THESIS FOR THE DEGREE OF DOCTOR OF PHILOSOPHY
IN PRODUCT AND PRODUCTION DEVELOPMENT

Influence of microstructure and batch variations on the machinability of steels

CHARLIE SALAME

Department of Mechanical Engineering

CHALMERS UNIVERSITY OF TECHNOLOGY

Gothenburg, Sweden 2026

Influence of microstructure and batch variations on the machinability of steels
CHARLIE SALAME

ISBN: 978-91-8103-400-4

Doktorsavhandlingar vid Chalmers tekniska högskola
Ny serie nr 5857
ISSN 0346-718X
https://doi.org/10.63959/chalmers.dt/5857

Department of Mechanical Engineering
Chalmers University of Technology
SE-412 96 Gothenburg
Sweden
Telephone + 46 (0)31-772 1000

Printed by Chalmers Reproservice
Gothenburg, Sweden 2026

To my mother, whose support is endless,
and my father, whose presence is permanent…

Influence of microstructure and batch variations on the machinability of steels

CHARLIE SALAME

Department of Mechanical Engineering
Chalmers University of Technology

Abstract

Material variations in steels – even within specific standards – can significantly influence machinability, leading to inconsistent tool wear behaviour that challenges process reliability, compels conservative machining strategies and increases production costs in industrial manufacturing. Although general trends are recognised within machinists, the machinability of steels is governed by a complex interplay of numerous factors that are difficult to isolate. This thesis investigates the influence of microstructural variations and non-metallic inclusion characteristics on the machinability of steels, with particular emphasis on tool wear behaviour and tribological interactions at the tool-chip interface. The thesis integrates experimental observations with modelling approaches to improve the understanding of thermo-mechanical conditions in machining. An enhanced semi-analytical model for predicting tool-chip interface temperature is developed, enabling more accurate estimation of thermal loads that govern wear mechanisms.

A multi-faceted experimental approach is adopted, combining detailed material characterisation with controlled machining tests across several steel grades, including case-hardening steels, micro-alloyed steels, bearing steels, and stainless steels. Microstructural features such as ferrite fraction, grain size, and pearlite morphology are quantified alongside non-metallic inclusion populations, including sulphides, oxides, and nitrides. These material characteristics are systematically correlated with tool wear mechanisms observed under well-defined cutting conditions. Across all investigated materials, the results demonstrate that even subtle variations in microstructure – such as reduced ferrite content, finer grain size, or decreased interlamellar spacing – lead to differences in tool wear response. In parallel, the role of non-metallic inclusions is shown to be equally critical. Soft, deformable inclusions such as MnS contribute positively to machinability by promoting chip segmentation and, in some cases, forming lubricating tribo-layers at the tool surface. In contrast, hard inclusions such as alumina-rich oxides and titanium nitrides act as abrasive particles, accelerating coating degradation and tool failure. Importantly, the findings highlight that machinability is not governed solely by inclusion quantity, but by a complex interplay of inclusion size, morphology, and chemical composition. A key contribution of this thesis lies in advancing the understanding of tribo-layer formation during machining. Through advanced characterisation techniques, including SEM, EDS, and FIB-STEM, the formation of protective layers composed of inclusion-derived material is identified as a decisive factor in tool performance. These tribo-layers can reduce friction and shield the tool surface; however, their formation is shown to be highly sensitive to both inclusion chemistry and tool coating composition.

The research further demonstrates that machinability must be interpreted as a system-level response, influenced not only by material properties but also by process conditions, geometric factors as well as cutting tool selection. Variations in tool-workpiece engagement, such as changes in effective depth of cut, are shown to significantly alter wear behaviour, particularly in industrial environments where such variations are difficult to control. The findings provide a foundation for improved material design through inclusion engineering, as well as for the development of predictive models and adaptive machining strategies aimed at achieving consistent and optimised tool performance in industrial applications.

Keywords: machining, tool wear, micro-alloyed steel, machinability, inclusion, thermal modelling

Preface

This doctoral thesis is based on the work performed at the Division of Materials and Manufacture, Department of Mechanical Engineering (former Department of Industrial and Materials Science) at Chalmers University of Technology between September 2021 and May 2026. The work is part of the WEAR-FRAME project funded by Vinnova (Sweden´s Innovation Agency) under FFI program (Project No.2020-05179). The thesis was supervised by Dr. Amir Malakizadi (main supervisor, 2021–2025) with Professor Uta Klement as co-supervisor, after which Professor Uta Klement served as main supervisor (2025–2026) with Dr. Amir Malakizadi as co-supervisor. The thesis was examined by Professor Peter Krajnik. The thesis consists of an introduction and summary of the work and the following appended papers. Parts of the work presented in this doctoral thesis have been previously published in a licentiate thesis by the same author.

Paper A — **An enhanced semi-analytical estimation of tool-chip interface temperature in metal cutting**
Charlie Salame, Amir Malakizadi
Journal of Manufacturing Processes, Vol. 105, No. 1, (2023), 407-430

Paper B — **On the influence of batch-to-batch microstructural variations on tool wear when machining C38 micro-alloyed steel**
Charlie Salame, Amir Malakizadi, Uta Klement
Wear, Vol. 562-563, No. 1, (2025), 205632.

Paper C — ***Batch-to-batch microstructural variations and their influence on machinability of a case-hardening steel***
Charlie Salame, Jonas Svensson, Amir Malakizadi
In Manuscript

Paper D — **A comparative investigation on machinability of stainless steels – influence of microstructure and mechanical properties on tool wear**
Charlie Salame, Denis Boing, Franck Lamirand, Christophe Bourgin, Amir Malakizadi
Submitted for publication

Paper E — ***Influence of microstructural batch variations on machinability and tribo-layer formation during turning of 100Cr6 bearing steel***
Charlie Salame, Daniel Andersson, Martin Aronsson, Rachid M Saoubi, Elias Vikenadler, Denis Boing, Enrico D'Eramo, Uta Klement, Amir Malakizadi
In Manuscript

The following papers are not appended to the thesis:

Paper F *Sensor-based identification of tool wear in turning*
Charlie Salame, Rico Rapold, Bülent Tasdelen, Amir Malakizadi
Procedia CIRP, Vol. 121, No. 1, (2024), 228-233

Paper G *Multi-sensor monitoring of wheel wear during cBN grinding of crankshaft steel*
Charlie Salame, Philipp Hoier, Peter Krajnik, Amir Malakizadi
MM Science Journal, (2025), 9165-9170.

Contribution to appended papers

My contribution to the appended papers is as follows:

Paper A I was involved in developing the thermal models and coding of the semi-analytical models in MATLAB. I also wrote the manuscript together with Amir Malakizadi.

Paper B I was involved in planning the cutting experiments and material characterisation together with the co-authors. I conducted all the cutting tests and characterisation work for the tools and workpiece materials. I also wrote the first draft of the manuscript. The physics-based model for simulation of tensile properties of micro-alloyed steel was developed by Amir Malakizadi.

Paper C I was involved in planning the cutting experiments and material characterisation together with the co-authors. I conducted the cutting tests at Chalmers, while the industrial cutting tests were conducted at Volvo Group Trucks, managed by Jonas Svensson. I performed all the characterisation work for the cutting tools and workpieces. I also wrote the manuscript together with Amir Malakizadi.

Paper D I was involved in planning the cutting experiments and material characterisation together with the co-authors. I conducted all the cutting tests with Amir Malakizadi. I performed all the characterisation of the worn cutting tools and workpieces, except the EBSD characterisation (done by Amir Malakizadi) and the thermo-mechanical properties (obtained from Ugitech). I wrote the manuscript together with Amir Malakizadi.

Paper E I was involved in planning the cutting experiments and material characterisation together with the co-authors. I supported Daniel Andersson and Martin Aronsson in the cutting tests at Chalmers. I was also involved in the temperature measurement tests at Seco Tools, Fagersta, Sweden. I performed all the characterisation work for the cutting tools and workpieces, including SEM, EDS and FIB-STEM. I also wrote the manuscript together with Amir Malakizadi and Uta Klement.

Table of Contents

1. Introduction

1.1. Background and motivation

To enable the development and optimisation of sustainable machining processes, it is essential to establish robust and reliable predictive models and simulation tools that can accurately capture the inherent complexity of machining operations. Equally important is a comprehensive understanding of the workpiece material characteristics that determine machinability, as even minor variations between batches, even within standard specifications, can significantly affect a material's machinability. Consequently, nominally identical materials from different suppliers or production batches do not necessarily exhibit the same machinability [1, 2]. Furthermore, given supply chain bottlenecks and increasing geopolitical uncertainty, manufacturing companies can often no longer rely on a single supplier for sustained production. This necessitates improved capabilities for managing material-related variations in production systems. The development of integrated and microstructure-sensitive modelling approaches that account for batch-to-batch variations plays a critical role in optimising production performance and effectively controlling process fluctuations. Otherwise, productivity losses or a compromise in product quality would occur.

A primary challenge in modern manufacturing is the lack of precision in tool life predictions, stemming from an incomplete understanding of how workpiece characteristics influence wear mechanisms. While predictive models are widely deployed, they often lack explicit consideration of microstructural effects, failing to account for the stochastic microstructural variations that drive batch-to-batch inconsistencies in machinability. Consequently, manufacturing facilities struggle to implement optimised tool-change schedules. From an economic perspective, such optimisation is of considerable interest to the manufacturing industry, as previous studies have shown that optimised tool change strategies can yield cost reductions of up to 40% in industrial production systems [3].

A better understanding of the influence of workpiece microstructure on machinability is therefore of central importance, as it supports compliance with stringent requirements for dimensional accuracy and surface integrity, while simultaneously increasing productivity and enabling lean and sustainable manufacturing methods. These improvements are typically reflected in performance indicators such as Overall Equipment Effectiveness (OEE) [4]. To achieve this, a systematic investigation of microstructural variations that lead to differences in machinability is required, combined with a thorough understanding of the underlying mechanisms of tool wear. This would complement the implementation of reliable physics-based and efficient modelling approaches to improve the understanding of tool wear progression during machining. To this end, this research is an initiative within the FFI project WEAR-FRAME, which aims to expand the existing knowledge in the aforementioned areas.

1.2. Research scope and focus

The first area of focus in this work is on the development of an efficient and reliable semi-analytical method for simulating the interface temperature during cutting. Thermally induced wear mechanisms, especially crater wear and plastic deformation, are strongly dependent on the temperature distribution at the interfaces between the tool, chip, and workpiece. Therefore, accurate simulation of tool wear and reliable prediction of tool life require precise determination of tool temperatures during machining. The complexity and limitations of experimental methods for measuring tool temperatures underscore the need for robust thermal models of the cutting process. In this context, the present work aims to further develop the established analytical thermal models of Komanduri and Hou [5-7] and Moufki et al. [8]. The modifications are intended to improve the accuracy of temperature predictions based on a physics-based understanding of the tribological conditions at the tool-chip interface. The results of this work were published in the first published article (Paper A) of this thesis work [9].

The second and most important focus in this work is to elucidate the influence of material microstructure on tool wear behaviour during machining. A major source of error that undermines the predictability of machining is the variation in workpiece material between different batches. These variations can be attributed to steelmaking processes and subsequent treatments such as heat treatment. These differences can influence microstructural phases, the type and distribution of non-metallic inclusions, and the thermo-mechanical properties of the material. Accordingly, this work focuses particularly on batch-to-batch microstructural variations that can influence the machinability of low-alloy steels and stainless steels. An attempt is made to determine the relationship between microstructural characteristics and tool wear response when machining two batches of modified C38 micro-alloyed steels under the same cutting conditions. The results are summarised in Paper B [2], appended to this thesis. A similar comparative study on the machinability of a high-carbon case-hardening steel is presented in Paper C. This study incorporates a stronger industrial perspective through machining tests performed on production lines at Volvo Group Trucks. Paper D extends the investigation and understanding of machinability to various stainless steel grades and provides a detailed comparative study of ferritic, martensitic, austenitic, super austenitic, duplex, and super duplex stainless steels.

While characterising the microstructural features of the workpiece is an essential first step in understanding its machinability, the inherent complexity of metal cutting processes requires a more in-depth investigation of the tribological interactions between tool and workpiece that occur at the tool surfaces in the cutting zone. Accordingly, the third focus of this work addresses the formation and stability of protective tribo-layers in the cutting zone. In this context, Paper E presents a detailed investigation of the tool surface and its compositional layers, examining the potential formation and stability of protective tribo-layers during the machining of different batches of 100Cr6 bearing steel. The study highlights the influence of such layers on tool wear and investigates their origin by comparing tools used for machining different steel batches.

1.3. Research objectives

By thorough investigations of the relationships between batch variation and tool wear progression, machining operations can be optimised to ensure higher productivity and improved workpiece quality. Despite extensive research in steel characterisation, the understanding of the influence of microstructural variations on the machinability of the material remains limited. Correspondingly, the predictability and simulation of tool wear (and by extension, tool life) are hindered by the many sources of variation in the complex machining processes, including batch-to-batch microstructural variations. This limits effective process optimisation and underscores the need for a deeper understanding of workpiece machinability. Accordingly, a main objective of this research is to answer the following research questions (RQ):

RQ1 - Does a physics-based approach to quantify tribological conditions at the tool-chip interface improve the accuracy in simulating the stress and thermal conditions during turning?

Despite the extensive body of work on tool temperature modelling in metal cutting, discrepancies persist in the underlying assumptions regarding heat generation and partitioning at the tool-chip interface. Existing models differ in their treatment of heat flux and heat partition distributions, with assumptions alternating between constant and variable quantities [10-13]. Moreover, several models do not reflect the established tribological conditions at the interface, where shear stress, sliding velocity, deformation rate and heat generation vary according to the sticking-sliding partition [11, 12]. The omission or oversimplification of these physics-based mechanisms has led to inconsistent predictions of both maximum temperature and temperature distribution along the tool rake face. An accurate representation of the tribological conditions at the tool-chip interface also enables a clearer understanding of their influence on protective layer formation on the tool surfaces (RQ3), as well as improved insight into thermally and mechanically driven wear mechanisms. These advantages motivate the need for improved thermal modelling that explicitly accounts for the tribological phenomena at the tool-chip interface. This research question is addressed in Paper A, where a physics-based approach is developed to quantify interfacial tribological conditions and assess their influence on the simulated stress and thermal distributions during turning.

RQ2 - How do microstructural properties influence the machinability of various grades of steels?

Machinability of steel grades is often assessed using standard certificate properties such as hardness, tensile properties and chemical composition. However, such properties alone do not adequately and fully reflect the complex interactions governing machining behaviour [14]. In fact, even microstructural variations between different batches of nominally-identical steel grades, within standard specifications, have been shown to strongly influence their machinability [14]. From an industrial perspective, this variability directly influences production efficiency and process predictability, as it impacts tool life

and, consequently, tool change intervals. However, the specific factors driving these differences remain poorly understood. In the absence of a systematic, material-specific analysis, it remains difficult to identify which microstructural properties are most critical to the machining performance of such materials. Papers B, C, D and E address this gap by characterising microstructural properties in different grades of steels. Papers B, C and E focus on the machinability variation of batches within specific steel grades, while Paper D compares machinability between different stainless steel grades. Relationships between material-specific properties and experimentally observed tool wear are then established to identify key factors governing the machinability of these materials.

RQ3 - Can workpiece microstructural variations influence the formation and stability of protective tribo-layers on the cutting tool?

Material transfer at the tool-chip interface is a key phenomenon influencing machinability during cutting. The transfer of workpiece material onto the cutting tool modifies the effective interface between the tool and chip, thereby altering the prevailing tribological conditions [15]. Interactions of a chemical, oxidative, and diffusional nature between the tool, chip, and surrounding environment are well recognised contributors to tool wear. Under certain conditions, however, the combined interaction of the tool, coating, workpiece material, and atmospheric oxygen can promote the formation of tribo-layers that reduce wear progression [15-18]. Variations in chemical composition, microstructure, thermo-mechanical properties, and inclusion content can influence the tool-workpiece contact conditions, which govern the formation and stability of these tribo-layers [15, 17, 19]. Despite this, the influence of such variations on tribo-layer development is not sufficiently examined in a systematic manner. Paper E addresses this research gap, specifically in bearing steels, by linking batch-specific properties of 100Cr6 to post-machining analyses of tribo-layer formation on different grades of cutting tools.

The research approach and sequence adopted in this work are schematically presented in Fig. 1, highlighting the relevant research questions within each area of focus.

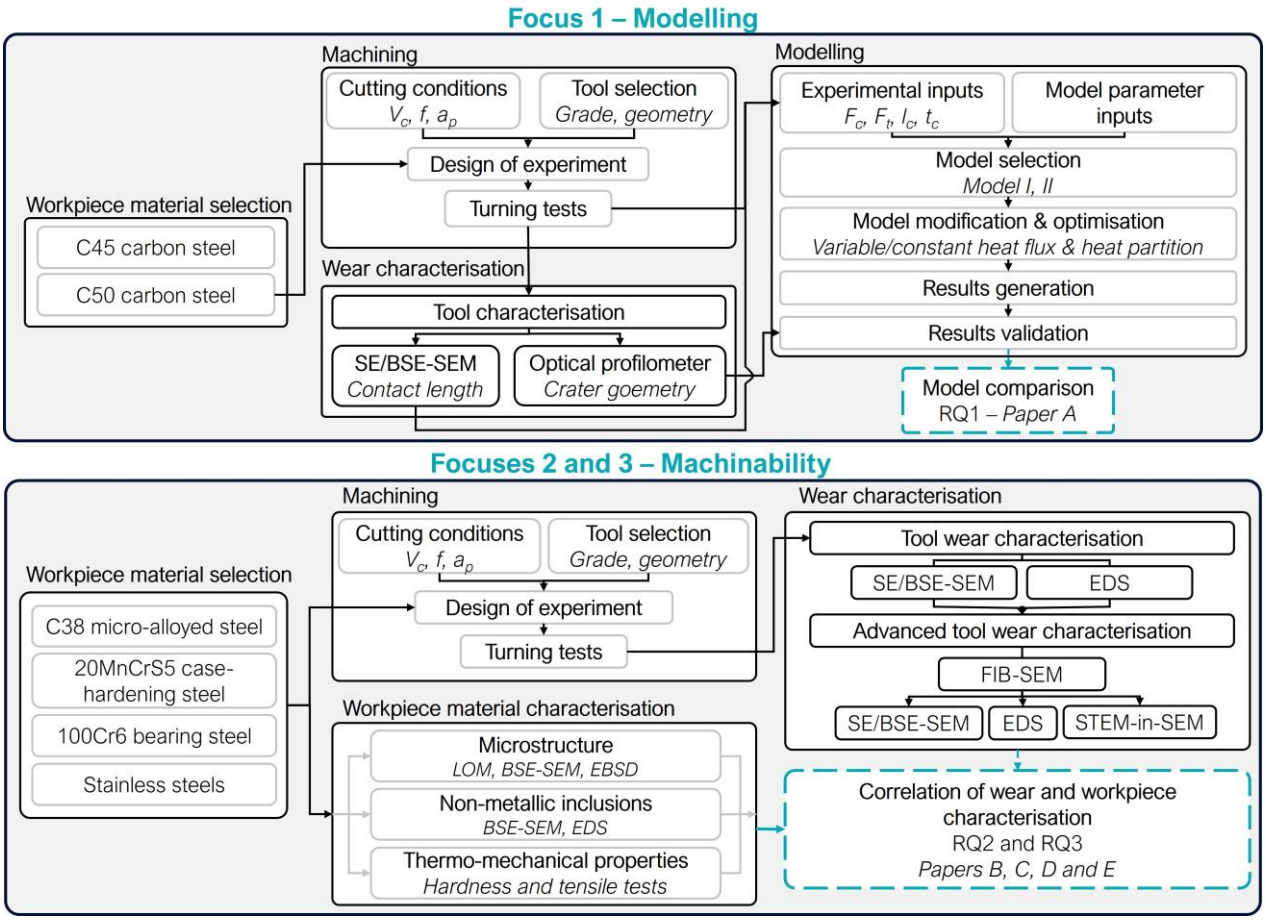

Fig. 1. Schematic representation of the research approach and sequence adopted in this research.

2. Tool wear during turning

This chapter provides an overview of the basic turning principles as well as the types and mechanisms of tool wear.

2.1. Fundamentals of turning

Metal cutting is the process of removing material from a workpiece using a cutting tool to create a desired shape that is symmetrical about its axis of rotation. In turning, the workpiece is clamped in a rotating chuck, while the tool is fed into the workpiece to remove material in the form of chips, as shown in Fig. 2. In longitudinal turning, shown in Fig. 2(a), the cutting tool is fed parallel to the axis of rotation of the workpiece. The directions of the cutting force (F_c), the feed force (F_f) and the passive force (F_p) that correspond to this type of turning are also shown. Longitudinal turning was employed in Papers C and D. In contrast, during facing operations, as shown in Fig. 2(b), the tool feed is radial to the workpiece's axis of rotation. The cutting, feed, and passive force directions for face turning are also shown. Facing is used in Papers A, B and E.

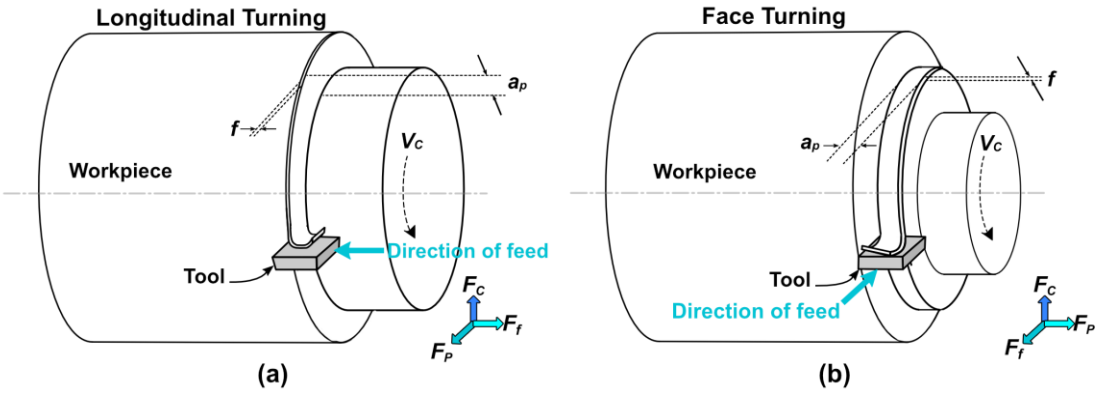

Fig. 2. Schematic illustrating (a) longitudinal turning and (b) face turning showing the main cutting parameters: cutting speed V_c, feed f and depth of cut a_p.

2.2. Cutting tools

In order for cutting tools to be suitable for machining workpiece materials, they must meet a number of strict requirements. Primarily, they must have high hardness to resist abrasive wear, while also maintaining sufficient toughness and compressive strength to withstand fracture and plastic deformation [20]. In addition, chemical stability and inertness with respect to the workpiece material are required. Given these demands, ceramics, polycrystalline diamond, and cubic boron nitride are employed as cutting tool materials; however, their properties (and cost) may limit their applicability in certain domains. Tungsten carbide (WC), when combined with a suitable durable coating, offers a more favourable combination of high bulk hardness and toughness over a broad temperature range, making it the most widely used cutting tool material [20]. Cemented tungsten carbide (WC-Co) is a composite material produced by powder metallurgy through liquid phase sintering and serves as a substrate in approximately 53% of cutting tools on the market [21]. In addition to the inherent hardness and wear resistance of the tungsten carbide grains, the binder phase – typically cobalt (Co) – provides toughness and

improves the material's resistance to fracture. The mechanical properties of Co-based cemented carbides can be tailored through modifications in WC grain size, binder content, or the addition of secondary carbides such as TaC, NbC, or TiC, enabling optimisation of the material for specific machining applications.

To further improve their mechanical, chemical, and thermal stability at elevated temperatures, cemented carbide tools are coated with protective layers, as is the case in 80-90% of such tools [21]. These coatings are applied predominantly using chemical vapour deposition (CVD) or physical vapour deposition (PVD). For steel machining, the CVD coatings often consist of different combinations and thicknesses of titanium carbonitride (Ti(C,N)) and alumina (Al_2O_3). Ti(C,N) increases the abrasive resistance and mechanical stability of the tool, while alumina provides chemical inertness, low thermal conductivity and sufficient mechanical stability at the elevated temperatures encountered during metal cutting [22, 23]. The tools used in this work are described in Chapter 6.

2.3. Tool wear in turning

The thermal and mechanical loads experienced by the cutting tool during machining lead to degradation of the cutting edge until its eventual failure. It is generally known that a worn tool has a detrimental effect on the functional properties and dimensional accuracy of the produced component and therefore must be replaced once the wear exceeds the application-specific threshold.

2.3.1. Tool wear types

Tool wear can broadly be classified into progressive and stochastic types. Progressive wear develops gradually over time, increasing with cutting duration, whereas stochastic wear occurs suddenly and unexpectedly. Owing to their gradual nature, progressive wear types can typically be modelled to provide an estimate of tool life and to predict, with reasonable accuracy, the timing of a required tool change. In contrast, stochastic wear cannot be reliably predicted through modelling and instead requires sensor-based monitoring due to its abrupt occurrence. Flank, notch and crater wear, shown schematically in Fig. 3, are considered progressive types of wear. Chipping is considered a stochastic wear type because it occurs suddenly by excessively high mechanical and thermal loads on the tool [24].

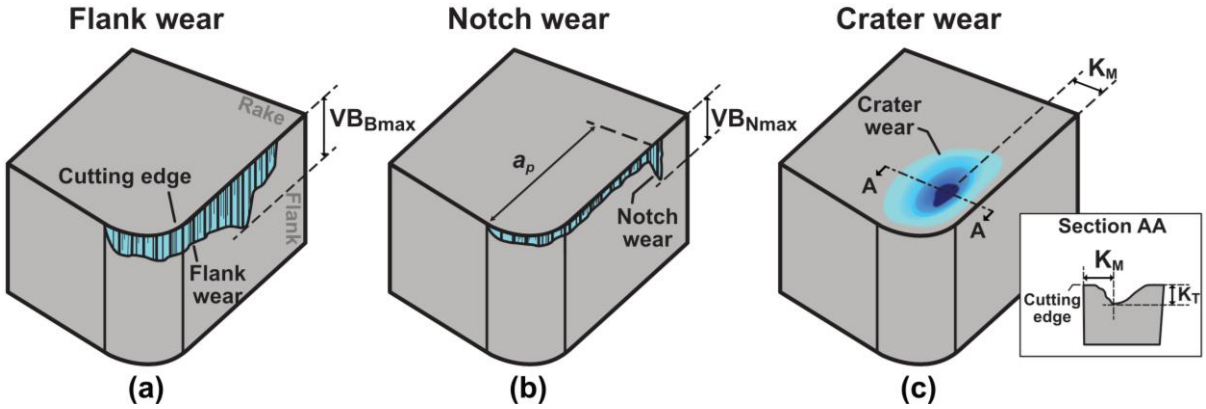

Fig. 3. Schematic representation of the main wear types investigated in this research and the main quantification parameters used.

Flank wear

One of the most common types of progressive wear in metal cutting is flank wear, which manifests as an increase in the contact area between the tool's flank surface and the newly generated workpiece surface. Flank wear typically develops in three stages, starting with an accelerated run-in phase, followed by a phase of steady wear, and ending in accelerated wear till failure [25]. The increased contact between tool and workpiece directly alters the mechanical, tribological, and thermal conditions in the cutting zone [26, 27]. Specifically, the feed and passive forces acting on the tool's flank tend to increase as flank wear progresses, which can lead to elevated temperatures, and reduced machining stability [28]. Flank wear is therefore a critical factor in determining tool life and the timing of tool changes in industrial practice. A common method to quantify flank wear is by measuring its maximum width, denoted as VB_{Bmax} in Fig. 3(a). It was monitored as a key indicator of wear and machinability in Papers B, C, D, and E.

Notch wear

Notch wear is another progressive wear type that develops at the depth-of-cut line, arising from a combination of high mechanical stress and increased local temperatures, and is often exacerbated by specific workpiece properties. Workpiece materials that exhibit high ductility and work hardening promote the formation of notch wear [29, 30]. These material properties lead to a work-hardened layer on the workpiece and the formation of work-hardened, and potentially serrated, chips during machining, which rub against the tool at the depth-of-cut line along the major cutting edge [31]. The complexity of notch wear is further increased by the influence of additional factor; for example, ambient oxygen content has been shown to influence notch wear for cemented carbide tools [32]. Notch wear on the major cutting edge often leads to tool chipping, whereas notch formation on the minor cutting edge degrades the surface integrity of the machined component [33]. A common method to quantify notch wear is by measuring its maximum width, denoted as VB_{Nmax} in Fig. 3(b). Given the high ductility and work hardening tendencies exhibited by various stainless steels, this type of wear was particularly observed in Paper D.

Crater wear

Crater wear is a thermally activated, progressive wear type that develops on the tool's rake face primarily due to the sliding action of the forming chips, particularly at elevated temperatures. The formation and growth of a crater reduces the strength of the cutting edge and compromises the structural integrity of the tool, increasing the likelihood of catastrophic failure, particularly when crater wear occurs in conjunction with significant flank wear [26]. Crater wear also influences the stress distribution at the tool-chip interface and can alter the heat generation during the process. Common indicators of crater wear are the maximum crater depth (K_T) and the maximum crater depth's distance from the cutting edge (K_M), shown in Fig. 3(c).

2.3.2. Tool wear mechanisms

The tool wear mechanisms underlying both progressive and stochastic wear can be abrasive, adhesive, diffusion-dissolution, or plastic-deformation based [34]. Abrasion

occurs when hard particles – originating either from the workpiece, such as non-metallic inclusions or carbides, or from fragments of the tool itself – penetrate the tool surface during relative tangential motion between the chip and the tool [35]. In his study on machining steels, Marinov [36] showed that the extent of abrasive wear depends on the tool material's hardness as well as the amount of abrasive inclusions in the workpiece. Xu et al. [37] demonstrated that resistance to abrasive wear in chemically identical steels is linearly correlated with some mechanical properties, mainly the hardness. In fact, the intensity of abrasive wear increases markedly when the hardness ratio between the abrading and abraded materials exceeds 1.25 [38, 39]. Given the thermal softening effect at the high cutting temperatures, it is the high temperature hardness of the material pair that determines whether the particle can abrade the tool material [40]. The extent of abrasion has also been shown to correlate to the size and shape of the abrasive particles, with larger and more angular particles leading to more pronounced abrasion compared to smaller and rounder ones [41]. Various studies by Ramalingam and Wright [42], Halila et al. [43], and Binder et al. [44] reported increased abrasive wear with higher concentrations of hard particles in the workpiece material.

Adhesion arises from the formation of micro-welds between the tool and workpiece materials, promoted by the high contact pressures in the cutting zone, which can be in the range of 2-3 GPa [45, 46]. The subsequent shearing action of the flowing chips may then cause material to separate from the tool rather than at the tool-chip interface, resulting in the gradual pullout of tool coatings and a loss of tool volume [47]. This mechanism is typically most pronounced in workpiece materials with high ductility, making it especially relevant in machining of stainless steels [48, 49].

Diffusion-dissolution occurs under sustained contact between tool and workpiece, leading to material loss either through diffusion of tool atoms into the workpiece [27] or, conversely, the incorporation of workpiece atoms into the tool, which can impair its wear resistance [27, 50]. During machining of stainless steel with cemented carbide tools, Saketi et al. [51] showed that crater wear can result from the diffusion of W, C and Co atoms into the chip. Plastic deformation, in contrast, is typically caused by excessive heat generation during cutting, which thermally softens the tool material and allows it to yield under the applied mechanical loads [52, 53]. In the case of cemented carbide tools, plastic deformation can occur by a combination of binder deformation, WC-grain deformation or WC-network deformation by grain boundary sliding [53, 54].

In practice, multiple wear mechanisms are usually active simultaneously, with their relative contribution governed largely by the temperature within the cutting zone. Such temperature changes may arise either from changes in cutting conditions, such as an increase in cutting speed, or from the gradual progression of tool wear. Wear mechanisms can generally be classified into three main groups: mechanical, thermal and adhesive [25]. Adhesive wear is dominant across a lower range of cutting temperatures compared to thermal mechanisms such as diffusion-dissolution wear, which prevail at higher temperatures [48]. When machining typical steel grades, mechanical wear mechanisms such as abrasion contribute progressively less to tool volume removal as temperature increases and lose prominence as thermal wear increases exponentially [55].

3. Thermal modelling of the cutting process

In metal cutting, experimental measurements and material characterisation can provide a partial understanding of the cutting process. However, many quantities of interest, such as local temperatures and stresses at the tool-chip interface, are difficult or impossible to measure with high accuracy [56, 57]. In addition, productivity requirements and practical constraints within production environments often limit the scope of experimental trials, making it challenging to systematically investigate the influence of multiple process parameters. In this context, modelling emerges as a valuable complementary tool, enabling the virtual evaluation of machining conditions and their effects on the thermo-mechanical loading of the cutting tool and the progression of wear. Not only do such models support the development of high performance machining in industrial applications, but they also improve the fundamental understanding of metal cutting. In particular, thermal models help improve the understanding of the prevalent tribological conditions during cutting and can, by extension, also give insight into tool wear evolution during cutting, especially for thermally induced wear types such as crater wear and plastic deformation [58]. The need for accurate thermal models is further underscored in light of the difficulties associated with measuring cutting temperatures experimentally.

Accurate modelling of the temperature distributions during metal cutting requires consideration of a wide range of factors, including the thermo-mechanical properties of the workpiece material, the applied cutting conditions, the tribological behaviour at the tool-chip-workpiece interfaces, and the geometry and thermal properties of the cutting tool. Accordingly, the motivation behind RQ1 is to improve the accuracy of semi-analytical thermal models, using physics-based quantification of the tribological conditions at the tool-chip interface. Such models account for the heat generation in the cutting zone using various assumptions related to the heat flux in the secondary shear zone (section 3.1) and tool micro-geometry (section 3.2). The challenges are elaborated in section 3.3.

3.1. Heat generation during turning

A schematic cross section of the tool and forming chip is shown in Fig. 4, highlighting the three shear zones that develop during cutting. The cutting process is initiated as the tool overcomes the shear strength of the workpiece, leading to intense, localised plastic deformation within the primary shear zone [59].

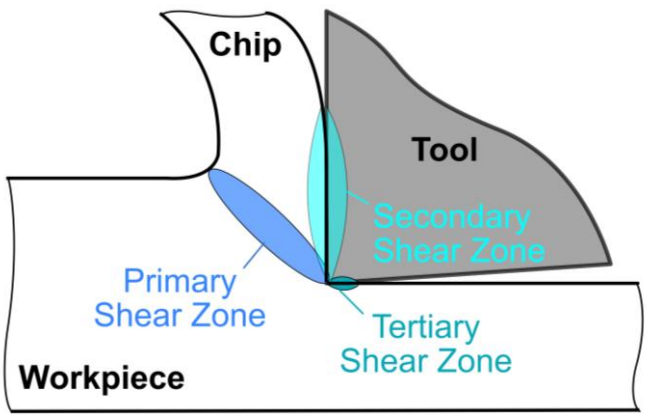

Fig. 4. Schematic illustration of the three main heat sources in metal cutting.

Owing to thermo-mechanical coupling, a significant portion of the mechanical work expended in this zone is transformed into heat, with the converted fraction commonly described by the Taylor-Quinney coefficient [60]. Incorporating the Taylor-Quinney coefficient into thermal models can be critical for improving their predictive accuracy, as several models in literature neglect this factor and instead assume that all mechanical work is converted into heat.

As the chip forms, it is further deformed while sliding along the tool rake face, where frictional resistance generates an additional heat source along the tool-chip contact length, known as the secondary shear zone [59]. This contact region can be subdivided into sticking, sliding, and transition zones, each contributing differently to heat generation at the tool-chip interface. A third, generally less dominant heat source originates from friction and deformation at the interface between the tool flank face and the newly machined surface, becoming increasingly relevant as flank wear progresses [59].

The fraction of heat entering the cutting tool plays a crucial role in determining cutting temperature, cutting forces, and tool life [61-64]. Fleischer reported that the fraction of cutting heat conducted into the tool, influenced primarily by the cutting conditions and workpiece and tool thermal conductivities, can range from approximately 2% to 18%, while 1-20% enters the workpiece and the remaining 74-96% is carried away by the chip [65]. A common simplification in thermal models reported in literature is the assumption of a uniform heat flux along the tool-chip interface, where the complex tribological conditions in the secondary shear zone is simplified to a single, constant value estimated using analytical expressions such as,

$$q_{SSZ} = \eta \frac{F_f V_{ch}}{l_c w} \tag{1}$$

where η is the Taylor-Quinney coefficient, F_f is the shear force on the rake face of the tool, V_{ch} is the chip velocity, l_c is the interface contact length and w is the width of the cut. Experimental and analytical studies, however, have demonstrated that the heat flux along the tool–chip interface is non-uniform in practice [56, 59, 66]. In fact, experimental observations indicate that the tool-chip interface comprises two distinct regions: a sticking zone characterised by complete seizure and a sliding zone governed by frictional sliding. Adjacent to the cutting edge, the tool-chip interface exhibits full material seizure due to the extreme normal stresses on the surface, causing the workpiece material to weld on the tool's rake face. Under these conditions, heat generated by intense plastic deformation is transferred predominantly into the tool by conduction, making this region a major contributor to heat flow into the tool [66]. In this sticking zone, the heat generated is proportional to the shear stress at the tool-chip interface (τ), which equals the shear strength of the workpiece material (k_{ssz}). In contrast, the sliding zone exhibits relative motion between the chip and the tool. The heat generation in this zone is governed by the shear stress distributions and the velocity distribution of the material flow [67]. To maintain material continuity along the tool-chip interface, there must be a transition region between the sticking and sliding zones, which combines both the equivalent heat generation mechanisms [67].

3.2. Tool edge micro-geometry

A large proportion of semi-analytical temperature models for orthogonal cutting rely on classical metal cutting models, such as the Merchant model [68], to estimate heat generation in the primary and secondary shear zones. To simplify the complex deformation behaviour within the cutting zone, these models commonly assume an idealised, perfectly sharp cutting edge. In reality, however, cutting tools possess a finite edge radius and are never truly sharp. This rounded geometry alters the material flow, leading to the formation of a stagnation point, or ploughing zone, around the cutting edge [69]. Material located above this stagnation point forms the chip, while material below it is displaced towards the flank face, as illustrated in Fig. 5. As a consequence of this non-ideal edge, the machining force is then split into two components: (1) a resultant force acting on the tool's rake face and (2) a ploughing force acting on the rounded edge and a section of the adjacent flank face [69, 70]. Consequently, there is an indication that the calculation of the heat generation on the rake face of the tool should exclude the ploughing force component [11].

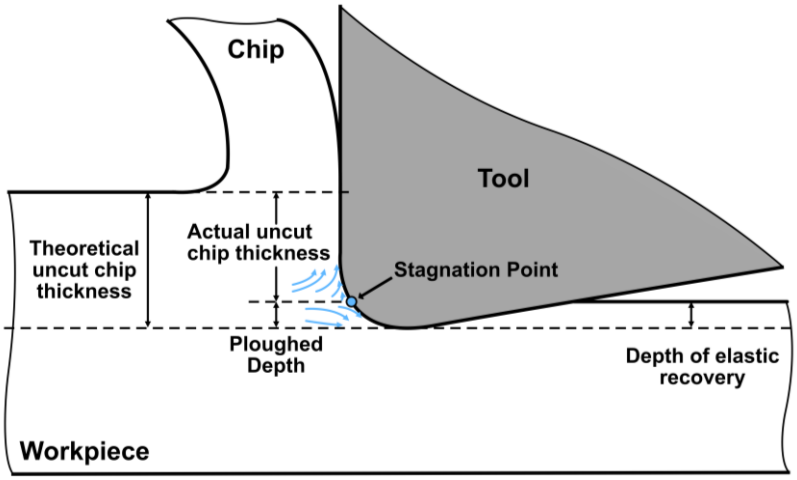

Fig. 5. Workpiece material flow showing the stagnation point on a rounded cutting-edge tool.

3.3. Challenges of semi-analytical thermal models

In addition to the assumptions outlined in the previous subsections, the accuracy of semi-analytical thermal simulations is hindered by various sources of error. For instance, part of the error in such models arises from their fundamental structure. Many existing models, such as those developed by Komanduri and Hou [5-7], depend on material- and process-specific parameters that require calibration for each tool-workpiece combination and cutting regime. These parameters are often challenging to determine experimentally, particularly across wide ranges of cutting conditions. Consequently, the development of robust, self-consistent models that minimise reliance on trial-and-error parameter selection and extensive experimental calibration remains an important objective within the field.

Analytical temperature models are also limited in their ability to accurately predict heat partition at the tool-chip-workpiece interfaces. The distribution of generated heat among these bodies is strongly influenced by cutting speed, contact pressure, sliding velocity,

interfacial conditions, and the temperature-dependence of thermophysical properties. In most analytical formulations, the heat partition coefficient is assumed constant or described using simplified expressions [25, 71, 72], which fail to capture the coupled and variable nature of interfacial heat transfer [5, 9]. Given the strong sensitivity of tool temperature to the fraction of heat conducted into the tool, even minor inaccuracies in the assumed partitioning can result in substantial deviations in predicted temperature fields.

Further, semi-analytical temperature models commonly account for the influence of a rounded cutting edge by incorporating the ploughing contribution into cutting forces and stress distributions, as discussed in the previous subsection. However, the associated heat generation in the immediate vicinity of the cutting edge and part of the flank face is often neglected or overly simplified [73]. This assumption can lead to an underestimation of local temperatures in these regions, where further thermo-mechanical interactions occur. A more accurate representation can be achieved by coupling finite element modelling (FEM) with semi-analytical thermal approaches, thereby enabling improved resolution of stress distributions and the corresponding heat sources around the cutting edge.

Additionally, the presence of tool coatings further complicates the accuracy of machining simulations. Different coatings (and coating combinations) behave differently under thermo-mechanical loads, which vary with cutting conditions. In addition, the varying nature of wear, i.e. progressive or stochastic, and its influence on temperature and stress distributions in the tool presents another challenge. Progressive wear can be modelled with a certain level of accuracy, but stochastic wear types, such as chipping, occur suddenly and remain difficult to predict, limiting the reliability of simulation-based tool life assessments.

4. Machinability

Modelling approaches that estimate stress and temperature distributions at the tool-chip interface provide valuable insight into wear mechanisms and tool performance. As such, they represent an important means of understanding machinability from a process-oriented perspective.

However, obtaining a more complete understanding of machinability – and the factors that influence it – also requires a thorough understanding of the workpiece material itself, since the material response under the extreme thermo-mechanical conditions of cutting is often governed by material-dependent microstructural and compositional features. This understanding becomes particularly important when comparing the machinability of batches with relatively subtle differences, given that even small variations in the material have been shown to result in measurable differences in machinability [2, 74-77]. Moreover, the characteristics of the cutting tool, e.g., its composition and microstructure, coating thickness and type as well as the cutting-edge radii can play a significant role in tool performance when machining a given grade of material, and thus its machinability. Therefore, a thorough understanding of material behaviour and its impact on machinability is essential, highlighting the need for a systematic investigation of tool-workpiece interactions driven by material-dependent variations (RQ2 and RQ3).

4.1. Definition, evolution and challenges

Machinability provides a broad conceptual framework for assessing how a workpiece material responds to mechanical cutting and has become a key consideration in the selection of cutting parameters, tool materials, and coolant strategies [78]. The inherent complexity of machinability stems from the large number of interacting parameters involved, as well as from the different definitions and evaluation criteria used by researchers and practitioners.

In one of its earliest definitions, machinability was viewed as an intrinsic property of the workpiece material, similar to mechanical properties such as yield strength or toughness [78]. Although these material properties can influence cutting performance, it has become widely accepted that the combined interaction of the workpiece, cutting tool, process parameters and machine setup ultimately determines the final performance. Even for a single workpiece material, machinability is strongly affected by factors such as machine rigidity, tool geometry and coating, cutting speed and feed, and cooling or lubrication strategy [78].

Researchers have long recognised these limitations, yet the need to maintain consistency for comparability is challenged by the need to understand workpiece material behaviour and evaluate new tool designs, coatings, lubricants, and machine configurations. To enable the relative comparison of machinability across different workpiece materials, a variety of methods have been developed, targeting different evaluation metrics.

The formal evaluation of machinability can be traced back to the pioneering work of F.W. Taylor [79] in the late nineteenth century. In his 1906 publication *On the Art of Cutting*

Metals, Taylor established the systematic variation of cutting parameters to determine force and tool wear coefficients within empirical power-law relationships. Building on this simple yet effective semi-empirical framework, subsequent research throughout the twentieth century expanded these concepts to enable comparative assessments of the machinability of different metal alloys, most often using readily measurable quantities such as cutting forces, chip morphology, and tool wear or tool life.

One of the earliest definitions of machinability was introduced by Sorenson and Gates [80] in 1929, who proposed a rating based on the ratio of cutting speed to hardness for hot-rolled SAE steels. Around the 1950s, Boulger et al. [81, 82] developed a machinability index defined by the machining speed at a tool life of 60 minutes (V60), expressed as a function of Brinell hardness, thermal conductivity, length of cut, and reduction in area from a standard tensile test. However, this index does not allow meaningful comparisons between different material classes and restricts machinability to a single parameter, namely cutting speed. Moreover, important aspects such as surface integrity and tool wear behaviour were not considered. In 1951, Woldman and Gibbons published an important work on the machinability and machining operations of various metal alloys. Machinability was primarily characterised in terms of workpiece properties such as strength, hardness, grain size, and microstructure, as well as their influence on tool wear, chip formation, ease of cutting, and surface finish [83].

In the 1980s, Mills and Redford [84] proposed a more focused definition based on tool wear under conditions that still ensure acceptable surface quality. They suggested that machinability should be understood primarily as a measure of how a given material contributes to the wear of a cutting tool during machining [85], while explicitly excluding cutting energy and surface quality from the machinability definition. Boothroyd [86] further emphasised that machinability is not a uniquely defined property but rather depends on the machining process and the criterion applied. Accordingly, a group of materials may be ranked differently depending on whether machinability is assessed in terms of tool wear rate, surface finish, or power consumption. Building on this concept, Enache et al. [87] distinguished between partial machinability, associated with individual criteria such as tool wear or surface roughness, and global machinability, which integrates multiple criteria into a single mathematical indicator.

According to Grzersik [88], machinability may be characterised using several primary criteria that depend on the machining parameters. These criteria include not only tool wear, energy consumption, material removal rate, surface roughness, and chip morphology, but also cutting forces, cutting temperature, and tribological parameters. Incorporating the latter enables a more detailed and physically grounded description of the cutting process. To facilitate quantification, coefficients relating machinability to cutting speed or feed rate are commonly employed, allowing the definition of machinability indices [89].

Sredanović et al. [90] proposed an approach in which the aforementioned machinability criteria are represented as normalised vectors within a rectangular coordinate system, enabling their combination into a single evaluation parameter. Through appropriate

selection and weighting of the criteria, machining performance can be assessed from the perspectives of productivity and economic efficiency. The choice of relevant criteria is typically determined by the end-user, based on the specific machining operation and the functional requirements of the component. More recently, sustainability-related metrics have been introduced to address legal, social, and economic constraints and expectations [91, 92].

Among the most widely used evaluation methods today are simple tool life assessments based on standards ISO 3685:1993 [93] and ISO 8688–1/2:1989 [94, 95] during turning and milling, respectively. Another commonly used comparison criterion is the American Iron and Steel Institute (AISI) machinability rating (Institute, 1960 #4422), which evaluates the relative tool life and surface finish in turning, using AISI/SAE B1112 carbon steel as a 100% baseline [78]. According to the AISI standard, cast aluminium achieves a relative machinability of 450%, while the superalloy Hastelloy X attains only 19%. Such evaluations of reductions (or elongations) in tool life are commonly regarded as central to the concept of machinability, which seeks to generalise or standardise the evaluation of ease with which a material can be cut.

Despite these developments, the multidimensional nature of machinability remains a source of ambiguity, as a material may exhibit favourable machinability with respect to one criterion while performing poorly according to another. The dependence of machinability on the machining system itself also makes comparison between different machinability studies challenging, as any variation in the system can influence the metrics used to define the material's machinability. In other words, comparing the machinability of different materials across two different machining systems is of limited practical value. For instance, a machinability ranking established for steel A relative to steel B using a certain tool grade cannot be directly generalised to another tool grade, as the process dynamics change significantly with any modification to the machining system. Although many studies and industrial practices have been carried out to evaluate machinability, most focus on specific materials and machining outcomes. To date, no comprehensive and universally accepted definition of machinability exists, nor is there consensus on standardised evaluation methods [78].

4.2. Evaluation of machinability

In the absence of a unified definition and standardised evaluation methodology, the concept of machinability has instead been approached through a set of practical indicators, which can be grouped into five broad categories: cutting forces and power consumption, chip morphology, cutting tool life, surface integrity of the machined workpiece, and environmental factors [14, 26]. In their review, Ånmark et al. [14] reported that approximately 85% of studies use flank wear as a machinability indicator, whereas only about 35% include cutting force measurements.

4.2.1. Tool life as a machinability indicator

The effective use of tool life as a machinability indicator requires systematic documentation and reporting of all relevant conditions, owing to the large number of

factors that influence tool wear behaviour. For instance, tool wear progression, as a machinability metric, is inherently dependent on the properties of the cutting tool. Among these, the choice of tool substrate material, together with the applied coating type, exerts a strong influence on wear behaviour and, consequently, on the assessed machinability [82]. A large body of work exists in literature investigating the influence of the tool grade on tool wear and tool life in the machining of steels and stainless steels [96-100].

Beyond substrate and coating composition, several other factors have been shown to significantly influence tool wear progression, including the coating deposition process, the structure of multilayer systems, coating texturing, and pre- and post-treatment of both the substrate and coating layers [97, 101-105]. Moreover, the cutting edge microgeometry - particularly the degree of edge sharpness or rounding - plays a critical role in governing stress and temperature distributions, wear mechanisms and tool life [106, 107], and thus directly impacts machinability. From a process perspective, it is well established that tool wear is also influenced by the applied cutting conditions and the chosen cooling-lubrication strategy.

These influences reveal that using tool wear as an indicator of machinability requires a holistic view of the machining process. To accurately assess variations in workpiece machinability, all other contributing factors - namely the cutting tools, process parameters, and machine setup - must be kept constant. This is particularly important when comparing machinability data across different studies, where variations in tooling, process parameters, or cooling strategies can significantly affect the observed wear behaviour. Within a single study, such influences must be minimised to enable a meaningful comparison of wear-based machinability.

4.2.2. Cutting forces as a machinability indicator

Similar to tool life, cutting forces are frequently employed as criteria for evaluating machinability. Although cutting force and cutting energy were initially considered of secondary importance for practical applications, their relevance has increased significantly in the context of today's energy-conscious manufacturing environment [74].

In general, it is well established that materials that are more difficult to machine generate higher forces during cutting [108]. However, the forces are strongly affected by the complex interactions between the tool and the workpiece, including cutting conditions and the applied cooling or lubrication strategy. Consequently, assessments of machinability based on cutting forces must also be interpreted within a well-defined, documented and reported context.

Another important aspect to consider when evaluating machinability based on process forces is the dynamic behaviour of the forces. For instance, the formation of built-up edges may lead to an overall reduction in average cutting forces, which would give the impression of improved machinability. However, the associated dynamic loading of the cutting edge and the resulting decline in surface quality would in contrast indicate poorer machinability [109, 110]. These dynamic intricacies are typically not captured when machinability is assessed solely on the basis of process force measurements.

Consequently, interpretations based on cutting forces alone may be misleading and defining the correct indicators for the intended application is crucial.

In literature, cutting forces are often interpreted in conjunction with cutting temperatures when assessing machinability. Materials with high thermal conductivity and relatively low tensile strength generally exhibit lower cutting forces and reduced cutting temperatures during machining [78]. Such workpiece materials are typically associated with slower tool wear rates, thus longer tool life and are often classified as having favourable machinability. In contrast, materials that are considered difficult to machine, such as duplex and super duplex stainless steels, combine high tensile strength with low thermal conductivity, resulting in elevated thermo-mechanical loads, accelerated tool wear, and adverse effects on workpiece surface integrity. Based on these and similar observations by machinists, readily available material properties are often used in practice as indicators of machinability. However, this approach represents a significant oversimplification of the complex and multi-faceted nature of machinability and does not consistently provide reliable assessments, particularly when attempting to explain or justify batch-to-batch variations.

4.3. Factors that influence machinability

The machinability of a material introduced into a production line depends on various interacting factors that can generally be classified into four categories: (1) workpiece material variations, (2) workpiece geometry variations, (3) cutting tool variations, and (4) process variations. Workpiece variations may be material-based, resulting from differences between batches or material grades, or geometry-based, arising from factors such as differences in forging conditions or prior machining processes. From a workpiece material's perspective, the factors that influence machinability include thermo-mechanical properties (e.g., flow stress properties, hardness, thermal conductivity), microstructural features (e.g. grain size, phase fractions) and the distribution and composition of non-metallic inclusions. From a broader perspective, the machinability of a material can be influenced by other factors, such as the cutting tool (e.g. tool grade, coating, geometry) as well as variations in the process itself (e.g. internal versus external turning, cutting conditions, clamping strategy). Accordingly, the machinability in this research is examined within the framework of these variations.

This subsection specifically addresses machinability variations arising from material-based differences in the workpiece material, whereas the remaining sources of variation are discussed in their respective publications (see Table 7). Despite extensive research on the influence of microstructural features on thermo-mechanical properties, the relationship between microstructure and machinability remains insufficiently understood due to the large number of interdependent factors involved. These factors collectively influence the flow stress behaviour of steels, underscoring the need for advanced, microstructure-sensitive models in machinability assessment. Despite earlier efforts to isolate the effects of individual microstructural features on steel machinability [75, 76, 111], it is impractical to modify a single characteristic without simultaneously affecting other interrelated properties [112-114]. This inherent interdependence is further

highlighted in Chapter 5, which demonstrates the complexity and intricacy of the steelmaking process.

4.3.1. Thermo-mechanical properties

Some thermo-mechanical properties such as tensile strength, yield strength, thermal conductivity, specific fracture energy, ductility, and strain hardening behaviour have been associated in literature with the machinability of workpiece materials. For instance, tensile and yield strength describe a material's resistance to plastic deformation and fracture. Therefore, they can provide an indication of the mechanical loads acting on the cutting tool, as well as the workpiece's cutting resistance, or specific cutting energy, defined as the mechanical work required per unit volume of material removed [47]. As discussed in Chapter 3, a large fraction of the cutting energy is converted into heat. As a result, high-strength materials impose elevated thermal and mechanical loads on the cutting tool, typically necessitating lower cutting speeds to achieve acceptable tool life.

Thermal properties of the workpiece and tool also strongly influence the temperature in the cutting zone. In particular, low thermal conductivity of the workpiece limits heat dissipation through the workpiece and chip, resulting in higher cutting temperatures [47]. Similarly, a low specific heat capacity leads to higher temperatures during machining. From a cutting tool perspective, these elevated temperatures accelerate thermally activated wear mechanisms, which rapidly degrade the cutting edge of tools [48]. The concentration of heat at the tool-chip interface can also cause thermal softening of the tool material, leading to plastic deformation of the cutting edge. From a product perspective, the high thermal gradients often induce tensile residual stresses and phase transformations on the machined surface, compromising the surface integrity and dimensional accuracy of the final component [115]. Consequently, materials with poor thermal conductivity often require reduced cutting speeds and feeds to control temperature, usually at the expense of productivity [47].

Further insight into the cutting temperatures can be obtained from the specific fracture energy, which can be calculated from the integration of the true stress-strain curves of the workpiece material. Although this property is derived from tensile tests under uniaxial loading - which do not fully replicate the complex conditions of machining - it still provides a useful indicator of heat generation during cutting and, consequently, of the prevalent thermal loads in the cutting zone [116, 117].

Ductility, typically quantified by elongation to fracture, serves as a primary indicator of a material's deformation capacity and its tendency to adhere to the tool's surface [47]. High ductility often promotes the formation of a Built-Up Edge (BUE), as the material undergoes extensive plastic flow and welds to the cutting edge, which can degrade surface finish and alter tool geometry [71, 118]. While reduced ductility can enhance chip breakability by facilitating fracture in the shear zone, extremely low ductility may lead to brittle splintering, increasing mechanical shock and accelerating abrasive wear on the tool's cutting edge [119].

Strain hardening is defined by the increase in a material's plastic flow stress as it undergoes strain. As described by Shaw [71], this occurs when dislocations – the primary carriers of plastic deformation – move through the crystal lattice and are impeded by grain boundaries, second-phase particles, or impurity atoms. These obstructed dislocations generate back stresses that hinder the motion of subsequent dislocations, resulting in an observable increase in both strength and hardness [71]. In machining, a workpiece that exhibits significant strain hardening requires progressively higher forces to sustain its plastic deformation. The larger deformation energy increases heat generation and thus temperatures rise in the cutting zone, creating a detrimental effect on tool wear. Strain hardening also affects the machined surface, leaving a hardened "skin" that increases surface roughness and tensile residual stresses. In multi-pass processes, the tool must penetrate this previously hardened layer, often leading to faster tool failure. This behaviour is particularly evident in materials such as stainless steels, which are well known for their strain hardening tendencies [120, 121].

4.3.2. Microstructural characteristics

While the aforementioned mechanical and thermal properties influence the workpiece response during cutting, they are fundamentally rooted in the workpiece's microstructure. Consequently, the investigation and comparison of microstructural characteristics can provide insights into a material's machinability. In low-alloy steels, critical factors include ferritic grain size, constituent volume fractions (such as the ferrite-to-pearlite ratio), and the presence of secondary precipitates. Conversely, in stainless steels, the influential characteristics are grade dependent. This subchapter discusses various key microstructural characteristics that are most relevant to the present investigation and their influence on machinability. Overall, it is important to recognise that these different factors are intimately linked; consequently, it can be misleading to rely on a single factor when evaluating a material's overall machinability.

While the influence of grain size on a material's mechanical properties is well established, its impact on machinability remains less clearly defined. According to the Hall-Petch effect, particularly at temperatures below half the material's melting point, smaller grains increase strength by impeding dislocation motion at the grain boundaries, making the material more resistant to deformation. The material's yield stress then varies according to

$$\sigma_y = \sigma_0 + k_y {d_g}^{-1/2}, \tag{2}$$

where d_g is the mean grain diameter, σ_0 is the internal stress required to move dislocations and k_y is a material-dependent constant. σ_0 is the sum of contributions from different sources of hardening, including solid-solution, precipitation, dislocation, and lattice hardening. This aspect is particularly significant in micro-alloyed steels containing small additions of vanadium, titanium, or niobium. In such steels, the nano-sized carbonitride precipitates exert a pinning effect on grain boundaries during rolling and subsequent thermal treatments, thereby controlling grain growth and the resulting microstructure [122, 123]. Depending on their size and volume fraction, these

precipitates also contribute to precipitation strengthening, leading to increased hardness and improved tensile properties of the steel [124]. Regarding the influence of grain size on machinability, an increase in grain size has been shown to correlate with higher notch wear and altered chip formation during the machining of various materials [125-127], including 316L austenitic stainless steel [1].

In addition to grain size, the hardness and yield strength of a material are also influenced by the volume fractions of its microstructural phases. In ferritic-pearlitic steels, an increased ferrite fraction is widely reported to improve machinability with carbide tools, primarily by reducing tool wear and promoting more favourable chip formation [76]. For duplex and super duplex stainless steels, the volume fraction of austenite to ferrite plays a role in determining the machinability, especially given the phases' vastly different thermo-mechanical properties. Austenite is known to exhibit high ductility and strain hardening rates, which promote adhesion and poor chip breakability, while ferrite possesses excellent thermal properties that positively influence the thermal conditions in the cutting zone [128]. Thus, it can be safely assumed that variations in the volume fractions of the constituent phases will have a significant impact on the machinability of the duplex material.

Variations in chemical composition can also influence machinability, particularly in micro-alloyed steels containing small additions of vanadium, titanium, or niobium. The presence of these elements renders the material sensitive to precipitation strengthening. In such steels, the holding temperature and time determine the precipitation of nano-sized carbonitrides in the matrix, which increase strength and hardness through their pinning effect on dislocation movement. The magnitude of this strengthening effect depends on factors such as the precipitate volume fraction (v_p), mean particle radius (r), and inter-precipitate spacing. Several models reported in literature describe this precipitation hardening, and its contribution is reflected in the value of σ_0 in Eq. (1). One such model is the well-known Orowan model [129],

$$\sigma_O = 0.8Gb/L, \tag{3}$$

where G is the shear modulus, b is the Burgers vector and L is the average spacing between neighbouring precipitates on the slip plane. The value of L is inversely correlated to the precipitate's volume fraction v_p and directly proportional to the particle mean radius r. According to the Orowan mechanism, an increase in the average inter-precipitate spacing L reduces the strengthening effect. However, Eq. (3) generally overestimates the contribution of precipitation hardening [129]. Therefore, the hardening effect in this work is estimated using the Ashby-Orowan model [130], which provides a more appropriate representation of precipitation strengthening in steel systems,

$$\sigma_{A-O} = \frac{0.8MGb}{2\pi L\sqrt{1-v}} \ln\left(\frac{x}{2b}\right) \tag{4}$$

where M is the Taylor factor (for instance, in ferrite M = 2.75), $v = 0.293$ represents the Poisson's ratio and x is the mean diameter of the cross section of the carbonitrides on the slip planes.

In austenitic stainless steels, the presence of δ-ferrite is a microstructural feature that can be relevant for machinability. δ-ferrite is a residual phase often found in austenitic castings that enhances the austenite's resistance against hot cracking. From a machinability perspective, the presence of δ-ferrite within an austenitic stainless steel matrix can create discontinuities in the steel that may disrupt steady-state chip formation during machining, thus leading to better chip breakability. Research also shows that WC has significantly lower solubility in ferrite than in austenite – approximately an order of magnitude lower across typical machining temperatures - thus a higher δ-ferrite volume fraction can reduce tool material dissolution during machining with an uncoated WC tool [1]. Annealing twins are also common features in austenite that effectively refine the microstructure and increase the material's overall strength. During machining, these twin boundaries act as additional barriers to dislocation movement, which increases the strain-hardening rate and the energy required for shearing. This increased work-hardening capacity often leads to higher cutting temperatures, significantly deteriorating their machinability.

Another feature of steel microstructure that can affect machinability is the crystallographic texture. Crystallographic texture can introduce anisotropy in the mechanical response of the workpiece, resulting in direction-dependent deformation behaviour. In machining, this anisotropy can manifest as systematic variations in cutting forces when the cutting direction changes relative to the dominant grain orientation, rather than as random force fluctuations. Strong textures may therefore contribute to uneven tool wear, directional differences in surface integrity, and reduced dimensional predictability, particularly in materials with pronounced rolling textures.

4.3.3. Non-metallic inclusions

In addition to thermo-mechanical properties and microstructural features, the population of non-metallic inclusions (NMIs) in steel exerts a strong influence on its machinability. Non-metallic inclusions are particles embedded in the matrix of metals and alloys, and they can be of various types: sulphides, nitrides, oxides or mixed. Minor variations in NMI content, even within standard specifications, may not have a substantial impact on the thermo-mechanical properties of the workpiece material; however, they have been shown to significantly influence the machinability of steels [78, 131-134]. For instance, in a study on the effect of oxide inclusions in a pearlitic-ferritic steel, an increase in the number of oxides led to a significant increase in flank wear despite the steel's macro-hardness remaining nearly constant [44]. Inclusions have been reported to be both beneficial and detrimental for tool life and machinability [14, 131, 132, 135]. The mode of action of these non-metallic inclusions, and thus their influence on machinability, is governed by various factors including their type, quantity, size, shape factor, and chemical composition which influences the NMI's hardness and plasticity. The inclusion characteristics that are of particular interest depend on the steel application. Therefore, the control of different characteristics of NMIs in steels, known as inclusion engineering, has been a subject of research for decades. Inclusion engineering is further elaborated in Chapter 5, which presents a detailed discussion of the steelmaking process and its influence on NMIs.

Types

The different NMI classes can be broadly categorised as either beneficial or detrimental to machinability, although important nuances exist within each class, as discussed in the following subsections. For instance, sulphides are regarded as beneficial to machinability, whereas nitrides are considered detrimental.

Sulphide inclusions, such as MnS and (Mn,Ca)S, are deformable and relatively malleable. From a fundamental perspective, the interface between a sulphide inclusion and the surrounding steel matrix is characterised by a mechanical mismatch, which gives rise to local stress concentrations. During machining, these sulphides can act as stress raisers in the primary shear zone, promoting void formation at the inclusion-matrix interface. With continued deformation, sulphides elongate in the shear direction, which facilitates crack propagation and enhances chip fragmentation [77, 136, 137]. This can also reduce the contact area between the tool and chip, leading to a deceleration of tool wear [14]. Another prevalent viewpoint suggests that sulphide inclusions affect the tribological conditions in the secondary shear zone by either reducing the coefficient of friction between the tool and chip, as initially proposed by Merchant and Zlatin [138], or by providing regions of easy shear and reducing the shear stress required for fracture [139, 140]. This leads to lower tangential forces on the cutting tool, an increased shear angle, and consequently a reduced cutting force [140].

Unlike malleable sulphide inclusions, non-deformable hard oxides and nitrides, exhibit brittle behaviour and tend to fracture rather than deform under the high-stress conditions of machining [136]. These hard particles act as abrasive agents when they come into contact with the cutting tool, inducing micro-rupturing and subsequent degradation of protective tool coatings [23]. Hard oxide inclusions (e.g. Al_2O_3, SiO_2, and mullite $3Al_2O_3$ SiO_2) can also fracture within the steel matrix, remaining as sharp, abrasive fragments that further accelerate flank and crater wear [14, 141].

The influence of mixed inclusions on machinability is highly dependent upon their specific chemical composition. In this study, the majority of such inclusions were determined to be oxysulphides, consisting of a hard oxide core encapsulated by a malleable sulphide shell. Generally, oxysulphides exert a more favourable influence on the machining process than pure oxides. This is attributed to the presence of the sulphide shell, which 'masks' the hard oxide core [137, 142]. By providing a softer outer layer, the overall abrasiveness of the inclusion is reduced, preventing (or delaying) the sharp oxide centre from coming in direct abrasive contact with the tool coating, thereby decelerating tool wear and positively influencing the material's machinability.

Shape factor

The performance of non-metallic inclusions is further affected by their morphology, typically characterised by the aspect ratio (the ratio of the inclusion's longitudinal axis to its transverse axis). It has been demonstrated that globular inclusions generally confer superior machinability compared to elongated or directional stringers, particularly regarding chip morphology and tool life [143, 144]. This is because in the case of globular

NMIs, the voids that nucleate at the interface under tensile stress are less prone to 'rewelding' or pressure-induced closure during deformation [144]. Consequently, they act as effective stress concentrators that facilitate micro-cracking and chip fracture, whereas elongated inclusions can allow for re-bonding, leading to less efficient chip breakability.

Size

The size of inclusions is also a key factor in determining their influence on machinability. This led Kiessling to classify NMIs into macro- and micro-inclusions based on a critical inclusion size [145]. For hard abrasive inclusions such as oxides and nitrides, smaller micro-inclusions are generally more favourable for machinability. In addition to reducing the contact area between these abrasive particles and the tool, the random interaction between larger inclusions and the cutting edge can generate impact loading, leading to unstable cutting forces, increased vibration, and degraded surface integrity [121].

For deformable sulphide inclusions, two contrasting viewpoints exist regarding the role of inclusion size, each attributing machinability benefits to different mechanisms. Several studies report improved chip breakability with smaller sulphide inclusions, primarily due to their reduced tendency to reweld, as discussed previously [2, 14]. In contrast, other researchers argue that very small sulphides are ineffective, for several reasons. Some suggest that they are unable to form or sustain a low-shear-strength lubricating film, thereby limiting their contribution to friction reduction [146]. Others, including Kiessling [136], emphasise stress concentration effects, noting that larger inclusions induce higher local stresses and are therefore more effective in promoting chip formation. Trent [140] further proposed that small inclusions may simply be entrained in the plastic flow without significantly influencing the shear zones. Taken together, these arguments suggest the existence of an optimal inclusion size range, where sulphides are sufficiently large to act as stress concentrators and form lubricating films, yet small enough to avoid rewelding. It should also be emphasised that all inclusions represent permanent defects in the final component, and larger inclusions – particularly those that introduce anisotropy, such as sulphides – should be carefully controlled and minimised.

Hardness

Beyond an inclusion’s morphology, its chemical composition strongly governs its hardness, which is a key factor influencing machinability. A common practice in steelmaking is calcium treatment of the melt, which alters the chemical composition and, consequently, the hardness of non-metallic inclusions. This Ca-treatment of sulphides introduces a dual effect, simultaneously influencing their lubricating behaviour and their abrasive interaction with the cutting tool. Experimental data shows that increasing calcium content in a sulphide significantly increases its hardness [147], as shown in Fig. 6(a). This increase in hardness significantly lowers the inclusion’s relative plasticity index (discussed further in the next subsection), thereby weakening its deformation ability during machining [148]. In essence, a trade-off exists: increased hardness provides the mechanical stability required for the inclusion to adhere to the tool rake face [149], yet it concurrently reduces the inclusion's ability to deform. Additionally, the increased hardness may itself be detrimental to machinability by promoting abrasive wear of the cutting tool.

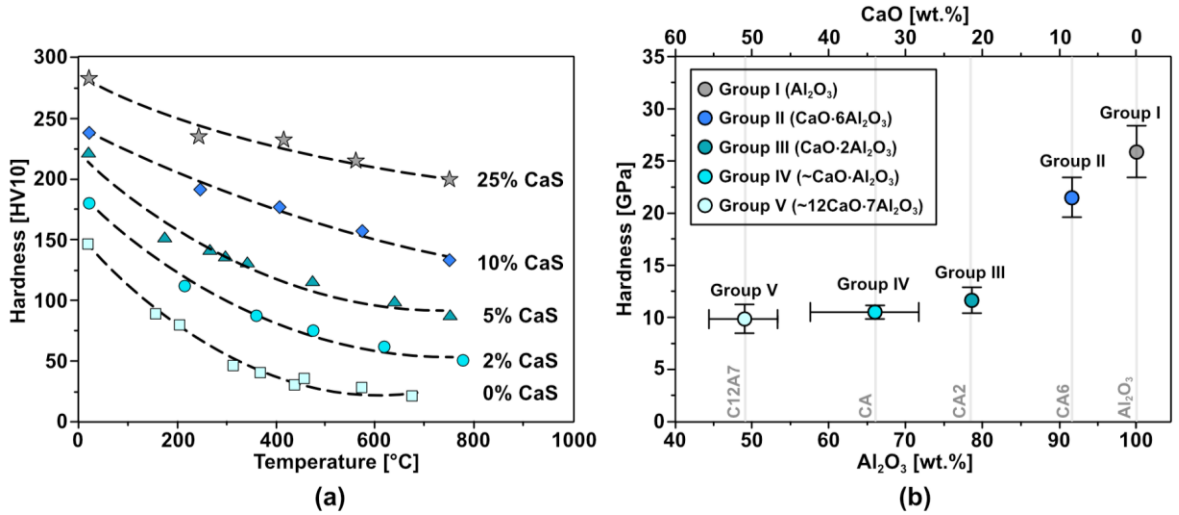

Fig. 6. (a) Influence of CaS wt% on the hardness of sulphide inclusions with respect to temperature, recreated from [147] and (b) average hardness of common groups of oxides based on their chemical composition, recreated from [150].

In contrast to its hardening effect on sulphides, calcium treatment softens abrasive oxide inclusions and renders them more malleable, while also promoting their envelopment by sulphides to form the aforementioned oxysulphides. Recently, Slagter et al. [150] measured the nano-indentation hardness of inclusion groups in the $CaO\text{-}Al_2O_3$ system, demonstrating a significant decrease in hardness with an increase in calcium weight percentage, as evident in Fig. 6(b). These calcium-rich oxides exhibit lower melting points and enhanced visco-plastic behaviour, which facilitate the formation of more stable protective layers at the tool-chip interface, thereby decelerating tool wear [14, 136, 151]. However, the effect of these Ca-rich oxides and oxysulphides is not exclusively beneficial. Recent studies have shown that calcium- and magnesium-rich oxides and oxysulphides can chemically interact with alumina tool coatings at elevated interface temperatures, forming calcium aluminate, spinel $MgAl_2O_4$, and calcium-magnesium aluminates [152]. Such reactions significantly reduce the hardness of the alumina coating, promoting groove formation and faster degradation of the tool coating.

Relative plasticity

Relative plasticity is also a commonly used metric to describe NMI behaviour, particularly when inclusion-specific properties are not available due to technological challenges [150]. Introduced in the 1960s, relative plasticity index is defined as the ratio of the true strain of inclusions to that of the surrounding steel [153]. A relative plasticity of zero indicates that the inclusion is rigid/brittle and will either remain intact or shatter upon being subject to forces. This is the case for most oxides and nitrides. In contrast, a plasticity of one indicates that the inclusion is perfectly plastic and will deform in the same manner as its surrounding steel matrix. This represents typical pure sulphide inclusions. Any value in between is referred to as semi-plastic behaviour, which is the typical behaviour adopted by modified sulphides and oxysulphides [136]. Rudnik [154] characterised the mechanical behaviour of non-metallic inclusions (NMIs) by categorising them into three distinct groups based on their relative plasticity indices. In the high-plasticity regime (0.5-1.0), the inclusion deforms in near-unison with the steel matrix. This high degree of strain

compatibility ensures that micro-cracking at the inclusion-matrix interface is largely avoided. At moderate plasticity levels (0.03-0.5), a differential flow occurs: while the inclusion's outer layers move with the matrix, the core remains relatively stationary. This mismatch results in a characteristic 'fish-tail' morphology and the formation of conical gaps at the poles of the inclusion before interfacial bonding can occur. Finally, in the case of non-deformable inclusions (≈0), such as oxides and nitrides, the steel matrix is forced to flow around a rigid body. This creates significant localised stress concentrations, leading to the development of prominent conical gap cracks within the material structure.

The behaviour of NMIs within these plasticity regimes depends strongly on various factors, such as chemical composition, hardness, and the prevailing temperature. In general, the relative plasticity of an inclusion is inversely related to its hardness [148]. In this context, as the inclusion is hardened – for instance, through chemical composition modification such as calcium treatment – its plasticity and capacity for plastic deformation is reduced [148]. Another notable example of these inter-dependencies are silicate oxides. These inclusions exhibit a rapid change in behaviour from brittle to plastic when the temperature exceeds a critical value [148]. This transition temperature increases with the increase of SiO_2 content in the silicate inclusion [148], further highlighting the coupled effects of chemistry and temperature on inclusion behaviour.

Thermal properties

Further expanding on the influence of temperature on NMI behaviour, the coefficients of thermal expansion (CTE) of NMIs differ from that of the steel matrix. Brooksbank and Andrews [155] showed that such CTE mismatches generate residual stress fields or voids around inclusions during cooling from prior forming processes. These residual stresses and voids are relevant to machinability as they help propagate cracks in the cutting zone and thereby reduce cutting forces and power consumption [14]. In fact, the magnitude of these stresses depends primarily on the difference between the expansion coefficients of the steel matrix and the non-metallic inclusion [14]. Consequently, inclusions may be categorised into three distinct groups according to this difference, as shown in Fig. 7.

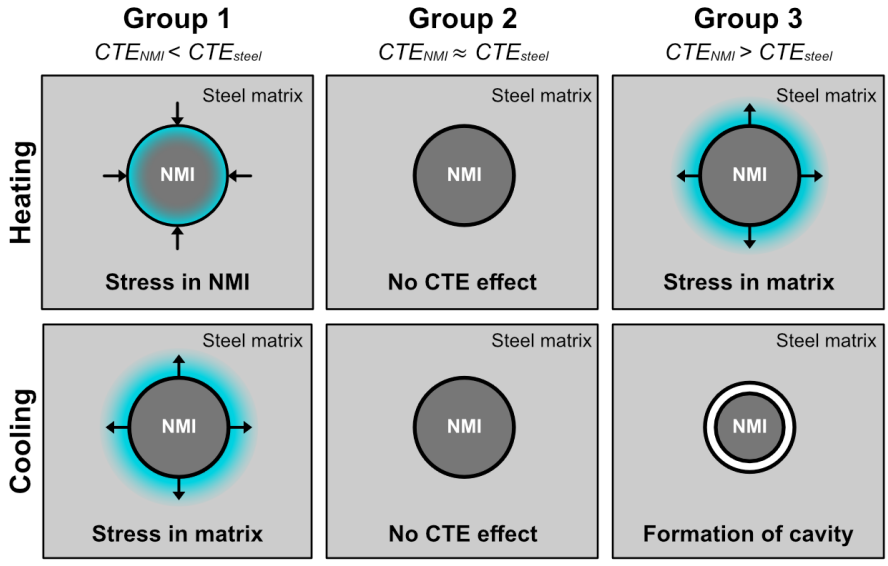

Fig. 7. Formation of stress fields and cavities around NMIs due to CTE mismatch. Recreated from [14].

From the perspective of residual stresses, non-metallic inclusions in Group 2 ($CTE_{NMI} \approx CTE_{steel}$) are expected to have minimal impact on machinability, as their thermal expansion closely matches that of the steel matrix. The beneficial influence on machinability described previously arises from the NMIs that belong to Group 1 ($CTE_{NMI} < CTE_{steel}$) and Group 3 ($CTE_{NMI} > CTE_{steel}$), which promote localised stress concentrations at the inclusion-matrix interface. During machining, these pre-existing stress fields facilitate the nucleation and propagation of micro-cracks within the primary shear zone, thereby lowering the energy required for chip formation and effectively reducing cutting forces.

In addition to the CTE, the melting temperature of an inclusion provides a useful indicator of its relative deformability during machining. Oxide inclusions with melting temperatures below or approaching the cutting temperature may soften or become partially molten, enabling their plastic deformation and elongation. In contrast, oxide inclusions with substantially higher melting points tend to remain rigid and resist deformation under the same conditions. A summary of the compositions and corresponding melting points of common Ca-rich oxides and sulphides is presented in Table 1.

Table 1. Chemical composition and melting temperatures of common Ca-rich oxides and sulphides [156].

NMI Class	Code	Phase	Chemical composition [wt.%]					Melting temperature [°C]
			CaO	Al_2O_3	Mn	Ca	S	
Oxide	$C_{12}A_7$	$12CaO \cdot 7Al_2O_3$	48	52				1455
	CA	$CaO \cdot Al_2O_3$	35	65				1605
	CA_2	$CaO \cdot 2Al_2O_3$	22	78				~1750
	CA_6	$CaO \cdot 6Al_2O_3$	8	92				~1850
	–	Al_2O_3	0	100				2054
Sulphide	–	CaS			–	55	45	>2000
	–	MnS			63	–	37	1610

4.4. Tribo-layer formation

Tribo-layer formation represents a key mechanism governing tool–workpiece interactions and is therefore closely linked to machinability, with variations in workpiece microstructure and inclusion characteristics influencing their formation and stability. These layers can locally modify the tribological conditions within the cutting zone, potentially reducing frictional stresses and consequently lowering the interface temperature. The thickness of such layers spans a wide range, from atomic monolayers to several tens of micrometres associated with severe plastic deformation [157]. Due to their complexity and multifaceted nature, these layers have been described using a variety of terms in the literature, including tribo-films, transfer layers, interlayers, agglomerated films, debris films, particle layers, and built-up layers [157-159]. However, the relationships between these terms, as well as their specific formation mechanisms and functional roles, remain insufficiently clarified. In the present work, the term *tribo-layer* is used in a general sense to describe surface layers that form at the tool-chip interface and influence the prevailing tribological conditions.

Such layers may develop through the mechanical smearing of non-metallic inclusions or wear debris onto the tool surface [160]. In addition, they can also form as a result of

chemical interactions between the workpiece material and the tribologically active tool surface [17]. A commonly adopted classification distinguishes tribo-layers based on whether they arise from surface transformation or deposition mechanisms [157]. Transformation-type layers originate from modifications of the underlying surface, such as plastic deformation or diffusion-driven processes affecting the near-surface region. In contrast, deposition-type layers form through the accumulation of externally supplied material, including non-metallic inclusions or wear debris, which may become compacted, tribo-sintered, and adhered to the tool surface. In the context of metal cutting, tribo-layers are most frequently reported to be of the deposition type [157].

Since real contact between tribological components occurs at the asperity level, the resulting tribo-layer has a decisive influence on friction in the cutting zone and subsequently wear. Local pressures at these micro-contacts can reach several GPa, leading to significant modifications of the near-surface region and the formation of a layer with properties rather distinct from the underlying material [157]. These modifications may include changes in surface topography (smoothing or roughening), micro-crack formation, phase transformations, deformation hardening, oxide formation, and material transfer from the counter surface. Under the extreme mechanical and thermal conditions present in the cutting zone, the tribo-layer material can undergo substantial changes due to plastic deformation, oxidation, and phase transformation, with many strengthening mechanisms typically associated with bulk materials being activated locally [157, 161].

Thus, tribo-layers can introduce substantially altered tribological conditions, as their properties may differ significantly from those of the underlying material, particularly on the tool side. During machining, these layers may be either beneficial or detrimental to machinability, depending on their composition and thermo-mechanical behaviour. However, their overall influence and prevalence remain insufficiently understood. For example, during the machining of tool steel with an uncoated cemented carbide tool, wear has been reported to proceed by the formation of a deposition-type tribo-film. Despite being mechanically weaker than the cemented carbide substrate, this tribo-film adheres sufficiently to promote gradual removal of the cobalt binder through diffusion. This is followed by fragmentation and removal of the WC grains, which are carried away as part of the shearing tribo-film [162, 163]. In contrast, beneficial influence of such tribo-layers is also reported in literature. Brant and Mikus [17] observed the formation of Al_2O_3-based protective layers on ceramic tools when machining steels with high alumina inclusion content, resulting in reduced crater and flank wear. Similarly, Matsui et al. [164] reported the formation of MnS-based inclusion layers on the rake face during machining of Ca-treated steels using carbide tools, which act to prevent direct tool-chip contact and reduce rake face wear. In a subsequent study, Matsui et al. [165] identified the formation of more complex oxide layers, including CaS at the interface, which contributed to reduced diffusional wear and improved tool life. In addition to inclusion-derived layers, tribo-oxidation mechanisms have also been reported. Yuan et al. [166] observed the formation of “protective/lubricious tribo-ceramic films” during machining of Inconel 718, which protect and lubricate the tool surface, thereby reducing wear and extending tool life. Furthermore, Song et al. [167] identified the formation of a stable built-up layer on the

rake face during dry cutting, which acts as a separating layer between the tool and chip and reduces both crater and flank wear, in contrast to unstable built-up edge.

Machining-induced tribo-layers reported in the literature predominantly comprise inclusion-derived layers, tribo-oxidation films, and built-up layers formed from adhered workpiece material. Inclusion-derived layers, often referred to as “Belag”, form by the deposition and smearing of non-metallic inclusions such as oxides and sulphides that adhere to the rake face and reduce tool wear by limiting direct tool-chip contact. Tribo-oxidation films, formed through chemical interaction between the tool, workpiece, and surrounding environment, are described as protective and lubricious layers that enhance wear resistance and extend tool life. In addition, built-up layers originate from adhered and plastically deformed workpiece material and can act as an intermediate layer at the rake face, thereby reducing crater and flank wear when stable. Across these studies, a consistent observation is that such layers, no matter their origin, can act to separate the tool and chip at the interface, thereby limiting direct abrasive contact between tool and workpiece and contributing to reduced wear.

The study of tribo-films has largely been conducted outside the context of machining, with substantial research focusing on coating materials such as alumina. While these investigations provide valuable insights, the conditions encountered during cutting are considerably more complex, particularly given the highly localised, extreme conditions of the tool-workpiece interaction. Consequently, further understanding is required. Without a clear understanding of how batch-to-batch variations influence the formation of these tribo-layers, and subsequently how these layers modify the tribological system, it remains challenging to reliably predict the friction and wear behaviour of materials under given conditions.

5. The production process chain: a machinability perspective

The production process chain, spanning from initial heat melt to final component production, dictates the intrinsic quality of the final workpiece. Chapter 4 presented the primary drivers of material and batch-to-batch variation, highlighting their critical effect on machinability and process predictability. Establishing robust control over these variations requires tracing them to their points of inception within the production sequence. Consequently, this chapter evaluates the process chain with an added focus on the primary upstream stages (i.e., secondary steelmaking, continuous casting and primary forming) in an attempt to identify critical stages that contribute to material inconsistency. Ultimately, identifying these areas of control provides industry with the insights necessary to mitigate batch-to-batch variations, helping standardise and optimise the machining process.

5.1. The steelmaking process

This subsection describes the steelmaking process, with a particular emphasis on its influence on microstructure and non-metallic inclusions. The steelmaking process consists of four main stages: primary steelmaking, secondary steelmaking, continuous casting and primary forming, as shown in Fig. 8. The specific steelmaking process may vary slightly depending on the grade of steel being produced.

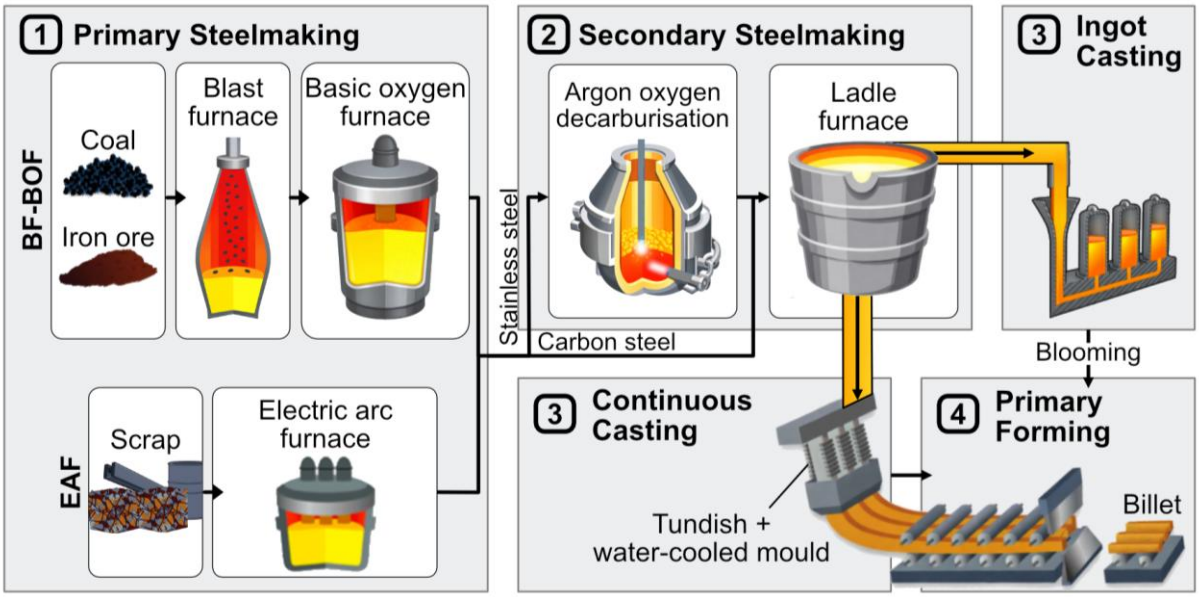

Fig. 8. Schematic representation of the general steelmaking process. Subfigures modified from [168].

5.1.1. Primary steelmaking

The first stage of steel production is primary steelmaking, during which crude steel is produced by converting iron-rich raw materials into liquid steel then removing excess carbon and impurities by oxidation reactions [169]. Primary steelmaking in the metallurgical industry follows two principal routes: the integrated blast furnace-basic oxygen furnace (BF-BOF) route and the electric arc furnace (EAF) route. The BF-BOF

process utilises iron ore and is the dominant production pathway, accounting for approximately 70% of global steel output [170]. The remaining share is predominantly produced via the EAF route, in which recycled steel scrap is melted and subsequently cast. The EAF route is the predominant steelmaking method for the production of stainless steels.

In the production of plain carbon and low-alloy steels, the majority of decarburisation is performed during the primary steelmaking stage, where oxygen is introduced to reduce carbon content in the steel melt. Conversely, for stainless steels, the high concentration of chromium necessitates that decarburisation is conducted in a more controlled environment during the next stage, secondary steelmaking.

5.1.2. Secondary steelmaking

The second stage of production is secondary steelmaking, commonly referred to as ladle metallurgy, during which steel cleanliness and chemical composition are carefully refined. At this stage, alloying element concentrations are precisely adjusted to meet the target steel grade specifications. For the secondary steelmaking of plain carbon and low-alloy steels, the melt is tapped from the BOF or EAF into a ladle furnace, where it undergoes various treatments including deoxidation, calcium treatment, desulphurisation, and alloying [156]. In contrast, the high chromium content of stainless steels necessitates an intermediate refining stage, typically within an Argon Oxygen Decarburisation (AOD) converter. This vessel allows for decarburisation of the stainless steel melt, by controlling the partial pressure of carbon monoxide to prevent the undesirable oxidation of chromium into the slag [156].

A critical risk during these transitions is atmospheric reoxidation, which occurs when the molten stream is exposed to air during transfers – such as from the BOF/EAF to the ladle or the AOD to the ladle. These pours can generate a significant population of large, uncontrolled non-metallic inclusions (NMIs) [156, 171]. Consequently, the tapping process is often considered a critical control point for the formation of NMIs and a primary driver of batch-to-batch variability in the final product.

Once the melt is transferred to the ladle, refining is achieved through various processes such as deoxidation, calcium treatment, desulphurisation, and alloying [156]. These processes also lead to the formation and control of non-metallic inclusions (explained further in the next subsection, see 5.2). For example, an excess of dissolved oxygen in the molten steel promotes the formation of blowholes in the steel ingot [156]; therefore, effective deoxidation is essential. However, the deoxidation of steels with aluminium and titanium leads to the development of hard oxides in the steel matrix, which requires the subsequent calcium treatment of these killed steels [151]. Calcium treatment is often employed to modify the morphology of harder oxide inclusions, such as alumina. The addition of calcium transforms these hard, angular inclusions into softer, lower-melting-point calcium aluminates with a more globular shape, thereby reducing their detrimental effects on tool wear and improving the overall machinability of the steel [156, 172].

Desulphurisation is another crucial process in which a reagent flux is added to the liquid steel, causing sulphur to react and form a slag that can be removed. This stage allows for precise adjustment of the sulphur and manganese concentrations, ensuring a favourable Mn:S ratio. This chemical balancing is essential to guarantee that sulphides precipitate as stable manganese sulphides (MnS) during continuous casting, rather than detrimental, low-melting-point iron sulphides (FeS), which can lead to hot shortness during subsequent thermomechanical processing [173]. From an application perspective, excess sulphur in steels reduces the fracture toughness and hot ductility [174, 175], yet from a machinability perspective, it can have a positive influence by controlling the volume fraction and distribution of beneficial manganese sulphide (MnS) inclusions.

Further, alloying of the steel is performed at this stage, and a summary of relevant alloying elements and their main functions is provided in Table 2 [176].

Table 2. Summary of alloying elements and their primary functions in steels

Element	Function / Influence
Aluminium	Acts as a deoxidiser. Restricts grain growth and promotes a finer grain structure.
Calcium	Enhances machinability by forming stringers, voids, and inclusions; may reduce overall steel strength.
Carbon	Forms steel. Increases hardness and wear resistance.
Chromium	Can form chromium carbides. Improves toughness and wear and corrosion resistance.
Cobalt	Forms cobalt carbides. Enhances heat resistance properties.
Manganese	Increases hardenability. Enhances machinability by forming stringers, voids, and inclusions; may reduce overall steel strength.
Silicon	Acts as a deoxidiser. Increases strength and toughness. Higher concentrations may reduce machinability and worsen surface finish.
Sulphur	Enhances machinability by forming stringers, voids, and inclusions; may reduce overall steel strength.
Titanium	Forms TiC carbides. Restricts grain growth. Can act as a deoxidiser.
Vanadium	Forms vanadium carbides. Restricts grain growth. Improves hardenability.

5.1.3. Continuous casting

Once the steel's chemical composition is refined in secondary metallurgy, casting can be carried out either through continuous casting or ingot casting. In continuous casting, the molten steel is teemed into an intermediate vessel, the tundish, from which it is continuously fed into a water-cooled mould. Solidification begins in the mould and proceeds as the strand is drawn, enabling direct primary forming into semi-finished products such as slabs, blooms, or billets [177]. Ingot casting on the other hand is a batch process where molten steel is poured into individual, stationary moulds to solidify into large blocks [156]. In contrast to traditional ingot casting, where the steel cools slowly in stationary moulds, the rapid cooling rates inherent to continuous casting result in a significantly more refined and uniform microstructure [178].

Casting plays a critical role in determining the final NMI population, as it is the primary birthplace for sulphides and nitrides [179, 180]. In continuous casting, this is mainly

caused by inter-dendritic micro-segregation, in which dissolved substances such as sulphur, nitrogen, and titanium are rejected by the solidifying crystals into the remaining liquid channels [181]. As the concentrations of these solutes increase in the late stages of solidification, their local enrichment in the remaining inter-dendritic liquid exceeds the solubility limits, leading to the precipitation of manganese sulphides (MnS) and cubic titanium nitrides (TiN) [181]. This mechanism of solute rejection also occurs in ingot casting; however, the prolonged solidification time in this type of casting allows for macro-segregation, leading to a much coarser and less homogeneous distribution of precipitates throughout the ingot volume, particularly at the top and centre line of the ingot [178].

The morphology of NMIs is also significantly influenced by this stage, due to the influence of the cooling rate during solidification: slow cooling can cause the inclusions to grow larger and cluster together, while rapid cooling produces smaller, more finely dispersed inclusions [182, 183]. Furthermore, the cooling rate dictates the thermal residence time within specific stability windows, which determines which NMI phases (specifically sulphides and nitrides) have sufficient time to nucleate and grow before the matrix solidifies. Consequently, ingot-cast steels typically exhibit larger inclusion clusters compared to the finer dispersion found in continuously cast billets, owing to their relatively longer cooling times [156, 178].

Conversely, the oxide population – which primarily formed during deoxidation in secondary metallurgy – is influenced by physical entrapment or reoxidation in this stage. Pouring the steel melt into the mould (teeming) can promote reoxidation if exposed to air, leading to the formation of large macro-inclusions (larger than 100 µm) that act as hard spots during machining and may cause sudden tool tip breakage [171]. This risk is often more severe in traditional ingot casting due to the open-stream pouring methods frequently employed, whereas modern continuous casting utilises ceramic shrouding and submerged nozzles to shield the melt from atmospheric oxygen [184].

5.1.4. Primary forming

Primary forming in this case consists of hot rolling, in which the cast billets are plastically deformed at high temperatures (900-1200 °C) in successive rolling stands to produce round steel bars of the required diameter [177]. Primary forming differs slightly between continuous-cast and ingot-cast steels. Although continuous-cast billets are often ready for hot rolling, ingot-cast steels must first undergo an additional primary breakdown stage known as blooming. This energy-intensive process is necessary to reduce the large cross-section of the ingot and apply the heavy deformation required to refine its coarse, as-cast structure and close internal porosity. Once reduced to the dimensions of a bloom or slab, the steel can then proceed to the final hot-rolling stands to produce the required bar profiles.

After casting, billets are sent to primary forming either via cold charging or hot charging routes. In the cold charging route, the cast billets are cooled to room temperature for inspection before being hot rolled. For micro-alloyed steels like C38, this sequence induces a double phase transformation (austenite to ferrite/pearlite and back to austenite upon reheating), which inherently refines the grain structure [185]. Generally, the faster

the steel is heated and cooled during this double transformation, the finer the final grain structure will be – an important control point to ensure microstructural consistency between batches. In the hot charging route, the solidified cast billet is directly transferred to the rolling mill while still at elevated temperatures. While more energy-efficient, this route requires sufficiently aggressive rolling deformation to mechanically break down the coarse, irregular as-cast austenitic grains that persist from the solidification process.

While primary forming does not alter the bulk chemical composition, it is critical in defining the steel's microstructure. The process mechanically breaks down larger austenitic grains, triggering dynamic recrystallisation where new, finer grains nucleate and grow [185]. Although morphologically equiaxed, these grains may still exhibit a preferred crystallographic orientation (rolling texture) associated with the rolling direction. The subsequent rate of cooling immediately after hot working strongly influences the phases that form – such as pearlite, ferrite, or martensite – and their respective grain sizes. Slow cooling enables diffusion-controlled transformations, promoting the formation of ferrite and pearlite with relatively coarse interlamellar spacing and colony size [161]. In carbon steels, such coarse pearlite is often beneficial for machinability due to its lower hardness and reduced resistance to chip formation. Conversely, rapid cooling or quenching suppresses diffusional transformations and promotes the formation of martensite, a body-centred phase characterised by high hardness and fine lath or plate substructure [161]. Controlled cooling techniques allow for the precise regulation of these phase constituents to ensure the steel achieves its required properties. The resulting microstructure then serves as the basis for any subsequent forming processes, such as forging, or subsequent heat treatments (see Section 5.3).

In addition to the microstructure, primary forming also plays a significant role in determining the morphology of the non-metallic inclusions. The characteristic deformation behaviours of various NMIs during hot rolling are illustrated in Fig. 9(a). In fact, these behaviours during hot rolling may be indicative of the general behaviour of these NMIs during machining. During hot rolling, relatively soft inclusions such as MnS are plastically deformed and elongated into stringers aligned with the rolling direction [186]. During machining, these elongated inclusions can act as internal lubricants and promote chip breakability during machining; however, their effect depends on orientation [187, 188]. Owing to their negligible plasticity, harder inclusions such as nitrides and oxides remain essentially non-deformable during the hot rolling process. Instead of elongating with the steel matrix, these inclusions typically undergo brittle fragmentation (i.e. shattering and dispersing along the rolling direction) or retain their original morphology while inducing the formation of micro-voids at the inclusion-matrix interface. This phenomenon, often referred to as interfacial decohesion, results from the significant kinematic mismatch between the rigid inclusion and the flowing steel. Mixed inclusions, such as oxysulphides, demonstrate heterogeneous deformation behaviour; the ductile manganese sulphide (MnS) shell undergoes plastic elongation, while the rigid oxide core – typically consisting of alumina or silicates – either undergoes rearrangement or brittle fragmentation. This depends on the thickness of the sulphide layer and the local stress concentrations at the

oxide-sulphide interface during rolling. Clusters of NMIs are generally fragmented and rearranged along the rolling direction.

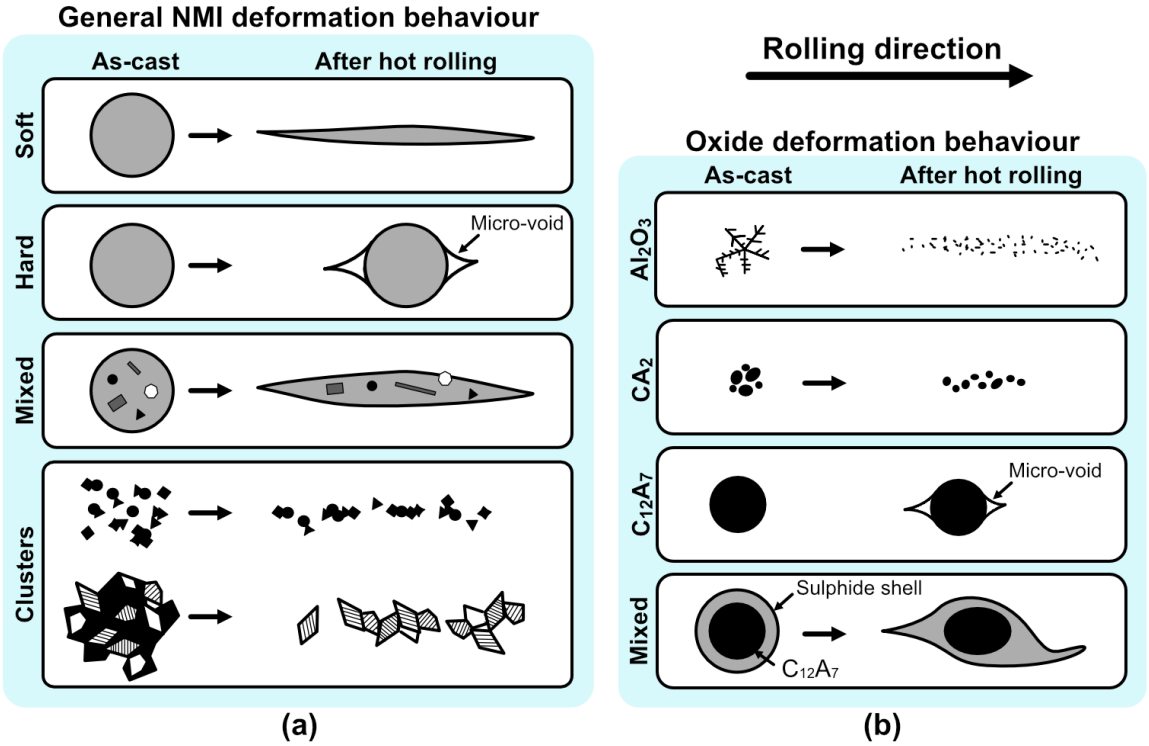

Fig. 9. General deformation behaviour of (a) soft, hard, mixed and clustered NMIs and (b) common oxide groups during hot rolling. (a) is recreated from [148] and (b) is recreated from [189].

As shown in Fig. 9(b), pure alumina Al_2O_3 inclusions exhibit brittle behaviour, undergoing fragmentation and dispersion along the rolling direction [189]. These fragmented particles remain highly abrasive, leading to significant abrasive wear on tool surfaces during subsequent machining operations. Similarly, calcium-aluminate phases with high alumina content, such as CA_2, retain substantial hardness at forging temperatures and consequently undergo similar fragmentation and dispersal [189]. In contrast, calcium-rich oxides like $C_{12}A_7$ are typically softer and exhibit higher plasticity. Rather than fracturing, these inclusions tend to promote the formation of micro-voids at the matrix-inclusion interface [189]. These voids can serve as critical crack initiation sites, potentially enhancing chip breakability during metal cutting. Mixed oxysulphides represent a complex case where the inclusion morphology is determined by the interaction between the constituents. Typically, the ductile sulphide shell undergoes significant elongation along the flow lines, whereas the harder oxide core is shielded, resulting in minimal deformation.

5.2. Control of NMIs during steelmaking

The control of non-metallic inclusions during steelmaking represents a compromise between enhancing machinability and preserving the functional performance of the steel. In fact, improvements in steelmaking over the past century have led to steel grade developments with remarkably low levels of impurities or inclusions. These steel grades have been labelled as “clean” steels, and offer notable improvements in their mechanical properties, including fatigue strength and impact toughness. However, the improvement

in their mechanical properties has come at the expense of their machinability. Machining these clean steels is generally accompanied by increased cutting forces, high power consumption, accelerated tool wear and high manufacturing costs [14]. Because of the technological challenges associated with developing these clean grades of steels, metallurgists have instead focused on tailoring the inclusions within steels to enhance machinability as an alternative to removing them. These steels have since become known as “free-machining” steels. Historically, lead (Pb) was added to these grades to improve their machinability, but its use is now rare due to environmental regulations and health concerns. Consequently, other alloying elements, such as sulphur, have become more prevalent alternatives in modern metallurgy to develop machinability-enhanced steels.

It is important to emphasise that, although machinability is a relevant consideration in modern metallurgy (especially from a machinist’s perspective), the ultimate and overriding priority from a holistic view is to achieve the required functional performance of the finished product.

5.2.1. Origin of NMIs

The appropriate control strategy for non-metallic inclusions depends on whether they are endogenous or exogenous in origin. This classification was introduced by Sims [190] and Forgeng [191], who grouped NMIs according to their origin during steelmaking and casting.

Endogenous non-metallic inclusions are the products of precipitation reactions within the molten steel or during its subsequent solidification [136]. In the ladle, inclusion formation is primarily driven by chemical supersaturation following the addition of deoxidisers. In contrast, those forming within the casting mould are driven by two distinct factors [156]. Firstly, the continuous decrease in temperature shifts chemical equilibria, reducing the solubility of oxygen, sulphur, and nitrogen and favouring the formation of oxides, sulphides, and nitrides [192]. Secondly, during cooling, the solid phase exhibits significantly lower solubility for these solute elements than the liquid, leading to solute partitioning at the solid-liquid interface [192]. This micro-segregation enriches the remaining inter-dendritic liquid, generating local supersaturation conditions that promote inclusion precipitation, often concentrated between growing dendritic branches [192].

The majority of nitrides and sulphides are endogenous, primarily originating during the solidification stage of continuous casting [193]. Due to their higher thermodynamic stability, nitrides such as TiN begin to precipitate at higher temperatures during the early stages of the solidification [190]. This provides a longer window for diffusion-led growth, resulting in the characteristic large, cubic morphologies. Abrasive sub-micron nitrides can also form in the solid steel during later stages of cooling depending on the cooling rate [194]. In contrast to nitrides, sulphides (MnS) typically have higher solubility in the melt and only precipitate during the final stages of solidification when the remaining liquid is heavily enriched with sulphur due to micro-segregation [190]. This late-stage formation, combined with the rapidly decreasing temperature, limits their growth window and typically results in a smaller, more finely dispersed initial population compared to nitrides.

Exogenous inclusions, on the other hand, are primarily oxides that arise from two principal sources. The first involves mechanical and chemical erosion of refractories in contact with the molten steel, such as ladle linings, tundish materials, and nozzles [195]. Specifically, any degraded refractory particles become entrained in the steel melt and typically display irregular morphology and composition. According to Pickering [195], the erosion of silicate refractories, followed by reactions with primary deoxidation products, gave rise to most of the troublesome inclusions, especially oxides and oxysulphides. The second source of exogenous inclusions is oxygen pickup during pouring or transfer. The exposure of the teeming stream to air promotes oxide formation through reactions with alloying elements, resulting in oxide clusters that deteriorate steel cleanliness [195]. McLean and Somerville [9] reported that macro-inclusions exceeding 100 μm frequently originate from reoxidation of the steel stream during teeming. Such reoxidation products are often enriched in comparatively low-stability oxides, including FeO and MnO, despite their large size. Similar observations have been documented by numerous researchers [156, 173, 196]. Comprehensive descriptions of the various sources of exogenous inclusions formed during steelmaking, along with their key elements, have been provided by Kiessling [197], as summarised in Table 3.

Table 3. Sources of exogeneous NMIs during steelmaking.

Stage	Source	Key element(s)
Furnace	Furnace slags	Ca
	Furnace refractories	Ca
	Ferroalloys	Cr, Al, Si
Tapping	Launder refractories	Mg, Ti, K
	Reoxidation	FeO, MnO
Ladle	Deoxidation	-
	Ladle slag	Ca, Mg
	Ladle refractories	Mg, Ti, K
Teeming	Stopper and nozzle refractories	Mg, Ti, K
	Reoxidation	FeO, MnO
	Deoxidation	-
Ingot mould	Refractories	Mg, Ti, K
	Deoxidation	-

In fact, inclusions rarely maintain their initial composition throughout steelmaking. Pre-existing inclusions can serve as heterogeneous nucleation sites for subsequent precipitation reactions, frequently resulting in complex oxide-sulphide mixed inclusions. Scanning electron microscopy combined with energy-dispersive X-ray spectroscopy (SEM/EDS) has demonstrated that many inclusions exhibit compositional heterogeneity. In numerous cases, inclusions possess a core-shell morphology, where the core consists of one phase and the outer layer of another. Representative examples include the sequential formation of alumina, galaxite, and manganese aluminosilicate during reoxidation of aluminium-killed steel, as well as the formation of CaS coatings on calcium

aluminate particles in calcium-treated aluminium-killed steel. Silicate inclusions may likewise display significant compositional variation from centre to periphery.

5.2.2. Strategies for NMI control

Given the various origins of NMIs, control strategies are implemented across the entire production chain to ensure steel cleanliness. To address the formation of endogenous inclusions, primary emphasis is placed on deoxidation and desulphurisation practices during secondary metallurgy. Optimisation of deoxidiser type and addition sequence, together with precise control of oxygen activity, can minimise the formation of undesirable oxides. Another key strategy for NMI control involves the removal of detrimental inclusions from the molten steel. The physical removal of existing NMIs is facilitated by gas stirring (argon purging) and vacuum degassing, which promote the flotation of inclusions to the surface slag layer through buoyancy. In cases where inclusions cannot be entirely eliminated, inclusion engineering, such as calcium treatment, is commonly employed as a modification strategy.

To mitigate exogenous NMI sources, control strategies focus on process cleanliness and containment. These include the use of high-quality, erosion-resistant refractories for ladle linings, as well as optimised tundish fluxes and mould powders designed to limit reoxidation and promote the absorption of rising inclusions. In addition, protection of the steel stream during transfer and casting – through shrouding, inert gas protection, or fully enclosed pouring systems – is essential to minimise reoxidation.

The selection of control strategies – whether to promote formation, facilitate removal, or enable modification of NMIs – is further tailored to the type of NMI as well as the intended application of the final component.

Control of sulphides

While elongated MnS inclusions have been shown to aid machinability, this type of morphology introduces severe mechanical anisotropy in the steel which can lead to its premature and catastrophic failure during the component's service life. Consequently, the control strategy for sulphides during steelmaking often prioritises the elimination of large inclusions and formation of small, globular sulphides characterised by limited relative plasticity [198].

The composition and morphology of sulphides is governed by the various stages of steelmaking. In particular, the morphology of sulphide inclusions is governed by their relative plasticity, alongside specific thermomechanical processing parameters [148]. Consequently, effective control of the final sulphide morphology after steelmaking requires considerations of its multiple stages: first, increasing sulphide hardness via alloying or chemical treatments (such as Ca-treatment) during secondary steelmaking, which increases its relative plasticity; second, regulating cooling rates during continuous casting to prevent the formation of large NMI clusters; and finally, optimising temperatures and reduction ratios during primary forming to manage the steel matrix's microstructure and hardness and thereby the relative plasticity [148]. However, these methods must be

carefully calibrated to avoid industrial complications such as nozzle clogging during casting or undesirable alterations to the final steel microstructure.

Control of oxides

The control of oxide inclusions, particularly in aluminium-killed steels, primarily revolves around process optimisation following calcium treatment. Standard strategies focus on the removal of large-scale modified inclusions through refined secondary metallurgy, such as extending the argon soft-blowing duration and optimizing the timing of calcium addition [199, 200]. While calcium treatment is designed to modify solid alumina Al_2O_3 into lower-melting-point calcium aluminates to prevent nozzle clogging, it introduces a trade-off regarding deformability. Research indicates that well-modified, plastic calcium aluminates can, during rolling, elongate into undesirable "stringers" that introduce anisotropy if they exceed 20 µm in original size [199, 201]. To counteract this, some strategies propose "incomplete" calcium treatment to maintain a higher melting point and brittle nature, thereby preventing elongation [148]. However, this approach must be managed with extreme caution, as high-melting-point inclusions are more difficult to remove from the melt and increase the risk of nozzle clogging.

The control of silicate inclusions is predominantly focused on chemical composition rather than rolling parameters alone. Since the plasticity of silicates is largely governed by their SiO_2 content, as discussed previously, the target composition is typically selected based on the intended application. Control of silicate deformation should be considered in conjunction with the intended rolling temperature. When the temperature is below the brittle-plastic transition, the inclusion's deformation is inversely proportional to its Young's modulus [148]. At higher temperatures, deformation is influenced by the silicate's melting point and is inversely proportional to its viscosity [148].

5.3. Further deformation and heat treatments

After the steelmaking process is complete, the steel – typically in the form of billets or blooms – can undergo a series of mechanical and thermal stages to achieve its desired properties before final machining. These stages are often distributed across several facilities, moving from the steel mill to specialised forging plants, and finally to the manufacturing facility, such as car and truck producers. The sequence of these operations is vital because it determines both the final microstructure of the steel matrix and the population of the non-metallic inclusions.

After primary forming, the steel may be subject to further bulk deformation, such as forging. Forging is a solid-state process usually performed at high temperatures (hot forging), where metal is shaped using localised compressive forces. During hot forging, the application of intense, multi-directional compressive forces at elevated temperatures triggers dynamic recrystallisation. This process ensures that the coarse, relatively elongated primary grains are replaced by a new population of significantly smaller, equiaxed grains [114]. This fundamental grain refinement is the primary reason forged components exhibit superior toughness; the process effectively reduces the grain size and mitigates the structural heterogeneities inherent in as-cast or primary-rolled steel.

Similar to the influence of primary forming on the NMI population, the specific influence of forging on inclusion morphology is determined by their relative plasticity at forging temperatures [197]. Generally, soft manganese sulphides are elongated into high-aspect-ratio stringers, whereas brittle inclusions like alumina or titanium nitrides remain undeformed or fragment into smaller, isolated particles [190, 197].

In most cases, the steel undergoes subsequent thermal processing to tailor its machinability or final engineering properties. By heating the steel above critical phase transformation temperatures, the existing microstructural constituents are redistributed or transformed into new microstructures, such as pearlite, ferrite, bainite, or martensite, depending on the cooling rate and alloy chemistry. The choice of treatment dictates microstructural features such as grain size and hardness, which directly impact cutting forces. For instance, annealing involves heating the steel above the critical temperature followed by controlled slow cooling to form a coarse pearlitic-ferritic microstructure that is beneficial to machinability. Alternatively, normalising involves holding the steel above its critical temperature then air cooling it to produce a more refined and uniform grain structure. In medium-carbon steels, normalising leads to grain refinement and removal of coarse pearlite or ferrite bands, which may influence machinability. In stainless steels, solution annealing is performed to retain alloying elements in solid solution, preventing the formation of hard grain-boundary carbides that can promote corrosion, act as abrasive sites, and increase tool wear during machining.

While heat treatments strongly influence the steel matrix and its microstructure, their effect on non-metallic inclusions is comparatively limited. Heat treatments do not have a major effect on the size and distribution of NMIs in the steel matrix [202]. Since standard heat treatments do not reach the temperatures required to induce plasticity in these inclusions, their shapes remain unchanged in the absence of mechanical deformation [202]. The interaction between the heat treatment and NMIs is primarily indirect, manifesting in two ways. First, changes in the matrix properties and differences in thermal contraction during cooling may generate interfacial stresses, potentially leading to micro-void formation at the matrix-inclusion boundary. Second, diffusion across the NMI-matrix boundary may lead to compositional changes in the inclusions. For example, Liu et al. [202] reported that increasing the heat treatment temperature resulted in higher Mn contents and lower Ca contents in sulphide and oxide inclusions, particularly in smaller particles such as CaS, MgO-Al_2O_3-CaO-CaS and MgO-Al_2O_3-CaO inclusions. It is also noteworthy that manganese sulphides can undergo minor spheroidisation during prolonged high-temperature soaking to reduce their surface energy [203].

6. Experimental details and analysis techniques

In this chapter, the investigated workpiece materials and the cutting tools used in the machining tests are presented. The characterisation techniques and analytical methods are also described.

6.1. Workpiece materials

The workpiece materials selected for machinability investigation are categorised into two broad groups based on their metallurgical classifications and industrial applications. The first group comprises low-alloy engineering steels, specifically (1) a medium-carbon micro-alloyed C38 steel (Paper B), (2) a 20MnCrS5 case-hardening steel (Paper C), and (3) a 100Cr6 high-carbon bearing steel (Paper E). The second group consists of a diverse range of (4) stainless steels (Paper D), including ferritic, martensitic, austenitic, super austenitic, duplex and super duplex grades. The details related to the steelmaking of these various materials are summarised in Table 4. Due to confidentiality, the details related to the secondary steelmaking are not included.

Table 4. Steelmaking and heat treatment details related to the various investigated materials (pre-machining). For heat treatments, CC: controlled cooling, A: annealing, SA: solution annealing, QT: quenched and tempered.

Class	Material	Primary steelmaking		Casting		Heat treatments
		BF-BOF	EAF	Continuous	Ingot	
Low-alloy steels	C38	✓		✓		CC
	20MnCrS5		✓	✓		CC
	100Cr6		✓		✓	CC
Stainless steels	Ferritic		✓	✓		A
	Martensitic		✓	✓		QT
	Austenitic		✓	✓		SA
	Super austenitic		✓	✓		SA
	Duplex		✓	✓		SA
	Super duplex		✓	✓		SA

6.1.1. C38 micro-alloyed steel

C38 is a medium-carbon steel utilised for components requiring high fatigue strength within high-volume production environments. Typical applications include connecting rods, axle stubs, and crankshafts – the latter being the specific application for the material investigated in this work. C38 grade is categorised as a low-alloy steel due to its total alloying content remaining below 5%. In this case, it is classified as micro-alloyed due to additions of vanadium and nitrogen which, despite their relatively low concentration, fundamentally alter the grain structure and mechanical properties through precipitation hardening. C38 possesses a ferrite-pearlite matrix achieved through controlled cooling. For this study, two distinct batches of vanadium-micro-alloyed C38 were investigated in their as-received condition. These batches were sourced from the same supplier at different intervals, representing two separate melts (heats). The difference in machinability of these two batches is described in Paper B.

6.1.2. 20MnCrS5 case hardening steel

The second material investigated in this work is a 20MnCrS5, a low-carbon alloy steel specifically engineered for case-hardening applications. The material was machined in its soft state, with a fully pearlitic-ferritic microstructure. Typically, these case hardening steels are further subject to induction hardening, a process utilised to create a high-strength, wear-resistant martensitic surface layer while preserving a relatively ductile and tough ferrite-pearlite core. This combination of properties is essential for gear components that must withstand high surface contact pressures and cyclic loading without brittle failure. The machinability of four distinct batches of this material (in soft state) was evaluated; two batches were subjected to controlled laboratory cutting tests, while the remaining two were machined within an industrial production environment. This comparative investigation is described in Paper C.

6.1.3. 100Cr6 bearing steel

Another material examined in this research is 100Cr6, a high-carbon chromium alloy steel widely used in the manufacture of rolling-element bearings due to its high fatigue strength and wear resistance. For this study, the material was investigated in an unspheroidised, pearlitic state, characterised by the presence of cementite along the grain boundaries. The investigation involved two nominally identical batches of 100Cr6. These batches were subjected to cutting tests using four different tool grades to assess the interaction between the material's microstructural constituents and various tool coatings and substrates. The methodology and findings regarding the performance of these tool-material combinations are presented in Paper E.

6.1.4. Stainless steels

The fourth group of materials examined comprises various stainless steel families, specifically ferritic, martensitic, austenitic, super austenitic, duplex, and super duplex grades. The machinability of these materials was investigated and compared across a range of cutting conditions. These studies are described in Paper D.

Ferritic

Ferritic stainless steels are primarily alloyed with chromium (typically 10.5% to 27%) and possess a body-centred cubic (BCC) crystal structure that remains stable at all temperatures. Their microstructure consists of ferrite grains, often containing fine carbide precipitates, which provide moderate corrosion resistance and excellent resistance to stress corrosion cracking. These steels are commonly utilised in automotive exhaust systems and kitchenware. While they generally cannot be hardened by heat treatment, they undergo annealing to relieve internal stresses and improve ductility following cold working.

Martensitic

Martensitic stainless steels are high-carbon, chromium steels that can be heat treated to achieve high levels of strength and hardness. Their microstructure is transformed from austenite to a distorted body-centred tetragonal (BCT) martensitic lattice through rapid

quenching. This high-strength steel is subject to a tempering cycle to balance hardness with toughness, making it ideal for applications requiring high wear resistance and edge retention, such as surgical instruments, turbine blades, and cutlery.

Austenitic and super austenitic

Austenitic stainless steels are the most widely used category, containing high levels of chromium and nickel to stabilise the face-centred cubic (FCC) austenite phase at room temperature. Their microstructure consists of equiaxed austenite grains with annealing twins, providing excellent ductility, toughness, and corrosion resistance. This makes them suitable for chemical, food processing, and pharmaceutical applications. Super austenitic stainless steels are highly alloyed variants with increased molybdenum and nitrogen content to improve resistance to pitting and crevice corrosion in aggressive chloride environments. Although fully austenitic, their microstructure is more highly strained due to the elevated alloying levels, and they are typically used in demanding applications such as seawater heat exchangers and desalination plants. Both grades require controlled solution annealing to retain alloying elements in solid solution and prevent intergranular carbide precipitation.

Duplex and super duplex

Duplex stainless steels exhibit a balanced dual-phase microstructure of approximately equal proportions of austenite and ferrite, combining the stress corrosion cracking resistance of ferritic grades with the toughness of austenitic steels. They are commonly used in the oil and gas industry and in marine structural applications, with performance strongly dependent on maintaining the 50/50 phase balance through controlled solution annealing and appropriate cooling rates to prevent brittle intermetallic phases such as sigma (σ). Super duplex stainless steels contain higher levels of chromium, molybdenum, and nitrogen, resulting in a refined dual-phase structure that provides exceptional strength and corrosion resistance in highly acidic or saline environments, such as subsea manifolds and chemical processing equipment. Owing to their high alloy content, super duplex grades are highly sensitive to thermal history and require strict solution annealing procedures to avoid rapid secondary phase formation, which can cause embrittlement and reduced machinability.

6.2. Workpiece characterisation

The workpieces were characterised following the procedure summarised in Fig. 10. Three metallographic samples per batch were cut using a Struers cutting machine and hot-mounted in conductive Struers PolyFast bakelite with the transverse surface exposed. Samples were then sequentially polished using a Struers TegraPol with 9, 3, and 1 µm diamond suspensions. Two samples were then ready for direct characterisation, while the third was etched to reveal the microstructure. Low-alloy steels were etched with 2% Nital for approximately 10 s each, while stainless steels underwent electrochemical etching in 10% oxalic acid for times varying per grade.

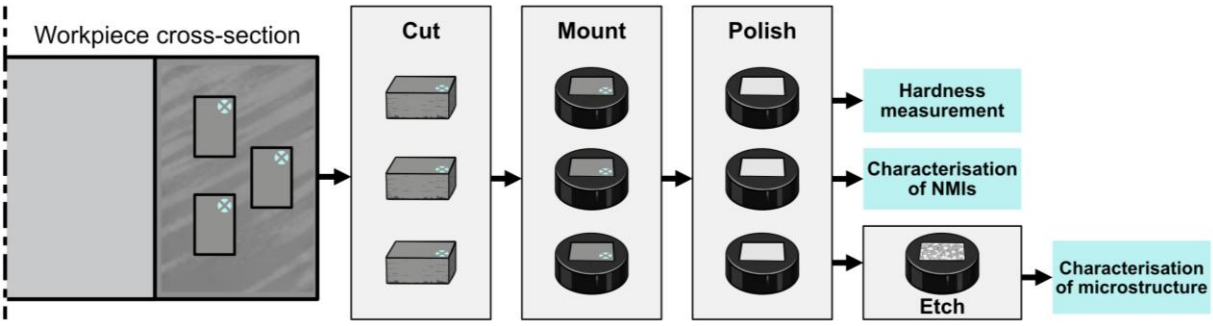

Fig. 10. Schematic depicting the process of workpiece material characterisation adopted in this work.

Once the samples were ready, the characterisation of the workpiece materials was conducted using multiple microscopes, detectors, and testing instruments, as detailed below:

- Scanning electron microscopy (SEM) was performed using the Zeiss Gemini 450 FEG-SEM.
- Energy-dispersive X-ray spectroscopy (EDS) was carried out using the Oxford Ultim Max 100 silicon drift detector mounted on the Gemini 450 FEG-SEM.
- Light optical microscopy (LOM) was performed using the Leitz DRMX microscope.
- Automated hardness testing for each sample was conducted using the Struers DuraScan-70 G5.

6.2.1. Microstructure characterisation

Depending on the material, the relevant microstructural features were then characterised. For materials exhibiting dual-phase microstructures, the area fraction of each phase was quantified using light optical microscopy. Micrographs covering a minimum surface area of 4.0 mm^2 per sample were acquired in an unbiased manner at 50× magnification. The area fraction analysis was subsequently performed using MATLAB image processing (versions R2020b and R2025a). The micrographs were converted to grayscale, contrast-enhanced, then binarised using an individually selected global threshold to ensure accurate phase distinction, as shown in Fig. 11. Accordingly, the area fraction of ferrite (A_F) was calculated as the ratio of ferritic pixels (P_F, pixels with a value of 1) to the total number of pixels (P_T) in the processed image.

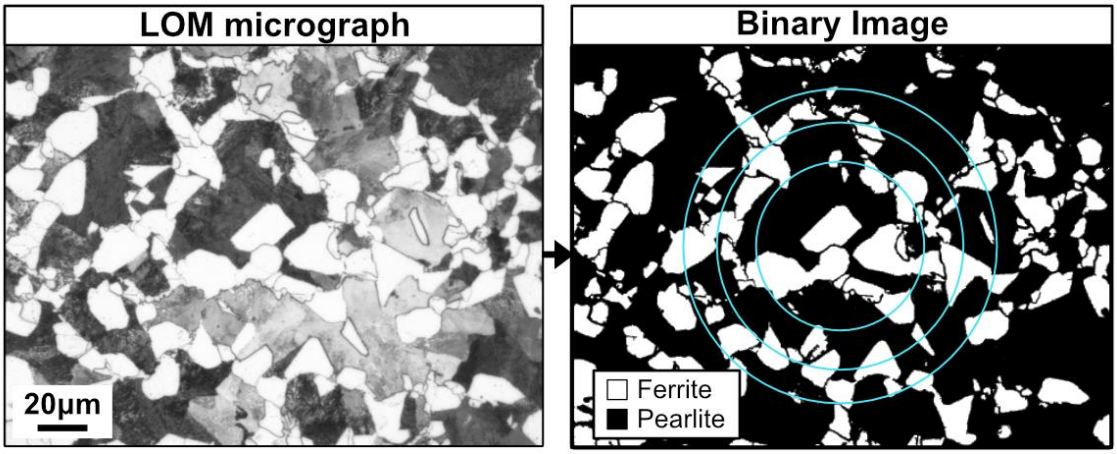

Fig. 11. Conversion of LOM micrographs to binary for the quantification of microstructural phases.

It is well established that the area fraction and volume fraction of microstructural constituents may be considered equivalent when the two-dimensional measurements are obtained from a statistically representative surface area [204]. Therefore, it is assumed that the measured area fractions correspond to the volume fractions of the respective microstructures.

The average grain size was determined from the binary images in accordance with ASTM E112 using the intercept method for multiphase specimens. The images were then converted to uint8 type, where three concentric circles were superimposed (Fig. 11). The number of intersections with ferritic grains was then automatically calculated by image subtraction and connected component analysis. With the number of intersections (N_α), the total test line length C_α (defined as the sum of the circumferences of the three inserted circles), the optical magnification M_α, and the ferrite area fraction A_F, the mean intercept length of the ferrite grains L_α was calculated as follows,

$$L_\alpha = \frac{A_F(C_\alpha/M_\alpha)}{N_\alpha} \tag{5}$$

Once the mean intercept length of the ferritic grains was determined, the average grain size was interpolated. In a similar manner, the mean true lamellar spacing of the pearlitic colonies was characterised by superimposing a circular test grid of diameter (D_c) onto the microstructure and counting the intersections between the cementite lamellae and the grid. A circular test grid was employed instead of a linear grid in order to minimise the influence of the sectioning plane effect, which may otherwise reduce the accuracy of the measurements [205]. Rather than LOM micrographs, high-magnification SEM images were acquired from etched specimens using the secondary electron (SE) detector and subsequently binarised following the methodology described previously. The circular grids were then positioned in an unbiased manner, and the number of intersections with the cementite lamellae (N_P) was recorded, as illustrated in Fig. 12. The lamellar mean true spacing (σ_t) was then calculated as follows:

$$\sigma_r = \frac{\pi D_c}{2N_P} \tag{6}$$

For each sample, at least 60 distinct pearlite colonies distributed across the entire specimen surface were characterised to ensure a representative determination of the mean true lamellar spacing.

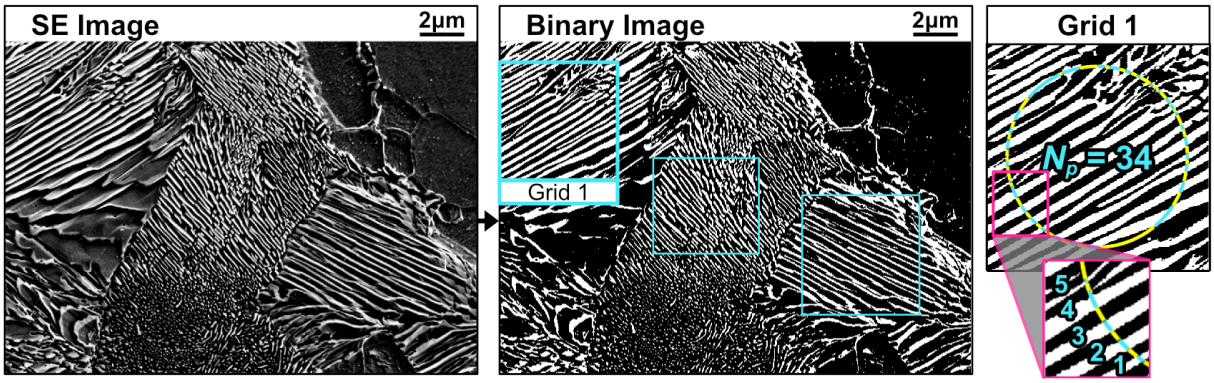

Fig. 12. Process used for determining the mean true lamellar spacing with help of an inserted grid.

6.2.2. Characterisation of non-metallic inclusions

To obtain a representative characterisation of the non-metallic inclusions in the materials, automated feature analysis combined with EDS was conducted using the Oxford AZtecSteel® software. The feature analysis module identifies NMIs based on colour contrast within the steel matrix in the backscatter electron (BSE) image, and EDS is subsequently performed on each detected inclusion to determine its chemical composition. This allows each inclusion to be assigned to its appropriate class – oxides, sulphides, nitrides, or oxysulphides – with further subclassification where applicable. For example, sulphides are subdivided into MnS or (Mn,Ca)S. A brief visual overview of this procedure is provided in Fig. 13.

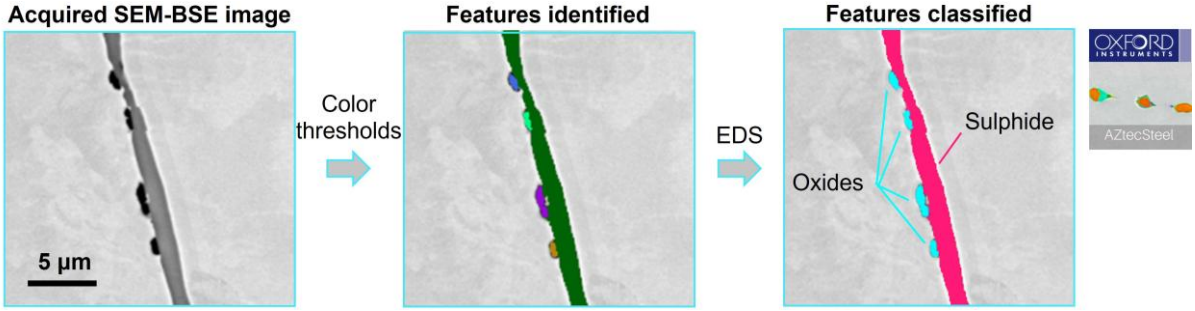

Fig. 13. Visualisation of the feature analysis algorithm employed for NMI characterisation.

The adopted classification scheme depends on the material type. For low-alloy steels, the built-in "high quality steel" scheme was used, whereas stainless steels were classified according to the built-in "inclusion clean steel" scheme. In both cases, inclusions are assigned to a class and subclass only if they satisfy the specific criteria for that category. For example, an inclusion is classified as a "sulphide" if its sulphur content exceeds a defined weight-percentage threshold. To determine the appropriate subclass, the weight percentages of other relevant elements, such as manganese and calcium, are evaluated. Based on these values, the inclusion is then assigned either to the MnS subclass or the (Mn,Ca)S subclass. This methodology enables the calculation of the area fraction for each inclusion class and subclass, as reported in Papers B-E. Similar to microstructural area fractions, the measured area fraction of a given NMI class can be considered equal to its true volume fraction if a statistically representative area is analysed [206, 207].

6.2.3. Hardness measurements

The hardness profile was measured along the radial direction of the workpieces using the Struers DuraScan-70 G5 hardness tester, according to ASTM standard E92. Several measurements were made at each location along the radial direction for statistical accuracy. For the C38 (Paper B) and 100Cr6 (Paper E) materials, the Vickers hardness method with an HV10 indent was used. For the 20MnCrS5 (Paper C) and stainless steels (Paper D), an HV5 indent was used instead.

6.3. Machining tests

6.3.1. Experimental details

The laboratory machining tests were carried out on a CNC-lathe (EMCO TURN 365) mounted with a three-component dynamometer (Kistler 9257A) for force measurements.

In particular, Fig. 14 shows the experimental setup used for the machining of micro-alloyed C38 steel in Paper B. The tool configuration varied depending on whether the cutting operation was longitudinal turning or facing.

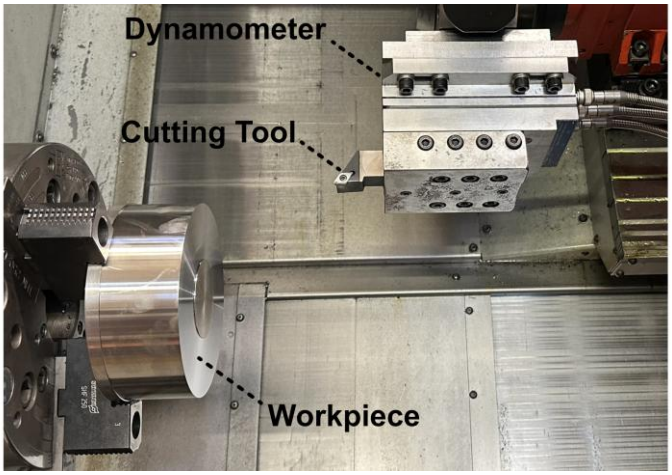

Fig. 14. Experimental setup used for machining in Paper B.

The cutting conditions and detailed parameters for each test are summarised in Table 5. The setting specifies whether the experiments were conducted in the laboratory or on industrial production lines. In contrast to the other cutting tests which were all conducted under dry cutting conditions, the machining of stainless steels (Paper D) was conducted under wet conditions using a cutting fluid with a 6% oil concentration. The end-of-test criterion denotes the condition at which the tools were examined, defined either by a specified spiral cutting length (SCL) or by the number of workpieces machined.

Table 5. Summary of cutting conditions used in machining tests

	Paper B C38	**Paper C** 20MnCrS5			**Paper D** Stainless steels	**Paper E** 100Cr6
Setting	Lab	Lab	Industry		Lab	Lab
Turning	Facing	Longitudinal	Profile	Internal	Longitudinal	Facing
Cooling	Dry	Dry	Dry	Dry	Wet	Dry
V_c [m/min]	300, 400, 500	300, 400, 500	330	330	150	200
f [mm/rev]	0.1	0.1	0.5	0.4	0.25	0.1
a_p [mm]	1	1	1.12	0.67	1.5	1.5
End of test	SCL 1200m	SCL 1200m	WPC 120	WPC 220	SCL 1500m	SCL 2000m
Insert geometry	DCMT111T304	DCMT111T304	WNMG080412		CNMG120408	CNMG120408
Chip breaker	M3	M3	M6		MM	M3
Grade	TP2501	TP2501	TP1500		GC2025, 2220	G1, G2

The insert grades were also varied to evaluate their influence on machinability, particularly in Papers D and E. In Paper D, two grades were investigated: GC2025 and GC2220. The differences between these grades relate to both the substrate and the coating system, as detailed in Table 6. In Paper E, four custom-made grades were examined, designated G01, G02, G03, and G04 (Table 6). Notably, these grades shared the same substrate, with variations introduced in the coatings. To minimise extraneous sources of variation, the tools' edge radii were measured prior to the cutting tests, and tools with the smallest variation were selected. Furthermore, the cutting conditions were kept constant in all

comparisons, and all compared cutting tools were used under identical cooling-lubrication strategies.

Table 6. Details of tool grades used in Papers D and E, including substrate and coating properties

		Paper D		Paper E	
	Tool grade	GC2025	GC2220	G1	G2
Substrate	Composition	WC-Co	WC-Co	WC-Co with γ-phase (TiC, TaC, NbC)	
	Cobalt content	14.5 vol%	13.8 vol%	5.5 wt%	
	Hardness [kg/mm^2]	1350 HV3	1400 HV3	1570 HV10	
	Grain size [µm]	1	0.96	2.2	
Inner coating	Composition	Ti(C,N)	Ti(C,N)	-	Ti(C,N)
	Thickness [µm]	2.5	3	-	2
Outer coating	Composition	alternating κ-Al_2O_3-TiN	α-Al_2O_3	Ti(C,N)	α-Al_2O_3
	Thickness [µm]	2	2.5	10	8

6.4. Characterisation of the cutting tools

Following the cutting experiments, the cutting tools were subjected to characterisation using advanced microscopy and compositional analysis techniques, as shown in Fig. 16. Tool wear types and underlying wear mechanisms were examined by means of BSE and SE imaging using the Zeiss Gemini 450 FEG-SEM. Surface chemical composition was analysed using EDS. To further elucidate coating degradation, selected tools were chemically etched in hydrochloric acid (HCl) at 60 °C for 3 h in order to dissolve adhered workpiece material. This procedure enabled clearer assessment of coating degradation that would otherwise be obscured by material adhesion (Paper D).

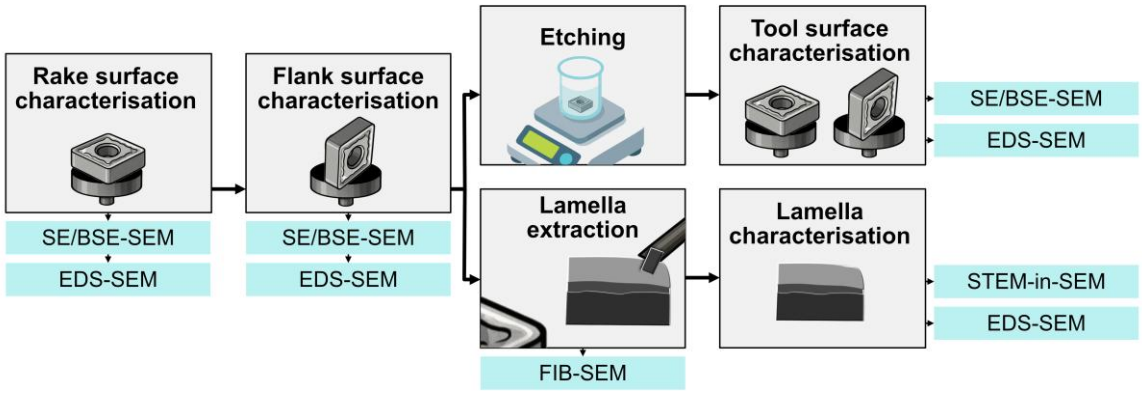

Fig. 15. Characterisation procedure applied to the cutting tools following the cutting experiments.

Specimen preparation for tribo-layer analysis was carried out by producing cross-sectional lamellae using a focused ion beam (FIB) on a dual-beam FEI Versa 3D system (Paper E). The thinned lamellae were subsequently characterised in scanning transmission electron microscopy (STEM-in-SEM) and analysed chemically by EDS using the Zeiss Gemini 450 equipped with a bright-field annular STEM (aSTEM) detector. Analyses were performed at 30 kV accelerating voltage and 500 pA probe current.

7. Summary of appended papers

This chapter summarises and discusses the principal findings presented in the appended papers. Section 7.1 addresses RQ1 by outlining the results obtained from the modification of the semi-analytical models for temperature prediction at the tool-chip interface (Paper A). Section 7.2 addresses RQ2 by presenting the machinability variations observed in different batches of the various workpiece materials and identifying the factors responsible for these variations. Finally, section 7.3 addresses RQ3 through an examination of tribo-layers and an analysis of their chemical composition.

7.1. Thermal modelling of the cutting process (Paper A)

Aim of the study presented in Paper A is to develop an improved semi-analytical model for predicting the tool-chip interface temperature during cutting. The proposed formulation builds upon established solutions to the heat conduction-advection problem with a moving heat source. Two reference models are considered: the model proposed by Komanduri and Hou (Model I) [5-7] and that developed by Moufki et al. (Model II) [8]. A detailed analysis is carried out to formulate a variable heat flux distribution along the tool-chip interface, accounting for the non-uniform heat generation within the sticking and sliding regions during chip flow. Furthermore, the influence of cutting-edge geometry, specifically ideal sharp and rounded edges, on the resulting temperature fields is examined. The robustness of the developed models is evaluated for the machining of plain carbon steels using uncoated carbide tools. The assessment focuses on two primary criteria: the accurate prediction of the maximum interface temperature and the precise determination of its location. For clarity, the notation (C) designates the original formulation assuming a constant heat flux, whereas (V) denotes the modified formulation incorporating a variable heat flux. Accordingly, Model I (C) refers to the original model of Komanduri and Hou, while Model I (V) represents the model with the proposed variable heat flux implementation.

Fig. 16 illustrates the maximum temperature along the tool-chip interface predicted by the different models for C45 carbon steel, considering both ideal sharp and rounded cutting edges. The modified formulations incorporating a variable heat flux, namely Models I (V) and II (V), exhibited behaviour comparable to their respective original versions, Model I (C) and Model II (C), under both edge geometries. For an ideal cutting edge, Model I demonstrated substantially higher accuracy than Model II in predicting the maximum interface temperature. The maximum errors associated with Models I (C), I (V), II (C), and II (V) were 17%, 18%, 70%, and 63%, respectively. The overestimation observed for Model II under the ideal edge assumption was attributed to an overprediction of the heat partition coefficient derived from empirical correlations. When a rounded cutting edge was considered, a reduction in the predicted maximum temperature was observed for all cutting conditions. This decrease is linked to the omission of the ploughing force component in the calculation of thermo-mechanical loads acting on the rake face. Under these conditions, the reduction in temperature effectively compensated for the previously overestimated heat partition coefficient in Model II, resulting in improved predictive

accuracy compared with the ideal edge assumption. It should be emphasised, however, that neglecting the contribution of the ploughing component within the secondary shear zone, without accounting for the associated heat generation in the tertiary shear zone, may lead to significant underestimation of the interface temperature, as evidenced in the present analysis. Future developments of these semi-analytical approaches should therefore focus on a correct estimation of the heat partition, as well as incorporating the influence of ploughing on the flank face and around the cutting edge.

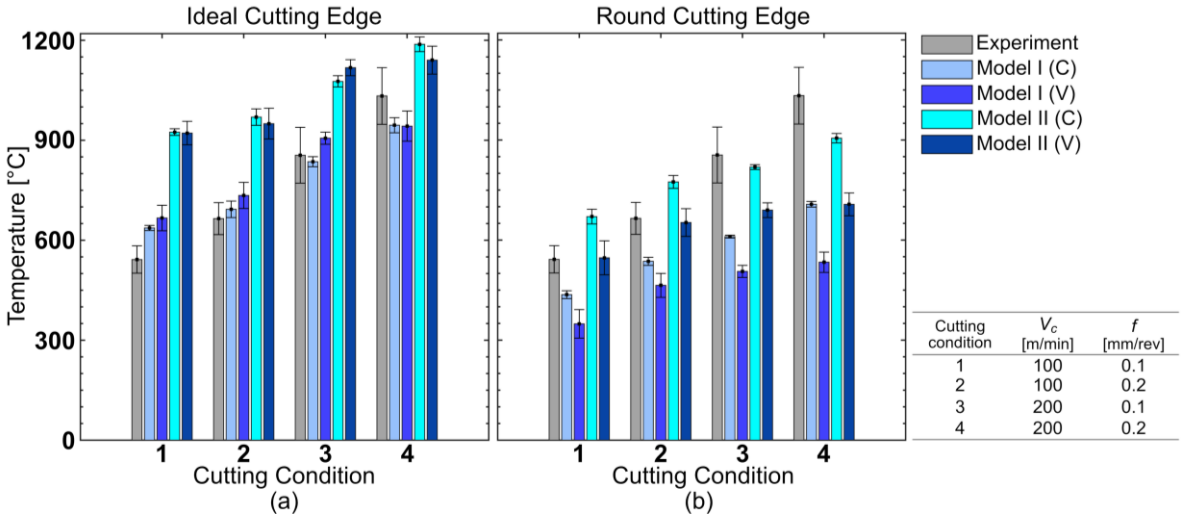

Fig. 16. Comparison of maximum temperatures obtained using the different models for C45 carbon steel using an ideal and round cutting edge.

Regarding the location of the maximum temperature along the tool-chip interface, Models I (V) and II (V) demonstrate a substantially lower error across all cutting conditions, as illustrated in Fig. 17. The average error amounts to 8% for Model I (V) and 22% for Model II (V), whereas the corresponding original formulations, Model I (C) by Komanduri and Hou and Model II (C) by Moufki et al., yield considerably higher average errors of 169% and 197%, respectively. This improvement can be attributed to the variable heat flux formulation, in which the heat flux attains its maximum at the end of the transition zones along the interface. Fig. 18 presents one set of the calculated stress, velocity and heat flux profiles along the tool-chip interface, for the case of orthogonal cutting of C45 steel with cutting conditions V_c = 200 m/min, f = 0.2 mm/rev and a_p = 2 mm. Evidently, the heat flux is variable and attains its maximum value immediately following the transition region. Here, the heat from both the plastic deformation in the sticking zone and the friction in the sliding zone superimpose, leading to the maximum heat flux in this area.

By accounting for the distinct mechanics of the sticking and sliding zones, the model incorporates a physics-based estimation of the heat generation along the tool-chip interface. As a result, the predicted position of the maximum temperature shifts closer to the cutting edge, in better agreement with experimental observations. Owing to their enhanced predictive accuracy, these improved models provide a more reliable foundation for advanced wear modelling, particularly for thermally driven mechanisms such as dissolution-diffusion wear.

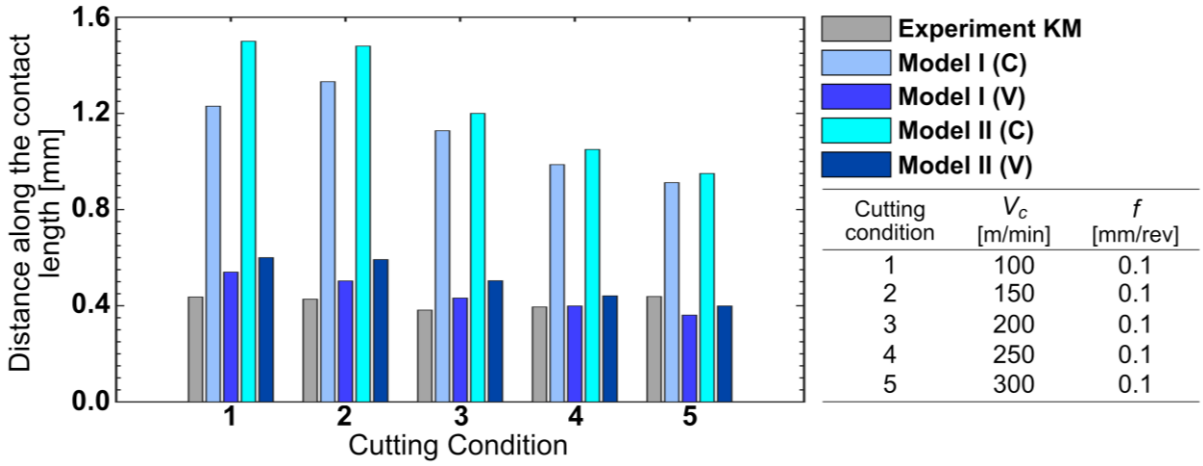

Cutting condition	V_c [m/min]	f [mm/rev]
1	100	0.1
2	150	0.1
3	200	0.1
4	250	0.1
5	300	0.1

Fig. 17. Comparison of the location of maximum crater wear KM with the location of the maximum temperature for cutting conditions of C50 steel using an ideal cutting edge. Recreated from Paper A [9].

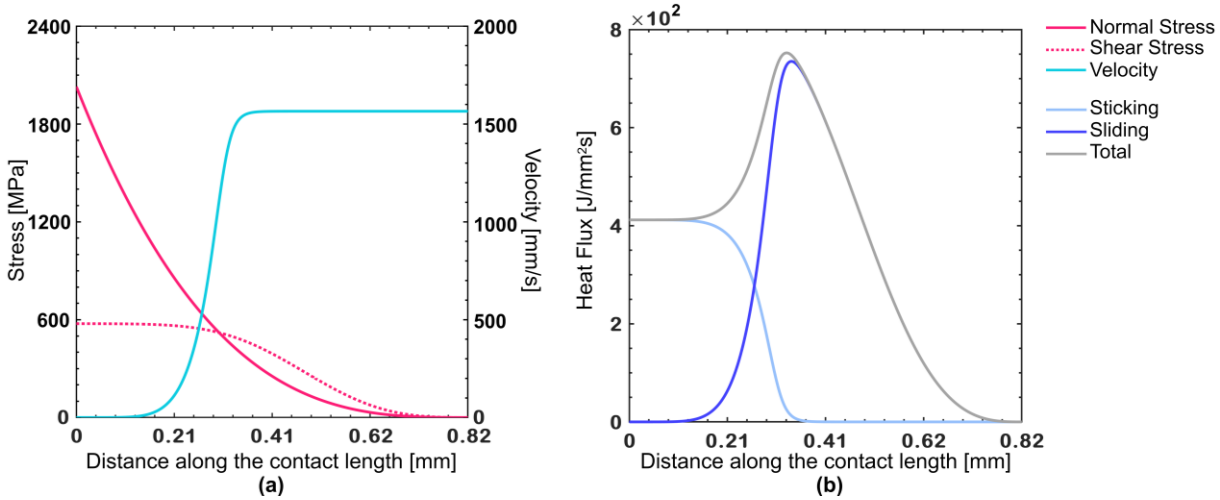

Fig. 18. (a) Stress and velocity profiles and (b) heat flux contributions from the sticking and sliding zones along contact length of an ideal cutting edge (C45, V_c = 200 m/min, f = 0.2 mm/rev). Adopted from [9].

7.2. Factors influencing machinability

Throughout Papers B-E, multiple sources of machinability variation were identified and classified according to their origin – namely workpiece material, workpiece geometry, cutting tool and process. As outlined in Table 7, these groups are examined across different publications and discussed in their respective subsections in this chapter.

Table 7. Different sources of machinability variation and their associated publications

Source of variation		Paper B C38	Paper C 20MnCrS5	Paper D Stainless Steels	Paper E 100Cr6
Workpiece material	Batch	✓	✓		✓
	Grade			✓	
Workpiece geometry			✓		
Cutting tool				✓	✓
Process		✓	✓		

7.2.1. Batch-to-batch workpiece variation

Papers B, C, and D investigate batch-to-batch variations and their corresponding effects on machinability. This section is divided into two subsections: the first presents the

differences observed in key machinability indicators, namely tool wear and cutting forces, while the second synthesises the common trends identified across the three papers that account for these variations.

Differences in machinability indicators

Significant differences in tool wear were observed between the different batches, with a representative example for each material presented in Fig. 19. Across all investigated cutting speeds (300, 400, and 500 m/min) for C38 steel, Batch B consistently exhibited lower tool wear than Batch A, with significantly reduced flank wear and noticeably less crater wear at identical spiral cutting lengths. At the highest speed, Batch A showed substantial crater development, coating spalling, and even exposure of the WC-Co substrate – effects not observed in Batch B, as shown in the BSE micrographs and EDS elemental maps in Fig. 19. Additionally, the maximum flank wear depth was also lower in batch B across all cutting conditions, as shown in Fig. 20.

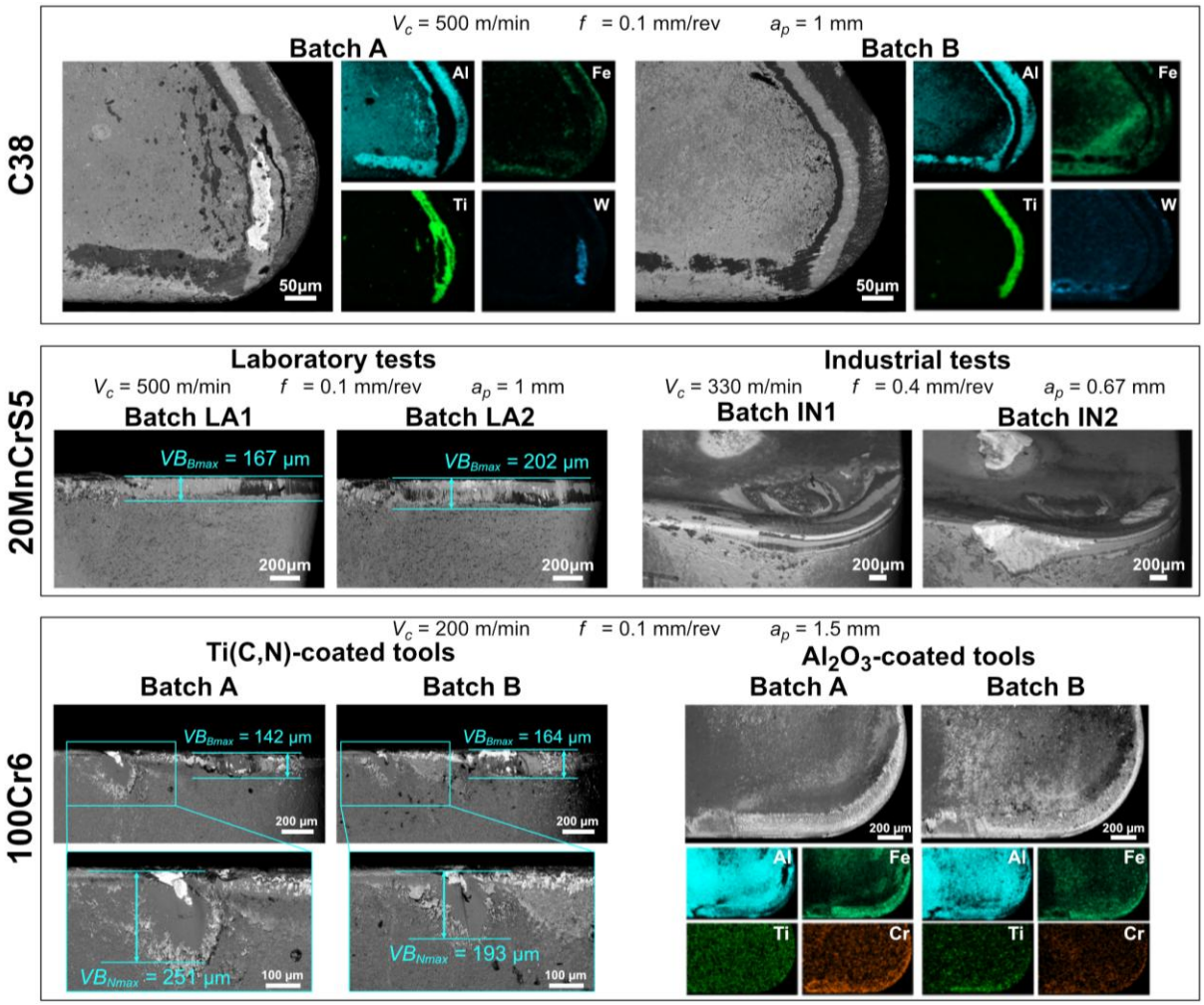

Fig. 19. BSE micrographs showing wear variation between the different batches of the low-alloy steels. Images acquired at 20kV.

Regarding material 20MnCrS5, batch LA2 consistently produced more advanced tool wear than LA1 in all investigated cutting conditions, as confirmed by BSE-SEM micrographs and flank wear measurements shown in Fig. 19 and Fig. 20. Similar to

machining of C38, the main wear types observed for this material were crater wear and flank wear. In the industrial machining tests, IN2 produced substantially more wear than IN1 in both OD and ID turning. When performing OD turning, the flank wear was 171 µm for IN2 vs. 124 µm for IN1, a 28% increase, and IN2's insert showed substrate exposure on the rake face, unlike IN1. In ID turning, the disparity was even more pronounced: IN2 generated severe notch wear with WC-substrate exposed, whereas IN1 did not (see Fig. 19). The maximum flank wear depth reached 617 µm for IN2, a 135% increase compared to IN1. IN2 also displayed more severe coating removal and damage at chip-breaker regions.

For 100Cr6, both coated tools resulted in a pronounced reduction in machinability for batch B, as illustrated in Fig. 19. In the Ti(C,N)-coated tools (G1), the rake surface of the tool used for batch A largely retained its coating compared to batch B, where significant coating degradation occurred leading to exposure of the substrate. For the Al_2O_3-coated tools (G2), both batches retained the coating; however, differences in adhesion behaviour were observed. Batch A exhibited a higher concentration of adhered Fe and Cr on the rake surface, while batch B showed a pronounced presence of Ti-rich deposits, particularly near the cutting edge. These had an influence on the formation of tribo-layers, as discussed further in section 7.3. In terms of flank wear, machining of batch B resulted in a substantial increase in maximum flank wear depth compared to batch A, with increases of 123% for tool G1 and 20% for tool G2, as shown in Fig. 20. Regarding notch wear, no measurable notch wear was observed for tool G2. In contrast, for tool G1, batch A exhibited approximately 40% greater maximum notch wear depth than batch B (231 µm versus 165 µm).

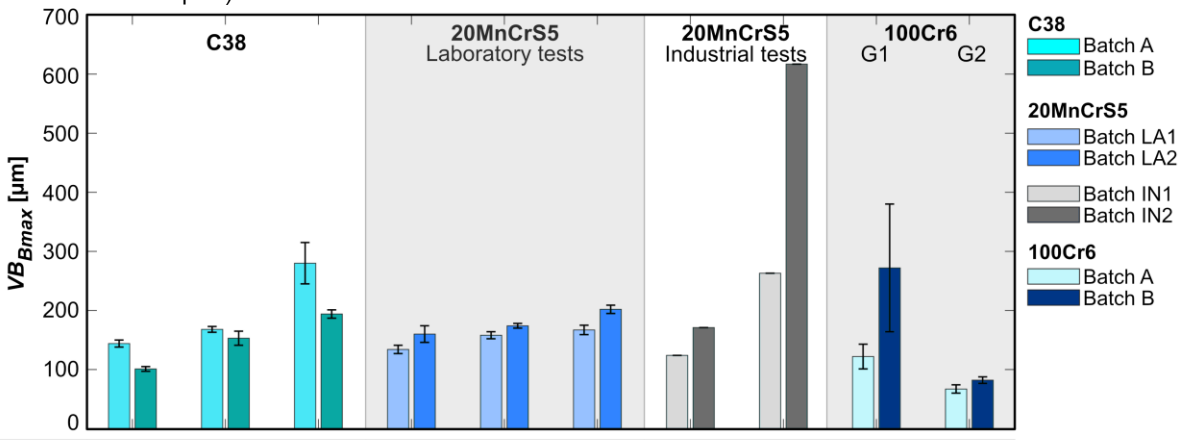

V_c [m/min]	300	400	500	300	400	500	330	330	200	200
f [mm/rev]	0.1	0.1	0.1	0.1	0.1	0.1	0.5	0.4	0.1	0.1
a_p [mm]	1	1	1	1	1	1	1.12	0.67	1.5	1.5

Fig. 20. Comparison of maximum flank wear depth (VB_{Bmax}) for machining different batches of low-alloy steels at different cutting conditions (cutting speed V_c, feed f and depth of cut a_p)

As an indicator of the thermo-mechanical loads acting on the cutting tool, the mean cutting force during the first 10 seconds of machining was assessed, considering the tool is largely unaffected by wear at that stage. For example, Fig. 21 presents the measured forces. In the case of 20MnCrS5, Batch LA2 consistently exhibited a slightly higher cutting force: on average 3%, 4% and 8% higher for the cutting, feed and passive forces. For

100Cr6, batch A exhibited only a marginal increase relative to batch B, averaging approximately 3% for the Ti(C,N)-coated tools and 5% for the Al_2O_3-coated tools. However, in the case of C38, no consistent variations are observed across all cases. It is then evident that forces alone do not constitute an independent indicator of machinability differences for all materials. Consequently, cutting force must be interpreted in conjunction with additional indicators, such as tool wear.

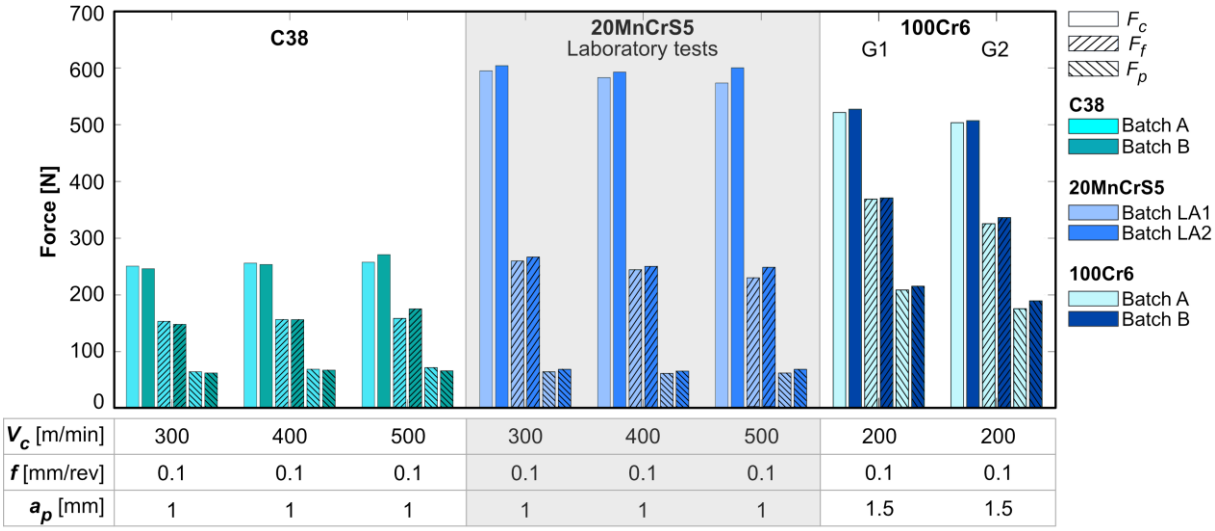

V_c [m/min]	300	400	500	300	400	500	200	200
f [mm/rev]	0.1	0.1	0.1	0.1	0.1	0.1	0.1	0.1
a_p [mm]	1	1	1	1	1	1	1.5	1.5

Fig. 21. Comparison of initial cutting (F_c), feed (F_f) and passive (F_p) forces for the different low-alloy steels.

Batch-to-batch material variations

The primary source of variation influencing batch machinability originates from differences in the workpiece material. These differences may be attributed to variations in (1) microstructural characteristics, (2) thermo-mechanical properties, and (3) non-metallic inclusion population. This subsection outlines the observed trends; however, it is important to emphasise that this does not imply that specific features can be categorically regarded as universally beneficial. Rather, the identified trends apply to the materials and cutting conditions investigated in this study, particularly considering that comparisons across different materials may lead to fundamentally different machinability responses. For clarity in the correlation analysis, the batch that exhibited inferior machinability (based on tool wear) is denoted with a "–" suffix (e.g., Batch A^-), whereas the batch with superior machinability is marked with a "+" suffix (e.g., Batch B^+).

From a microstructure point of view, it can be seen in Fig. 22 that there are remarkable differences between batches of nominally identical steels. The numbers at the top of each micrograph indicate the mean ferrite area percentage [%], mean ferrite grain size [µm] and the mean HV hardness [kg/mm^2]. In fact, the batches exhibiting superior machinability consistently displayed characteristics associated with lower flow stress and lower thermo-mechanical loading of the cutting tool. Particularly, the batches with superior machinability exhibited microstructures with higher ferrite fraction and lower hardness. For C38, Batch A^- contained a lower ferrite volume fraction (19% vs. 28%) and a harder outer diameter (261 vs. 241 kg/mm^2). It can reasonably be assumed that batches containing a higher ferrite fraction – given that ferrite exhibits greater thermal conductivity than pearlite [208, 209] – will display increased overall thermal conductivity.

Consequently, such microstructures are expected to reduce the thermal load imposed on the cutting tool. In the case of 20MnCrS5 steel, these superior-machinability batches further showed a coarser ferritic grain size (compare $LA1^+$ (9.8 µm) vs $LA2^-$ (8.8 µm), and $IN1^+$ (11.2 µm) vs $IN2^-$ (9.2 µm)). Additionally, the batch with superior machinability in 100Cr6 showed larger interlamellar spacing (85 vs. 73 nm) as well as lower hardness (350 kg/mm^2 vs. 357 kg/mm^2).

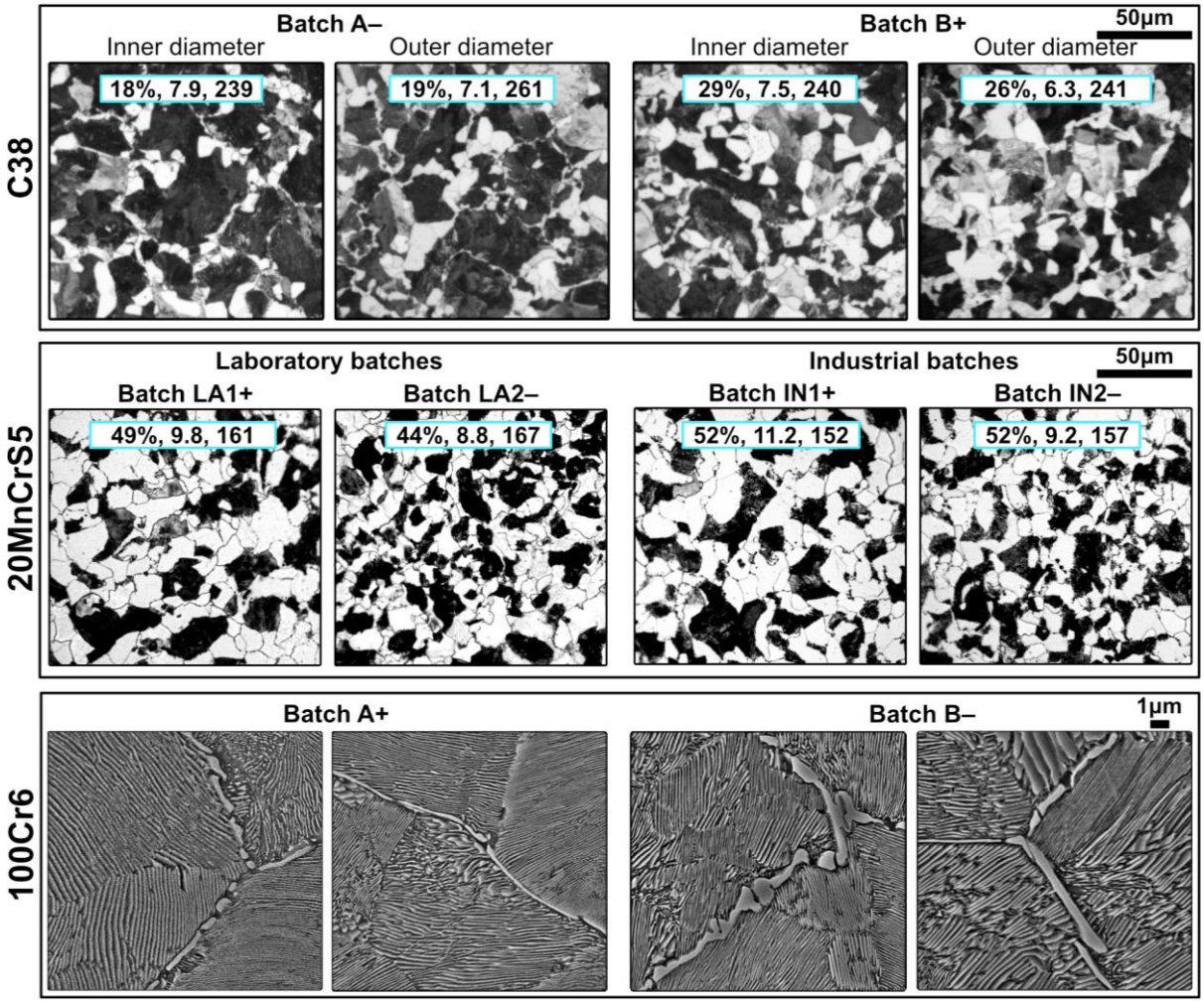

Fig. 22. Comparison of microstructures of different batches of various materials investigated. The numbers at the top of each micrograph provide the mean ferrite area percentage [%], mean ferrite grain size [µm] and mean HV hardness [kg/mm^2].

From the perspective of non-metallic inclusions, the increased wear observed in the inferior batches may be associated with a less favourable inclusion population. Although the isolation of individual contributing factors remains challenging, certain overall trends can nevertheless be identified. The area fractions of NMI classes are presented in Fig. 23.

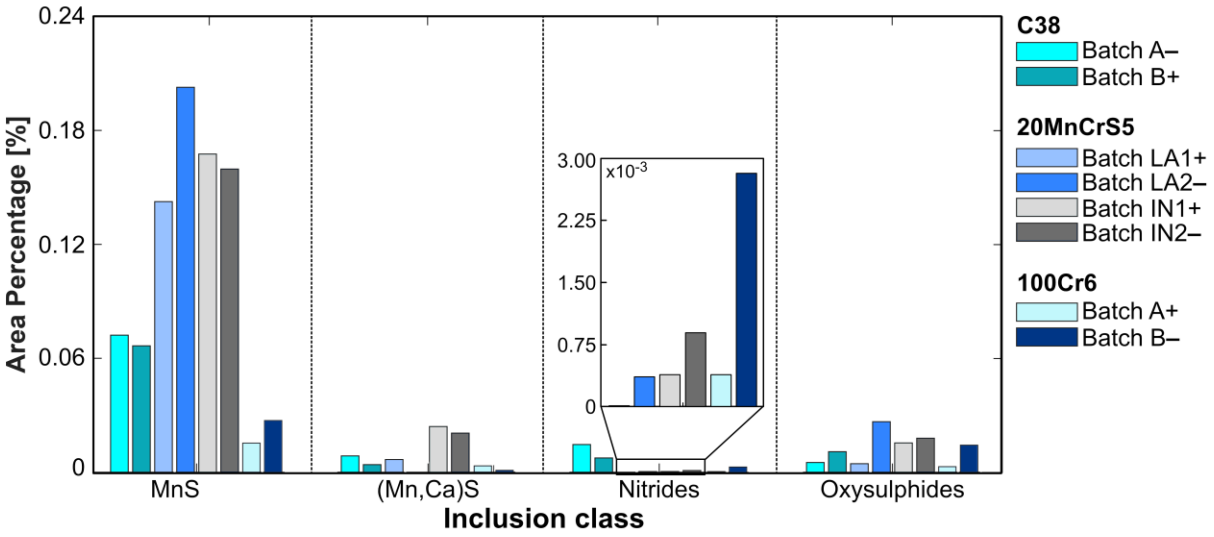

Fig. 23. Comparison of area percentage [%] of NMI classes between batches of low-alloy steels.

One trend that can be observed with these materials is the greater number and volume fraction of nitrides present in every batch that exhibited inferior machinability. This is the case for C38 [batch A^- (1431) vs. B^+ (1046)], the laboratory batches of 20MnCrS5 [batch $LA1^+$ (1) vs $LA2^-$ (25)], its industrial batches [batch $IN1^+$ (44) vs $IN2^-$ (77)], as well as the 100Cr6 batches [A^+ (82) vs B^- (190)]. These high-hardness particles can accelerate coating degradation by abrasive ploughing and promote earlier exposure of the WC substrate. Such hard nitrides can also destabilise the formation of tribo-layers, as further discussed in section 7.3. Another trend was observed regarding nitride size, where batches with larger nitrides consistently exhibited increased tool wear.

The influence of sulphides exhibits a more complex behaviour, depending on their composition, specifically whether they are pure MnS or calcium-rich (Mn,Ca)S. Batches with a higher proportion of MnS inclusions generally showed lower tool wear and improved machinability, likely through their function as crack initiation sites that increase chip breakability and promote the potential formation of lubricating tribo-layers. Notably, the quantity of sulphides seems to be a more representative metric than the area fraction. For instance, $LA1^+$ exhibits superior machinability – it has more sulphide inclusions than $LA2^-$ (1347 vs. 1025) but less sulphide area fraction (0.14% vs. 0.20%), probably also emphasising the role of the size of inclusions, as smaller sulphides (within a certain range) are considered more beneficial. The exception to this observed trend was the 100Cr6 batches, where batch A^+ showed better machinability with significantly less MnS sulphides. Calcium-rich (Mn,Ca)S sulphides are recognised for facilitating the formation of more stable lubricating layers at elevated temperatures compared to calcium-poor sulphides. No consistent trend in terms of quantity or area fraction of these sulphides was observed across the investigated materials. Regarding the influence of sulphide size and aspect ratio, Fig. 24 compares these characteristics for sulphides. A trend is observed for the size of (Mn,Ca)S sulphides, where smaller inclusions are consistently present for all the batches that exhibited superior machinability (C38-B^+, $LA1^+$, $IN1^+$ and 100Cr6-A^+).

Similar trends are identified for MnS – smaller and more globular MnS sulphides exist in superior batches; however, the exception to this is the 100Cr6 batches.

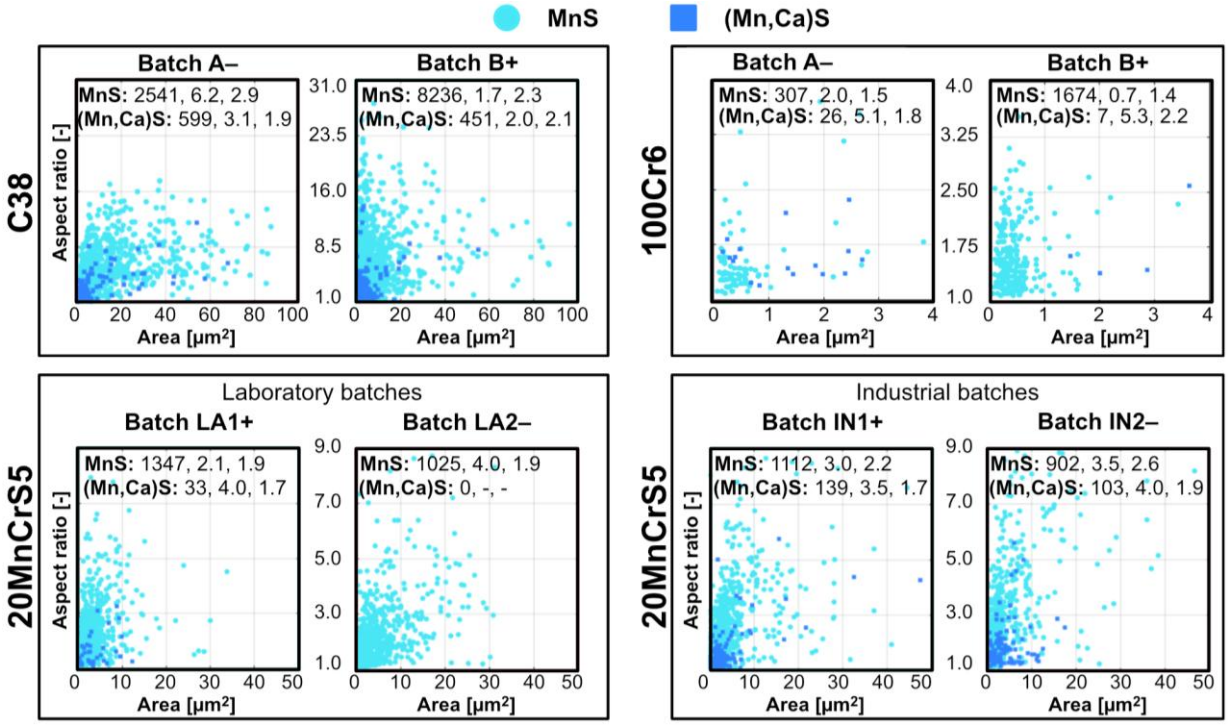

Fig. 24. Comparison of aspect ratio versus area of the sulphide inclusions in each batch of the low-alloy steels. The values at the top of each graph respectively denote quantity [-], mean area [µm^2], and mean aspect ratio [-] of each inclusion subclass.

Finally, oxides and oxysulphides generally contribute to micro-abrasion and abrasive ploughing of the tool coatings. However, the extent of their abrasiveness is difficult to assess without knowledge of their chemical composition, as their behaviour is strongly governed by properties such as hardness and plasticity. Given favourable composition and conditions, oxysulphides can instead form protective layers on the tool surfaces. Therefore, it is important to emphasise that evaluating oxysulphides solely based on their quantity or volume fraction, without accounting for their chemical composition, can be misleading. Thus, Table 8 summarises the average chemical composition of oxides/oxysulphides present in different batches.

Table 8. Average chemical composition per oxysulphide in weight percentage [wt.%]

	Batch	Al_2O_3	SiO_2	CaO	MgO	MnO	TiO_2
C38	A^-	30.2	0.4	5.5	4.4	55.7	3.9
	B^+	31.0	0.3	9.1	2.2	53.3	4.1
20MnCrS5	$LA1^+$	10.6	7.9	0.7	0.9	79.9	0.0
	$LA2^-$	28.9	0.6	7.1	1.9	61.5	0.0
	$IN1^+$	22.2	2.2	3.5	2.0	70.1	0.0
	$IN2^-$	32.6	0.0	7.3	2.0	58.1	0.1
100Cr6	A^+	25.3	8.9	3.2	1.1	59.8	1.7
	B^-	73.7	4.4	0.8	1.1	19.9	0.1S

For the C38 steel, Batch B^+ contains approximately twice the oxysulphide area fraction of Batch A^-. The chemical composition of the oxysulphides in both batches is similar, except for a higher calcium concentration in Batch B^+ (A^-: 5.5 wt.% vs. B^+: 9.1 wt.%).

Based on their chemical composition, Ca-rich oxysulphides exhibit lower hardness (Fig. 6), thereby reducing their contribution to the abrasive wear mechanism and instead, probably promoting the formation of protective layers on the tool surfaces. Thus, the oxysulphide composition seems to favour the machinability of Batch B^+.

For the 20MnCrS5 batches, similar trends in oxide composition were observed between both sets of batches. The batches that exhibited superior machinability ($LA1^+$ and $IN1^+$) both possessed a higher Mn- but lower Al- and Ca- content compared to their counterparts ($LA2^-$ and $IN2^-$). In fact, higher Mn-content renders oxides significantly softer with a lower melting temperature compared to Al-rich oxides [210]. Despite $IN2^-$ and $LA2^-$ exhibiting higher mean calcium content, the potential benefit associated with increased Ca in Al-rich oxides appears to be less influential than the elevated MnO concentration observed in $IN1^+$ and $LA1^+$ for these materials. Similar trends were also observed in the 100Cr6 batches. The batch that exhibited superior machinability (A^+) possessed oxysulphides with lower Al- and higher Mn- content. Further, the oxysulphides in batch A^+ possessed higher Ca-content, despite its low concentration. The influence of these oxysulphides on the machinability is further discussed in section 7.3. Across all investigated materials, there were no discernible trends regarding oxysulphide size and globularity, indicating that the influence of this inclusion class on machinability is primarily governed by its chemical composition rather than its morphology.

Table 9 summarises the investigated material features and their expected influence on machinability. For each feature, the condition anticipated to enhance machinability is defined (e.g., higher ferrite fraction). A check mark (✓) then indicates if the batch with superior machinability demonstrated this favourable characteristic, a cross (✗) denotes if it did not, and an equal sign (=) signifies that both batches exhibited comparable values for this feature. N/A signifies that one batch did not possess this type of NMI.

Table 9. Summary of investigated material features and their expected influence on machinability.

			C38	20MnCrS5		100Cr6
		Batch	B⁺	LA1⁺	IN1⁺	A⁺
Micro-structure		Higher ferrite fraction	✓	✓	=	N/A
		Larger grain size	✗	✓	✓	N/A
		Larger interlamellar spacing	=	=	=	✓
		Lower hardness	✓	✓	✓	✓
Non-metallic inclusions	MnS	More MnS sulphides	✓	✓	✓	✗
		Smaller MnS sulphides	✓	✓	✓	✗
		Globular MnS sulphides	✓	=	✓	✗
	(Mn,Ca)S	More (Mn,Ca)S sulphides	✗	✓	✓	✓
		Smaller (Mn,Ca)S sulphides	✓	N/A	✓	✓
		Globular (Mn,Ca)S sulphides	✗	N/A	✓	✗
	Nitride	Less nitrides	✓	✓	✓	✓
		Smaller nitrides	✓	✓	✓	✓
		Globular nitrides	=	✓	✓	✓
	Oxides	Smaller oxysulphides	✗	✓	✓	✓
		Globular oxysulphides	=	✗	✗	✗
		Less Al-rich oxides	=	✓	✓	✓
		More Mn-rich oxides	=	✓	✓	✓
		More Ca-rich oxides	✓	✗	✗	✓

7.2.2. Workpiece grade variation

While the other publications varied batches of nominally identical steels, Paper D examined machinability across different grades of stainless steel. Similarly, this section is split into 2 subsections: (1) differences in machinability indicators and (2) workpiece material characteristics that may explain the machinability differences.

Differences in machinability indicators

The cutting tool grade in these cutting tests was varied, leading to distinctly different flank and notch wear depths across the investigated materials, as observed in Fig. 25. For tool grade GC2025, VB_{Bmax} was lowest when machining the martensitic stainless steel (98 µm), 48.8% higher for ferritic, and most severe for the super duplex steel (480 µm).

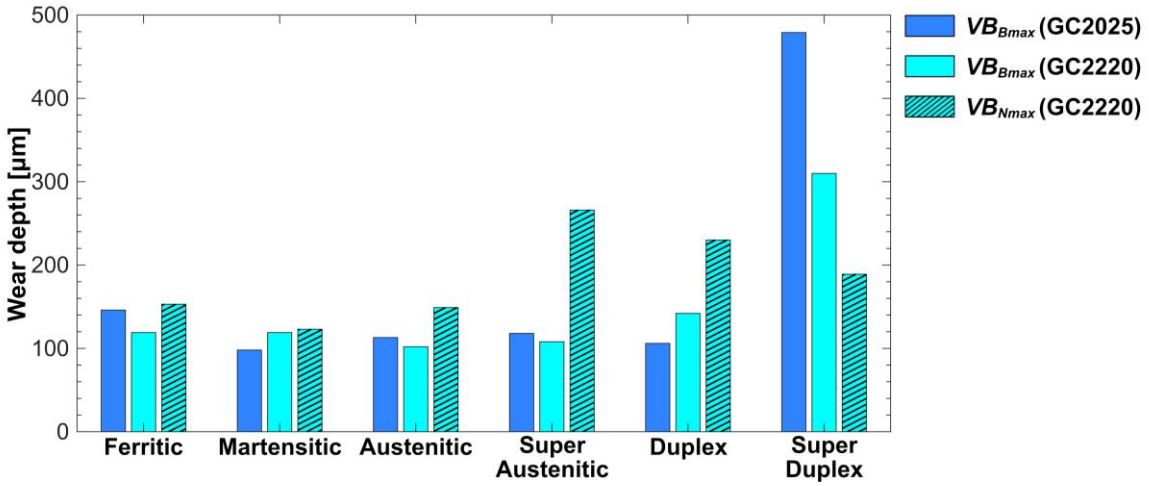

Fig. 25. Difference in maximum wear depths for various stainless steels using tool grades GC2025 and GC2220 with cutting conditions: V_c = 150 m/min, feed f = 0.25 mm/rev and depth of cut a_p = 1.5mm.

The coating degradation was also significantly different between materials, as shown in Fig. 26. The martensitic workpiece showed the least adhesion and coating degradation on both rake and flank surfaces compared to all other grades. Ferritic machining resulted in coating spallation, a feature not observed for any other stainless steel, while machining of super duplex steels produced the most severe wear, exhibiting loss of the cutting edge despite being machined to only half the SCL of other materials.

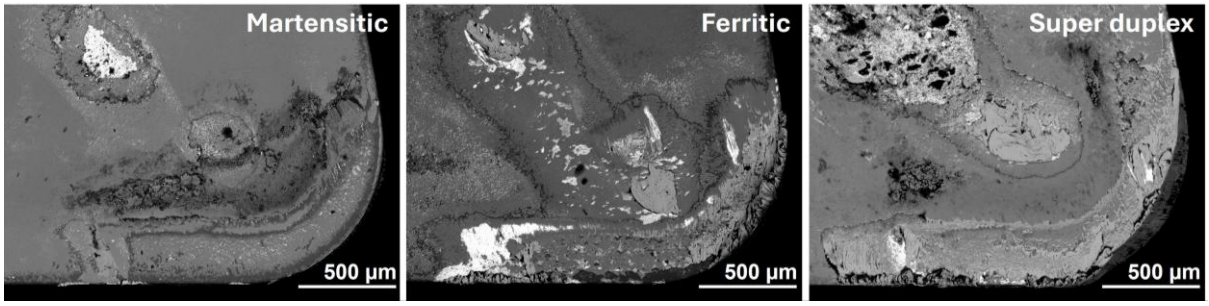

Fig. 26. BSE micrographs showing the worn rake surfaces of the GC2025 tools. Obtained at 20kV.

Notch wear was observed exclusively for tool grade GC2220 as shown in Fig. 27. The highest notch wear depths occurred for the super austenitic, duplex, and super duplex steels, all of which displayed substantial adhesion in the notch region. The ferritic tool showed advanced coating degradation with exposed substrate in the notch region. Martensitic machining again resulted in comparatively limited coating degradation and minimal adhesion compared to the other stainless steels. For the notch wear depth, VB_{Nmax} was 123.3 µm in martensitic, 153.3 µm in ferritic (+24%) and 189.1 µm in super duplex (+53%). For both tool grades, the cutting force yielded the highest values for super duplex steel and the lowest for ferritic steel.

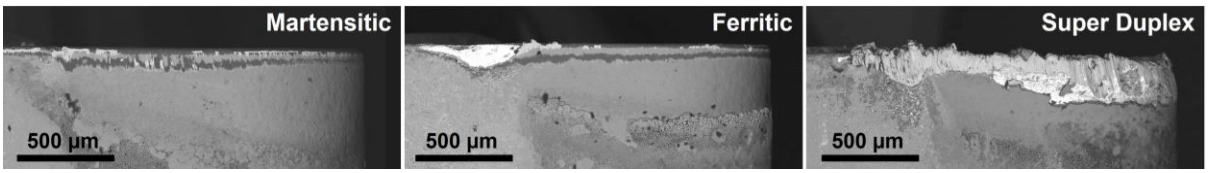

Fig. 27. BSE micrographs showing the flank surfaces of the cutting tools GC2220. Obtained at 20kV.

Workpiece material variations

The wear behaviour of the investigated stainless steels is strongly influenced by their thermo-mechanical properties, presented in Table 10, and microstructures, shown in Fig. 28. Martensitic steel combined the highest hardness with low specific fracture energy and relatively high thermal conductivity, generating low thermal loads despite higher forces. This can explain the minor adhesion and shallow crater wear observed for this material. Ferritic stainless steel caused comparatively low wear on the tool's rake face, but moderate flank and severe notch wear. From the perspective of thermo-mechanical properties, ferrite's low yield strength and low hardness promote lower cutting forces so the stresses on the tool are relatively low. Further, ferrite's low specific fracture energy and high thermal conductivity facilitate efficient heat dissipation, reducing thermal loads on the tool. Despite these favourable conditions, ferrite's inherent stickiness still leads to moderate adhesion on the tool surfaces, while the severe notch wear can be attributed to chip-induced cyclic loading at the depth-of-cut line. Austenitic and super austenitic steels'

low thermal conductivity, high ductility and strong strain hardening promoted adhesion and hardened material deposition, accelerating coating degradation. Duplex and super duplex steels, with their high strength, high ductility, limited thermal conductivity, and high specific fracture energy, generated the most severe thermo-mechanical stresses. This is consistent with the most aggressive wear and in super duplex, plastic deformation.

Table 10. Thermo-mechanical properties of the investigated stainless steel grades.

	Hardness	Yield strength	Ultimate tensile strength	Elongation at fracture	Reduction in cross-sectional area	Thermal conductivity	Specific fracture energy
	[kg/mm^2]	[MPa]	[MPa]	[%]	[%]	[W/mK]	[GJ/m^3]
Ferritic	147	264	382	20	18	25	0.119
Martensitic	294	767	942	18	52	30	0.107
Austenitic	162	326	591	59	79	15	0.260
Super Austenitic	187	384	617	41	82	12	0.222
Duplex	250	573	746	38	76	14	0.236
Super Duplex	276	579	802	42	80	15	0.272

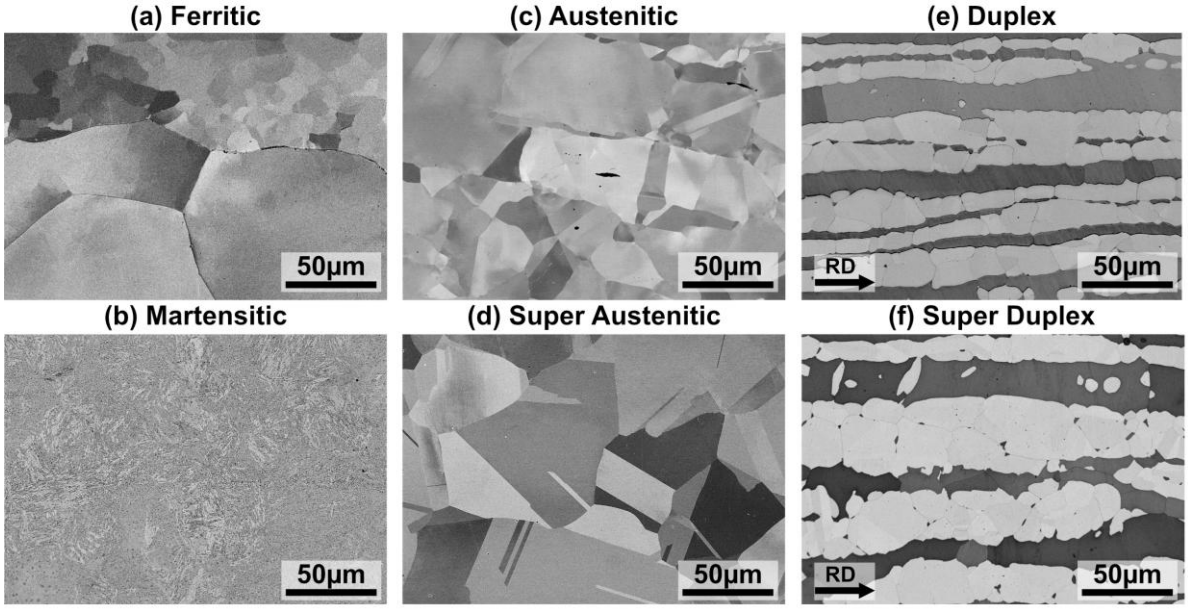

Fig. 28. BSE micrographs of microstructures for the investigated stainless steels obtained at 500x magnification and (a) 10 kV, (c) 3 kV, (d) 15 kV, and (b, e, f) 2kV, RD represents the rolling direction.

In addition to the differences in microstructure and thermo-mechanical properties, the non-metallic inclusions also vary substantially across the stainless steel grades, as shown in Fig. 29. The martensitic stainless steel was characterised by a high population of fine, globular MnS inclusions (7238; mean size 0.48 µm^2) which likely enhanced lubricity at the tool-chip interface, reducing adhesive and crater wear. However, larger Si-rich hard oxides (163) and oxysulphides (413) caused localised abrasive interactions, evidenced by the micro-grooves on the tool. Ferritic stainless steel was characterised by its high population of small, hard oxides (533; mainly Al_2O_3, MnO and TiO_2; see Fig. 30), which contributed to pronounced coating degradation and spallation. The absence of numerous MnS inclusions (19) reduced lubricity, exacerbating adhesion and adhesive pull-out.

In the austenitic grade, large and elongated sulphides (1154; mean size 1.82 μm^2; mean aspect ratio 3.5) were less beneficial for machinability, while a substantial and abrasive Si-, Ca- and Al-rich oxide/oxysulphide population (1173) contributed to extensive tool coating degradation and pronounced crater wear. Although calcium-rich inclusions may form protective layers under favourable conditions, this effect was not evident. The super austenitic grade contained significantly lower volume fraction of sulphides, further limiting lubricity and protective layer formation. In contrast to the other stainless steels, the duplex grade had low oxide and sulphide contents, suggesting a limited influence of NMIs on its machinability. The super duplex grade, however, contained numerous large Al_2O_3-CaO oxides (280; mean area 3.35 μm²; Fig. 30). Despite their reduced hardness at higher CaO contents, any potential protective effect seems to have been outweighed by the severe thermo-mechanical conditions.

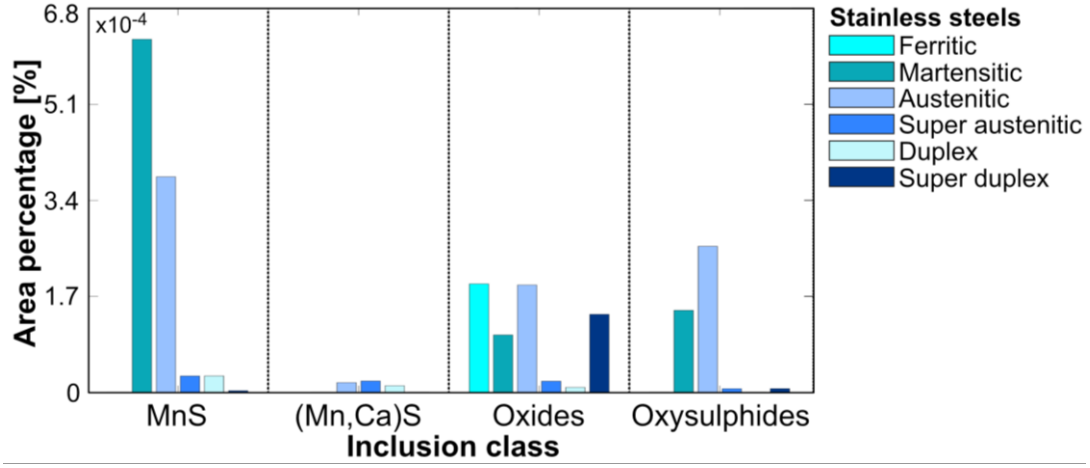

Fig. 29. Comparison of area percentage of NMIs by class between batches of stainless steels.

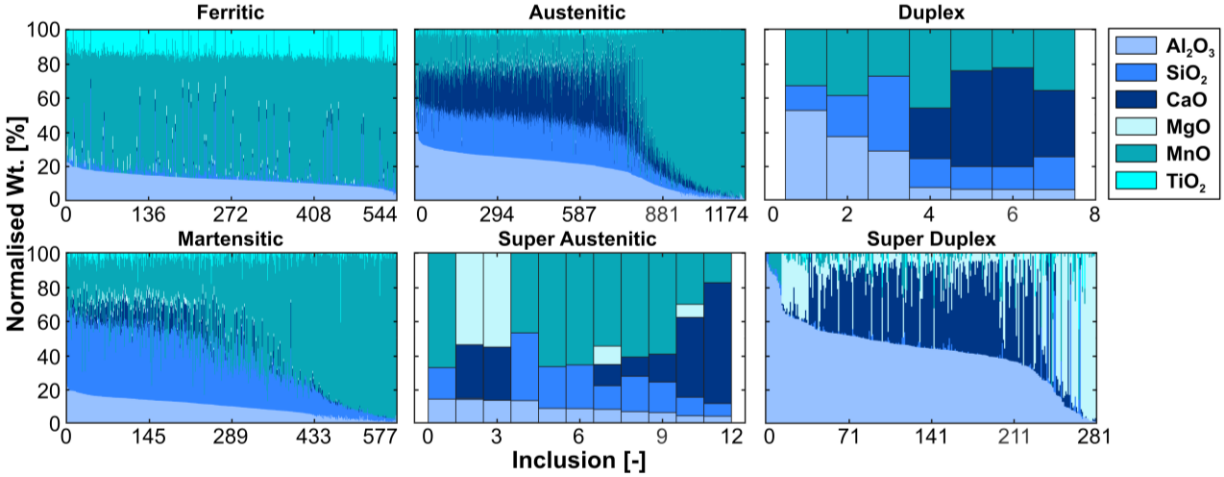

Fig. 30. Comparison of oxysulphide chemical composition for the investigated stainless steels.

7.2.3. Influence of workpiece geometry

Another source of variation in machinability arises from differences in workpiece geometry, which may result from upstream variability in forging precision between suppliers as well as clamping and fixturing inconsistencies during turning operations. The study presented in Paper C on the machinability of 20MnCrS5 provides clear evidence of these effects, where the effective depth of cut experienced by the tools in the industrial

lines differed significantly despite nominally identical machining conditions (see Fig. 31). This variation indicates that the mechanical loading on the tool is not uniform, leading to local fluctuations in cutting forces, contact conditions, and heat generation. Consequently, these variations influence tool wear progression, tribo-layer development, and overall machining stability, thereby contributing to differences in machinability.

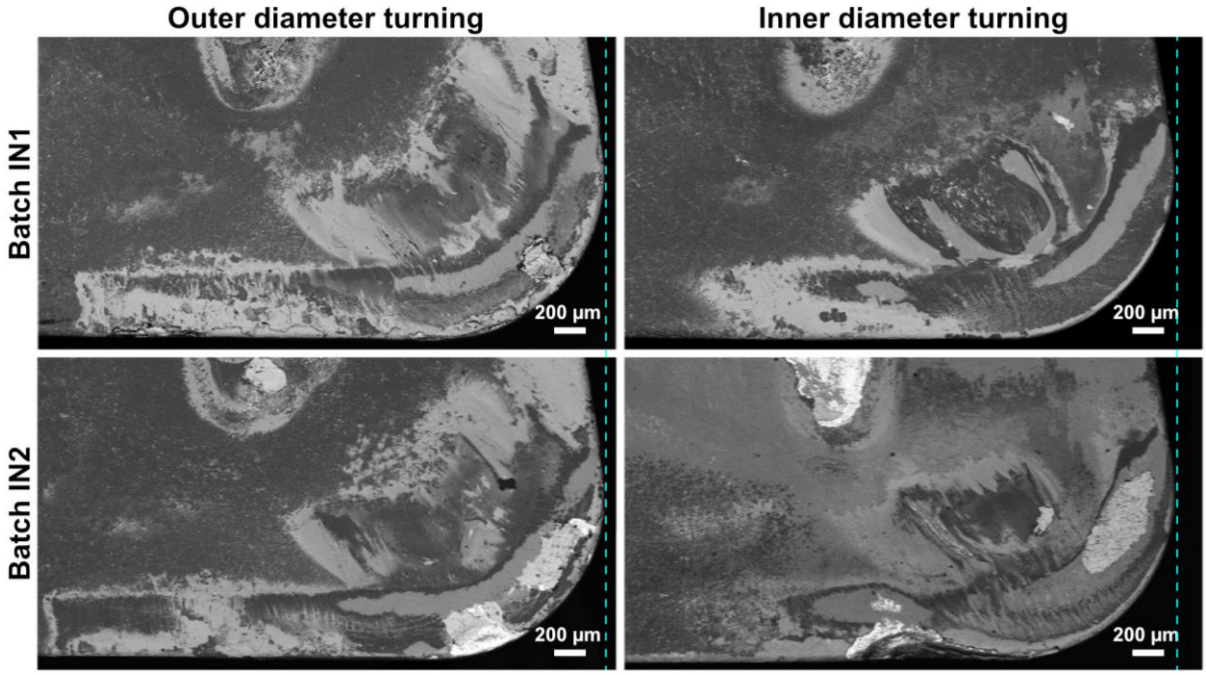

Fig. 31. Comparison of effective depths of cut for industrial tools used for machining the two batches ($IN1^{+}$ and $IN2^{-}$) of 20MnCrS5 with two different cutting processes (outer and inner diameter turning).

7.2.4. Influence of tool grade variations

The selection of tool grade plays a critical role in determining machinability, as different coating architectures and substrate properties can lead to markedly different wear behaviours under identical cutting conditions.

In Paper D, the machining of stainless steels was carried out using two tool grades, GC2025 and GC2220 (detailed in Table 6), which primarily differ in their coating compositions. The most pronounced distinction in their performance was observed in their notch wear behaviour. Notch wear was prominent in GC2220 (multilayer κ-Al_2O_3–TiN outer coating), whereas it was largely absent in GC2025 (single α-Al_2O_3 outer coating). For both tool grades, notch wear initiation is associated with brittle failure of the coating at the depth-of-cut line, followed by adhesion-driven material removal [23,24], as supported by the presence of adhered workpiece material in the notch regions (Fig. 21), particularly for GC2220. The observed differences can be attributed to the way each coating architecture accommodates crack initiation and propagation. In GC2025, the multilayer κ-Al_2O_3–TiN coating promotes a more gradual degradation process, where cracks propagate through successive layers via interlamellar spallation, resulting in a controlled, stepwise material removal. In contrast, GC2220 features a thicker single α-Al_2O_3 coating, which is more susceptible to notch failure due to the detachment of larger coating fragments, thereby accelerating notch wear. Consequently, the multilayer

structure in GC2025 enhances resistance to catastrophic coating loss, whereas the single-layer α-Al_2O_3 coating in GC2220 is more prone to large-scale material removal. This difference in wear response is further enhanced by the more homogeneous plastic deformation exhibited by α-Al_2O_3-coated tools, which is governed by basal slip mechanisms due to their {0001} texture, thereby enhancing their resistance to wear.

A similar trend is observed when machining 100Cr6 using with differently coated tools G1 and G2 (Table 6), which share identical substrates but differ in coating composition. The Ti(C,N)-coated tool (G1) exhibited more severe wear across all modes, including flank, crater, and notch wear, for both batches. Notch wear was exclusively observed in this grade. In contrast, the α-Al_2O_3-coated tool (G2) showed significantly improved wear resistance and no evidence of notch wear. Given that adhesion plays a key role in notch wear development, the lower chemical affinity of alumina compared to the Ti(C,N) coating likely reduces adhesion at the tool-chip interfaces, thereby delaying or suppressing notch formation.

7.2.5. Influence of process variations

For machining of C38 (Paper B) and 20MnCrS5 (Paper C), variations in flank and crater wear across different cutting conditions (see Fig. 19 and Fig. 20) indicate that the magnitude of batch-to-batch variations is condition-dependent. While consistent trends in machinability persisted across a range of cutting speeds, the severity of the differences was amplified under specific conditions, particularly at higher cutting regimes (V_c = 500 m/min).

In addition to variations within a given operation, the machinability response of identical batches can differ depending on the machining process, as demonstrated in the industrial cutting tests of 20MnCrS5 (Paper C). The disparity between $IN1^+$ and $IN2^-$ was more pronounced in internal turning than in external turning (see Fig. 31). This can be partly attributed to inherent differences in process kinematics, including tool-workpiece engagement and chip evacuation. In internal turning, restricted chip evacuation reduces heat dissipation and increases the likelihood of chip re-contact with the tool, leading to elevated friction, thermal loading, and accelerated wear. These conditions also promote repeated interaction between the tool and hard constituents within the chip, such as nitrides and oxides, thereby intensifying micro-abrasive wear. Overall, these findings emphasise that machinability should be considered a system-level response, governed by the combined effects of material characteristics and process conditions.

7.3. Formation of tribo-layers

The formation of tribo-layers was examined in Paper E following the machining of two batches of 100Cr6 with two different tools (see Table 5 and Table 6). STEM lamellae extracted from the rake surfaces revealed the presence of tribo-layers for both tools – Ti(C,N)-coated (grade 1) and α-Al_2O_3-coated (grade 2) – with more pronounced development observed in batch A, as shown in Fig. 32. For the Ti(C,N)-coated tool, a continuous Al–O-rich tribo-layer was identified on the Ti(C,N) rake surface, appearing as a dark contrast region. Within this layer, localised regions containing varying

concentrations of Fe, Cu, and Al were observed. Furthermore, discrete Fe-oxide deposits were found distributed along the length of this layer. This Al–O-rich tribo-layer is likely associated with the deformation and subsequent deposition of MnO–Al_2O_3-rich oxysulphide inclusions present in batch A^+. Such inclusions exhibit greater deformability than pure Al_2O_3 inclusions, enabling them to plastically deform and smear onto the tool surface rather than fracture and contribute to abrasive wear. Alumina-based layers are inherently hard and may undergo further strengthening due to severe plastic deformation prior to deposition [211], thereby enhancing their ability to protect the underlying tool coating from abrasive wear mechanisms. This is reflected in the observed tool wear behaviour, where machining of batch A^+ – which exhibited the presence of such layers – resulted in greater retention of the coating compared to batch B^-, whose tool experienced significantly more severe coating loss, leading to exposure of its underlying substrate. In fact, in contrast to batch A^+, no such tribo-layer was identified in the lamellae extracted from tools used for machining batch B^-. While it is important to acknowledge that lamellae represent highly localised regions and therefore do not allow for broad generalisation, this absence may nevertheless be linked to the underlying inclusion population. In particular, the significantly higher number and mean area of nitrides in batch B^- may promote shearing and destabilisation of any forming layers. Furthermore, the oxide inclusions in this batch are significantly richer in Al_2O_3 (73.7% vs. 25.3%, Table 8), resulting in higher hardness and reduced deformability, which limits their ability to plastically smear and contribute to stable tribo-layer formation.

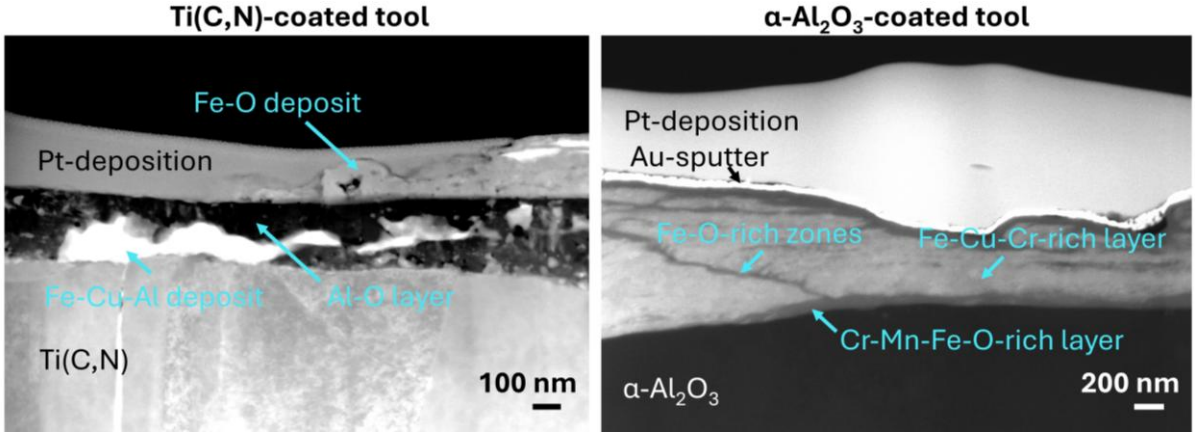

Fig. 32. HAADF micrographs showing the deposition of different tribo-layers on the different coatings of the tools used for machining batch A.

In contrast to the Ti(C,N)-coated tools, the α-Al_2O_3-coated tools promoted the formation of a thinner oxide layer enriched in Fe, Cr, and Mn (dark grey contrast) adjacent to its α-Al_2O_3 coating (black contrast). Within the adhered material (light grey contrast), elongated strands of Fe–O-rich phases were also observed. These Fe–Cr–Mn–O tribo-layers, which were detected in batch A^+ but not B^-, are likely to have contributed positively to the machinability of batch A^+ by altering the interfacial tribological conditions favourably and thus mitigating wear. However, further investigation into the physicochemical and mechanical properties of such tribo-layers is required to fully elucidate the mechanisms by which they influence tool-workpiece interactions.

8. Conclusions and future work

This chapter presents the conclusions of the thesis, formulated with respect to the research questions presented in Chapter 1. Some recommendations for future work are also provided.

8.1. Conclusions

RQ1 - Does a physics-based approach to quantify tribological conditions at the tool-chip interface improve the accuracy in simulating the stress and thermal conditions during turning?

Based on the investigations presented in Paper A, which examined the effect of incorporating a variable heat flux into two established semi-analytical temperature models, the following conclusions can be drawn:

- Incorporating a variable heat flux along the tool–chip interface has a limited influence on the magnitude of the maximum interface temperature; however, it significantly enhances the accuracy of its predicted location. In particular, the modified Komanduri and Hou model, Model I (V), demonstrates good agreement in predicting both the peak temperature and its position. This improved localisation is of critical importance for the accurate estimation of crater wear evolution during machining.
- The model proposed by Komanduri and Hou demonstrates improved accuracy in predicting the maximum cutting temperature compared to the model presented by Moufki et al. (Model II) when incorporating a similar heat flux distribution. This improvement is primarily attributed to the temperature coupling along the tool–chip interface inherent in Komanduri and Hou's formulation, which enables direct determination of the variable heat partition. In contrast, Model II requires prior specification of the heat partitioning coefficient, making its accuracy highly dependent on the reliability of the assumed partitioning relationships.
- The developed machine learning-based approach for identifying the heat partitioning parameters within Komanduri and Hou's model offers a promising framework, thereby enabling more efficient and reliable temperature predictions.
- Modelling a round-edged cutting tool results in a notable reduction in predicted cutting temperature, primarily due to the exclusion of the heat source associated with ploughing forces, as well as the corresponding decrease in normal and shear forces acting along the tool's rake face.

RQ2 - How do microstructural variations affect the machinability of various grades of steels?

Based on the investigations presented in Papers B–E, in which the machinability of different steel batches and grades was examined, the following conclusions can be drawn:

- The machinability of nominally identical steels can exhibit significant variation between batches, extending beyond what can be explained by the properties typically reported in material certificates.
    - Higher ferrite fraction, larger interlamellar spacing and lower hardness were consistently associated with the batch exhibiting superior machinability.
    - Nitrides were found to have a strong influence on machinability, with higher number density, area fraction, and mean size, as well as lower globularity, consistently associated with poorer machinability. Consequently, control of nitride characteristics during the steelmaking process appears to be of critical importance.
    - The influence of oxysulphides appears to be primarily governed by their chemical composition rather than their size or aspect ratio. While their morphology exhibited varied trends, batches containing oxysulphides with higher MnO content and lower Al_2O_3 content consistently demonstrated improved machinability. The concentration of CaO appears to be less influential than those of MnO and Al_2O_3.
    - In most materials, a higher presence of MnS sulphides was associated with improved machinability. Furthermore, smaller and more globular sulphides tended to correlate with better machinability.
    - Similarly, Ca-rich sulphides were more prevalent in batches exhibiting superior machinability. Although no clear trend was observed with respect to globularity, smaller Ca-rich sulphides were consistently associated with improved machinability.
- The machinability of different stainless steel grades was significantly influenced by their thermo-mechanical properties, with thermal conductivity, specific fracture energy, ductility and yield strength being most representative of their machinabilities.
- The influence of tool grade, process parameters, and workpiece geometry was shown to be significant in determining machinability. This highlights the importance of evaluating machinability as a system-level response rather than as an intrinsic property of the material alone.

RQ3 - Can workpiece microstructural variations affect the formation and stability of protective tribo-layers on the cutting tool?

Based on the investigations of tribo-layer formation during machining of 100Cr6 using two distinct tool grades, the following conclusions can be drawn:

- The type of tribo-layer formed is strongly influenced by the coating composition. Ti(C,N)-based coatings were found to promote the formation of Al_2O_3-rich layers during machining of 100Cr6, whereas Al_2O_3 coatings favoured the formation of Cr–Mn-rich oxide layers.
- The formation of tribo-layers is closely associated with the presence of deformable oxides, with $MnO{\cdot}Al_2O_3$ oxides promoting layer formation more readily than Al_2O_3-

rich oxides. Further, the preferential oxidation of chromium can also promote the formation of Cr-rich oxide tribo-layers.
- The formation mechanism of tribo-layers can be associated with the deposition of workpiece material into micro-grooves present in the tool coating.
- Hard inclusions, such as nitrides and Al_2O_3-rich oxides, can disrupt and destabilise the formation of tribo-layers on the tool surface.

8.2. Future work

Based on the findings of this thesis, some directions for future work are identified.

From a modelling perspective:

- Future developments of semi-analytical modelling approaches should place greater emphasis on accurately determining the heat partition between the tool and chip, as this remains a critical factor governing temperature prediction and, consequently, wear behaviour.
- More realistic representation of round-edged cutting tools requires explicit incorporation of ploughing effects, particularly along the flank face and in the vicinity of the cutting edge.

From a machinability perspective:

- Decoupling the respective influences of microstructure and non-metallic inclusions would provide deeper insight into their individual contributions to machinability. This could be achieved by applying controlled heat treatments to a single material batch to systematically vary microstructural features – such as ferrite fraction and grain size – while preserving a constant inclusion population. Conversely, remelted or inclusion-engineered steels could be utilised to tailor inclusion characteristics (size, morphology, and chemistry) while maintaining a comparable bulk microstructure. Such an approach would enable independent evaluation of inclusion-driven effects on tool wear and cutting behaviour. In particular, targeted control and deliberate variation of oxide populations would be of significant interest, allowing investigation of their role in machinability and in the formation and stability of tribo-layers at the tool-chip interface.
- The role of sulphides remains less consistent across the investigated batches; therefore, more detailed insight may be gained through systematic chip formation and chip morphology analysis.
- Advanced characterisation techniques (e.g. high-resolution SEM/TEM analysis) should be employed to understand the formation mechanisms and structural evolution of tribo-layers at the tool-chip interface.
- Further investigation into the physicochemical and mechanical properties of the tribo-layers, for example through techniques such as nano-indentation, is required to elucidate the mechanisms by which they influence tool-workpiece interactions.
- For the machinability analysis of 100Cr6, extending the study to include spheroidised microstructures would provide useful comparative insight into the microstructure's influence on the machinability of bearing steels.

Acknowledgements

First and foremost, I'd like to thank my supervisors Dr. Amir Malakizadi and Prof. Uta Klement. Amir - thank you for all the lessons, support and inspiration. I'm grateful that you've always had my best interest at heart. On my first day at Chalmers, you told me, "Aim high and I will support you" - thank you for sticking to your word. Uta - thank you for always helping me see the bigger picture and reminding me to think ahead. I'm grateful for our insightful conversations about my research, and equally for the ones about everyday life! Thank you for having my back. To my examiner, Prof. Peter Krajnik, thank you for the support, but also for all the shawarma lunches (sorry for the extra cholesterol). Your "sabah el kher" on some mornings was a nice reminder of home.

On a more formal note, this research was part of the WEAR-FRAME project funded by Vinnova (Sweden´s Innovation Agency) under FFI program (Project No.2020-05179). The supports received from Chalmers Area of Advance – Production and Chalmers Centre for Metal Cutting Research (MCR) are also acknowledged. I have learned a lot and received support from many people in this project, so I would like to acknowledge and thank: Dr. Rachid M'Saoubi, Elias Vikenadler, Jens Ringborg, Jimmy Emanuelsson, Dr. Martin Selin, Roope Roininen and Jonas Svensson. My gratitude also extends to Dr. Denis Boing, Christophe Bourgin, Franck Lamirand, Isabelle Calmet and Enrico D'Eramo.

To my colleagues and friends at Chalmers, Dr. Philipp Hoier and to-be-Dr. Daniel Andersson, thank you for making work fun. Our conversations and laughs about random things are some of my favourite memories at Chalmers. And thanks for constantly reminding me that Chalmers intranet exists. Philipp, you've been an amazing office mate.

I'm also grateful to Dr. Antonio Mulone, who on top of teaching and supporting me in various characterisation techniques, always had an open door for my questions. Dr. Sahith Kokkirala, it was fun to share this journey with you, milestone by milestone. Thank you for your invaluable help with the FIB. To all my other colleagues at Chalmers, including Bala, Sofia, Plinio, Rasmus, Dmitri, Satya, Kirill, and Angelica - thank you for the breaks, volleyball games, and after-works.

And finally, to my support system: Phil, merci vöumol for all the joy and adventure you constantly bring into my life, you made the tough days easier. Chebli, a voice from home - merci for calling (almost!) every day. Jamie, tack for all the warmth, laughs and free sodas. Maria and Christine, shukran for helping me sing through the sadder songs. Kriss, thank you for being there and listening when I needed someone to talk to. To my sisters, Kassandra and Daad, thank you for always cheering me on, especially when things felt a little out of reach. To my mother, Rima, I don't have enough words to thank you for helping bring my dreams into reach, day by day for a long 30 years. And to my father, Salame, who I am sure is watching from somewhere in the universe: Paps, thank you - we did it!

Gothenburg, 2026

References

[1] P. Hoier, A. Malakizadi, S. Friebe, U. Klement, and P. Krajnik, "Microstructural variations in 316L austenitic stainless steel and their influence on tool wear in machining," *Wear,* vol. 428, pp. 315-327, 2019.

[2] C. Salame, A. Malakizadi, and U. Klement, "On the influence of batch-to-batch microstructural variations on tool wear when machining C38 micro-alloyed steel," *Wear,* vol. 562, p. 205632, 2025.

[3] P. Stavropoulos, A. Papacharalampopoulos, E. Vasiliadis, and G. Chryssolouris, "Tool wear predictability estimation in milling based on multi-sensorial data," *The International Journal of Advanced Manufacturing Technology,* vol. 82, no. 1, pp. 509-521, 2016.

[4] T. Nauclér, M. Tyreman, and C. Roxburgh, "Growth and renewal in the Swedish economy: Development, current situation and priorities for the future," *McKinsey Global Institute, McKinsey Sweden,* 2012.

[5] R. Komanduri and Z. B. Hou, "Thermal modeling of the metal cutting process: part I—temperature rise distribution due to shear plane heat source," *International Journal of Mechanical Sciences,* vol. 42, no. 9, pp. 1715-1752, 2000.

[6] R. Komanduri and Z. B. Hou, "Thermal modeling of the metal cutting process—Part II: temperature rise distribution due to frictional heat source at the tool–chip interface," *International Journal of Mechanical Sciences,* vol. 43, no. 1, pp. 57-88, 2001.

[7] R. Komanduri and Z. B. Hou, "Thermal modeling of the metal cutting process—Part III: temperature rise distribution due to the combined effects of shear plane heat source and the tool–chip interface frictional heat source," *International Journal of Mechanical Sciences,* vol. 43, no. 1, pp. 89-107, 2001.

[8] A. Moufki, A. Molinari, and D. Dudzinski, "Modelling of orthogonal cutting with a temperature dependent friction law," *Journal of the Mechanics and Physics of Solids,* vol. 46, no. 10, pp. 2103-2138, 1998.

[9] C. Salame and A. Malakizadi, "An enhanced semi-analytical estimation of tool-chip interface temperature in metal cutting," *Journal of Manufacturing Processes,* vol. 105, pp. 407-430, 2023.

[10] F. Zhou, X. Wang, Y. Hu, and L. Ling, "Modeling temperature of non-equidistant primary shear zone in metal cutting," *International Journal of Thermal Sciences,* vol. 73, pp. 38-45, 2013/11/01/ 2013, doi: https://doi.org/10.1016/j.ijthermalsci.2013.05.014.

[11] R. M'Saoubi and H. Chandrasekaran, "Experimental study and modelling of tool temperature distribution in orthogonal cutting of AISI 316L and AISI 3115 steels," *The International Journal of Advanced Manufacturing Technology,* vol. 56, no. 9, pp. 865-877, 2011.

[12] C. Shan, X. Zhang, B. Shen, and D. Zhang, "An improved analytical model of cutting temperature in orthogonal cutting of Ti6Al4V," *Chinese Journal of Aeronautics,* vol. 32, no. 3, pp. 759-769, 2019/03/01/ 2019, doi: https://doi.org/10.1016/j.cja.2018.12.001.

[13] L. Li, B. Li, K. F. Ehmann, and X. Li, "A thermo-mechanical model of dry orthogonal cutting and its experimental validation through embedded micro-scale thin film thermocouple arrays in PCBN tooling," *International Journal of Machine Tools and Manufacture,* vol. 70, pp. 70-87, 2013/07/01/ 2013, doi: https://doi.org/10.1016/j.ijmachtools.2013.03.005.

[14] N. Ånmark, A. Karasev, and P. G. Jönsson, "The effect of different non-metallic inclusions on the machinability of steels," *Materials,* vol. 8, no. 2, pp. 751-783, 2015.

[15] T. Aiso, U. Wiklund, M. Kubota, and S. Jacobson, "Effect of Si and Al additions to carbon steel on material transfer and coating damage mechanism in turning with CVD coated tools," *Wear,* vol. 368-369, pp. 379-389, 2016/12/15/ 2016, doi: https://doi.org/10.1016/j.wear.2016.10.011.

[16] A. Bjerke *et al.*, "Thermodynamic modeling framework for prediction of tool wear and tool protection phenomena in machining," *Wear,* vol. 484-485, p. 203991, 2021/11/15/ 2021, doi: https://doi.org/10.1016/j.wear.2021.203991.

[17] G. Brant and M. Mikus, "The formation of protective layers when machining steel with ceramic cutting tools," *Wear,* vol. 118, no. 1, pp. 99-112, 1987/07/15/ 1987, doi: https://doi.org/10.1016/0043-1648(87)90007-X.

[18] E. Harju, S. Kivivuori, and A. S. Korhonen, "Formation of a wear resistant non-metallic protective layer on PVD-coated cutting and forming tools," *Surface and Coatings Technology,* vol. 112, no. 1, pp. 98-102, 1999/02/01/ 1999, doi: https://doi.org/10.1016/S0257-8972(98)00771-3.

[19] A. Helle, "On the interaction between inclusions in steel and the cutting tool during machining," 1995.

[20] M. Groppe, "Cemented Carbides," in *CIRP Encyclopedia of Production Engineering*: Springer, 2014, pp. 127-135.
[21] D. Boing, A. J. De Oliveira, and R. B. Schroeter, "Evaluation of wear mechanisms of PVD and CVD coatings deposited on cemented carbide substrates applied to hard turning," *The International Journal of Advanced Manufacturing Technology,* vol. 106, no. 11, pp. 5441-5451, 2020.
[22] S. Shoja, O. Alm, S. Norgren, H.-O. Andrén, and M. Halvarsson, "Calculated and experimental Schmid factors for chip flow deformation of textured CVD α-alumina coatings," *Surface and Coatings Technology,* vol. 412, p. 126991, 2021.
[23] S. Shoja, S. Norgren, H.-O. Andrén, O. Bäcke, and M. Halvarsson, "On the influence of varying the crystallographic texture of alumina CVD coatings on cutting performance in steel turning," *International Journal of Machine Tools and Manufacture,* vol. 176, p. 103885, 2022.
[24] A. E. Diniz, Á. R. Machado, and J. G. Corrêa, "Tool wear mechanisms in the machining of steels and stainless steels," *The International Journal of Advanced Manufacturing Technology,* vol. 87, no. 9, pp. 3157-3168, 2016.
[25] W. Grzesik, *Advanced machining processes of metallic materials: theory, modelling and applications*. Elsevier, 2008.
[26] S. J. Eric and A. Seco Tools, *Metal cutting theories and models*. Division of Production and Materials Engineering, 2012.
[27] E. M. Trent and P. K. Wright, *Metal cutting*. Butterworth-Heinemann, 2000.
[28] F. Klocke and A. Kuchle, *Manufacturing processes*. Springer, 2009.
[29] H. A. Youssef, *Machining of stainless steels and super alloys: traditional and nontraditional techniques*. John Wiley & Sons, 2016.
[30] H. Chandrasekaran and J. Johansson, "Chip flow and notch wear mechanisms during the machining of high austenitic stainless steels," *CIRP annals,* vol. 43, no. 1, pp. 101-105, 1994.
[31] U. S. Patel, S. K. Rawal, A. Arif, and S. C. Veldhuis, "Influence of secondary carbides on microstructure, wear mechanism, and tool performance for different cermet grades during high-speed dry finish turning of AISI 304 stainless steel," *Wear,* vol. 452, p. 203285, 2020.
[32] V. Bushlya, F. Lenrick, J.-E. Ståhl, and R. M'Saoubi, "Influence of oxygen on the tool wear in machining," *CIRP Annals,* vol. 67, no. 1, pp. 79-82, 2018/01/01/ 2018, doi: https://doi.org/10.1016/j.cirp.2018.03.011.
[33] J. Kong, Z. Xia, D. Xu, and N. He, "Investigation on notch wear mechanism in finish turning pure iron material with uncoated carbide tools under different cooling/lubrication conditions," *The International Journal of Advanced Manufacturing Technology,* vol. 86, no. 1, pp. 97-105, 2016.
[34] A. Hrechuk, K. Slipchenko, G. Maistro, and V. Bushlya, "Quantification of tool wear mechanisms in machining: The case of controlled-microstructure AISI 316L," *Wear,* vol. 570, p. 205944, 2025/06/01/ 2025, doi: https://doi.org/10.1016/j.wear.2025.205944.
[35] M. Fallqvist, M. Olsson, and S. Ruppi, "Abrasive wear of multilayer κ-Al2O3–Ti (C, N) CVD coatings on cemented carbide," *Wear,* vol. 263, no. 1-6, pp. 74-80, 2007.
[36] V. Marinov, "Experimental study on the abrasive wear in metal cutting," *Wear,* vol. 197, no. 1, pp. 242-247, 1996/09/01/ 1996, doi: https://doi.org/10.1016/0043-1648(96)06957-8.
[37] X. Xu, F. H. Ederveen, S. van der Zwaag, and W. Xu, "Correlating the abrasion resistance of low alloy steels to the standard mechanical properties: A statistical analysis over a larger data set," *Wear,* vol. 368-369, pp. 92-100, 2016/12/15/ 2016, doi: https://doi.org/10.1016/j.wear.2016.09.014.
[38] B. M. Kramer and P. K. Judd, "Computational design of wear coatings," *Journal of Vacuum Science & Technology A: Vacuum, Surfaces, and Films,* vol. 3, no. 6, pp. 2439-2444, 1985.
[39] E. Rabinowicz and A. Mutis, "Effect of abrasive particle size on wear," *Wear,* vol. 8, no. 5, pp. 381-390, 1965.
[40] J. A. Olortegui-Yume and P. Y. Kwon, "Tool wear mechanisms in machining," *International journal of machining and machinability of materials,* vol. 2, no. 3-4, pp. 316-334, 2007.
[41] I. Hutchings and P. Shipway, *Tribology: friction and wear of engineering materials*. Butterworth-heinemann, 2017.
[42] S. Ramalingam and P. Wright, "Abrasive wear in machining: experiments with materials of controlled microstructure," *Journal of Engineering Materials and Technology,* vol. 103, no. 2, pp. 151-156, 1981.
[43] F. Halila, C. Czarnota, and M. Nouari, "Analytical stochastic modeling and experimental investigation on abrasive wear when turning difficult to cut materials," *Wear,* vol. 302, no. 1-2, pp. 1145-1157, 2013.

[44] M. Binder, F. Klocke, and B. Doebbeler, "Abrasive wear behavior under metal cutting conditions," *Wear,* vol. 376, pp. 165-171, 2017.
[45] J. Gerth *et al.*, "Adhesion phenomena in the secondary shear zone in turning of austenitic stainless steel and carbon steel," *Journal of Materials Processing Technology,* vol. 214, no. 8, pp. 1467-1481, 2014/08/01/ 2014, doi: https://doi.org/10.1016/j.jmatprotec.2014.01.017.
[46] P. J. Arrazola, T. Özel, D. Umbrello, M. Davies, and I. S. Jawahir, "Recent advances in modelling of metal machining processes," *Cirp Annals,* vol. 62, no. 2, pp. 695-718, 2013.
[47] J. Ståhl, "Metal cutting: theories and models. Division of Production and Materials Engineering," *Lund University in cooperation with SecoTools AB, Lund/Fagersta, Sweden,* 2012.
[48] D. Jianxin, Z. Jiantou, Z. Hui, and Y. Pei, "Wear mechanisms of cemented carbide tools in dry cutting of precipitation hardening semi-austenitic stainless steels," *Wear,* vol. 270, no. 7, pp. 520-527, 2011/03/10/ 2011, doi: https://doi.org/10.1016/j.wear.2011.01.006.
[49] S. Fenglian, L. Zhenjia, J. Daming, and C. Bo, "Adhering wear mechanism of cemented carbide cutter in the intervallic cutting of stainless steel," *Wear,* vol. 214, no. 1, pp. 79-82, 1998/01/01/ 1998, doi: https://doi.org/10.1016/S0043-1648(97)00203-2.
[50] Y. Liao and R. Shiue, "Carbide tool wear mechanism in turning of Inconel 718 superalloy," *Wear,* vol. 193, no. 1, pp. 16-24, 1996.
[51] S. Saketi, U. Bexell, J. Östby, and M. Olsson, "On the diffusion wear of cemented carbides in the turning of AISI 316L stainless steel," *Wear,* vol. 430, pp. 202-213, 2019.
[52] G. Östberg *et al.*, "Mechanisms of plastic deformation of WC–Co and Ti (C, N)–WC–Co," *International Journal of Refractory Metals and Hard Materials,* vol. 24, no. 1-2, pp. 135-144, 2006.
[53] D. Mari, "Mechanical behavior of hardmetals at high temperature," 2014.
[54] G. Östberg and H.-O. Andrén, "Microstructural changes during wear by plastic deformation of cemented carbide and cermet cutting inserts," *Metallurgical and Materials Transactions A,* vol. 37, no. 5, pp. 1495-1506, 2006.
[55] T. Childs, *Metal machining: theory and applications*. Butterworth-Heinemann, 2000.
[56] R. Komanduri and Z. Hou, "A review of the experimental techniques for the measurement of heat and temperatures generated in some manufacturing processes and tribology," *Tribology international,* vol. 34, no. 10, pp. 653-682, 2001.
[57] J. Zhao, Z. Liu, B. Wang, J. Hu, and Y. Wan, "Tool coating effects on cutting temperature during metal cutting processes: Comprehensive review and future research directions," *Mechanical Systems and Signal Processing,* vol. 150, p. 107302, 2021.
[58] A. Malakizadi, H. Gruber, I. Sadik, and L. Nyborg, "An FEM-based approach for tool wear estimation in machining," *Wear,* vol. 368, pp. 10-24, 2016.
[59] G. Hao and Z. Liu, "The heat partition into cutting tool at tool-chip contact interface during cutting process: a review," *The International Journal of Advanced Manufacturing Technology,* vol. 108, no. 1, pp. 393-411, 2020.
[60] G. I. Taylor and H. Quinney, "The latent energy remaining in a metal after cold working," *Proceedings of the Royal Society of London. Series A, Containing Papers of a Mathematical and Physical Character,* vol. 143, no. 849, pp. 307-326, 1934.
[61] H. Puls, F. Klocke, and D. Veselovac, "FEM-based prediction of heat partition in dry metal cutting of AISI 1045," *The International Journal of Advanced Manufacturing Technology,* vol. 86, no. 1, pp. 737-745, 2016.
[62] I. Jawahir *et al.*, "Surface integrity in material removal processes: Recent advances," *CIRP annals,* vol. 60, no. 2, pp. 603-626, 2011.
[63] M. Saez-de-Buruaga, D. Soler, P. X. Aristimuño, J. A. Esnaola, and P. J. Arrazola, "Determining tool/chip temperatures from thermography measurements in metal cutting," *Applied Thermal Engineering,* vol. 145, pp. 305-314, 2018.
[64] X. Wang, T. Yu, X. Sun, Y. Shi, and W. Wang, "Study of 3D grinding temperature field based on finite difference method: considering machining parameters and energy partition," *The International Journal of Advanced Manufacturing Technology,* vol. 84, no. 5, pp. 915-927, 2016.
[65] J. Fleischer, R. Pabst, and S. Kelemen, "Heat flow simulation for dry machining of power train castings," *CIRP annals,* vol. 56, no. 1, pp. 117-122, 2007.
[66] N. Abukhshim, P. Mativenga, and M. A. Sheikh, "Heat generation and temperature prediction in metal cutting: A review and implications for high speed machining," *International Journal of Machine Tools and Manufacture,* vol. 46, no. 7-8, pp. 782-800, 2006.
[67] V. R. Marinov, "Hybrid analytical–numerical solution for the shear angle in orthogonal metal cutting—Part I: theoretical foundation," *International Journal of Mechanical Sciences,* vol. 43, no. 2, pp. 399-414, 2001.

[68] M. E. Merchant, "Mechanics of the metal cutting process. I. Orthogonal cutting and a type 2 chip," *Journal of applied physics,* vol. 16, no. 5, pp. 267-275, 1945.
[69] B. Denkena and D. Biermann, "Cutting edge geometries," *CIRP annals,* vol. 63, no. 2, pp. 631-653, 2014.
[70] C.-F. Wyen and K. Wegener, "Influence of cutting edge radius on cutting forces in machining titanium," *CIRP annals,* vol. 59, no. 1, pp. 93-96, 2010.
[71] M. C. Shaw and J. Cookson, *Metal cutting principles* (no. 3). Oxford university press New York, 2005.
[72] G. List, G. Sutter, and A. Bouthiche, "Cutting temperature prediction in high speed machining by numerical modelling of chip formation and its dependence with crater wear," *International Journal of Machine Tools and Manufacture,* vol. 54-55, pp. 1-9, 2012/03/01/ 2012, doi: https://doi.org/10.1016/j.ijmachtools.2011.11.009.
[73] D. J. Waldorf, R. E. DeVor, and S. G. Kapoor, "An Evaluation of Ploughing Models for Orthogonal Machining," *Journal of Manufacturing Science and Engineering,* vol. 121, no. 4, pp. 550-558, 1999, doi: 10.1115/1.2833050.
[74] H. Attia *et al.*, "Physics based models for characterization of machining performance – A critical review," *CIRP Journal of Manufacturing Science and Technology,* vol. 51, pp. 161-189, 2024/07/01/ 2024, doi: https://doi.org/10.1016/j.cirpj.2024.04.008.
[75] K. Björkeborn, U. Klement, and H.-B. Oskarson, "Study of microstructural influences on machinability of case hardening steel," *The International Journal of Advanced Manufacturing Technology,* vol. 49, no. 5, pp. 441-446, 2010.
[76] F. W. Boulger, "Machinability of steels," in *Properties and Selection: Irons, Steels, and High-Performance Alloys*: ASM International, 1990, pp. 591-602.
[77] S. Pytel and S. Rudnik, "The role of inclusion morphology on machinability of structural bar steels," in *International Conference on Processing, Microstructure and Properties of Microalloyed and Other Modern High Strength Low Alloy Steels*, 1991, pp. 13-21.
[78] Z. Liao *et al.*, "Review of current best-practices in machinability evaluation and understanding for improving machining performance," *CIRP Journal of Manufacturing Science and Technology,* vol. 50, pp. 151-184, 2024.
[79] F. W. Taylor, *On the art of cutting metals* (no. 1119). American society of mechanical engineers, 1907.
[80] J. Sorenson and W. Gates, "Machinability of steels," *Prod. Eng,* vol. 10, 1929.
[81] F. Boulger, H. Shaw, and H. Johnson, "Constant-pressure lathe test for measuring the machinability of free-cutting steels," *Transactions of the American Society of Mechanical Engineers,* vol. 71, no. 5, pp. 431-438, 1949.
[82] W. Boulger, M. HA, and G. TM, "Superior machinability of MX steel explained," *Iron Age,* vol. 67, pp. 90-95, 1951.
[83] N. E. Woldman and R. C. Gibbons, "Machinability and machining of metals," *(No Title),* 1951.
[84] B. Mills and A. Redford, "The concept of machinability," in *Machinability of Engineering Materials*: Springer, 1983, pp. 1-3.
[85] B. Mills, *Machinability of engineering materials*. Springer Science & Business Media, 2012.
[86] G. Boothroyd, *Fundamentals of metal machining and machine tools*. Crc Press, 1988.
[87] S. Enache, E. Strajescu, C. Opran, C. Minciu, and M. Zamfirache, "Mathematical model for the establishment of the materials machinability," *CIRP annals,* vol. 44, no. 1, pp. 79-82, 1995.
[88] W. Grzesik, "Modelling and Simulation of Machining Processes and Operations," *Advanced Machining Processes of Metallic Materials,* pp. 49-67, 2008.
[89] J. Kopac, "Cutting farces and their influence on the economics of machining," *Strojniski vestnik,* vol. 48, no. 3, pp. 121-132, 2002.
[90] B. Sredanović, G. Globočki-Lakić, D. Čiča, and S. Borojević, "A novel method for material machinability evaluation," in *Proceedings of the 12th International Conference on Management of Innovative Technologies & 4th International Conference on Sustainable Life in Manufacturing*, 2013.
[91] A. Damir, A. Sadek, H. Attia, and A. Tendolkar, "Characterization and optimization of machinability and environmental impact of machining of Ti–6Al–4V with minimum quantity lubrication," *Int. J. Robot. Mechatron,* vol. 4, no. 1, pp. 1-7, 2017.
[92] A. Damir, A. Sadek, and H. Attia, "Characterization of Machinability and Environmental Impact of Cryogenic Turning of Ti-6Al-4V," *Procedia CIRP,* vol. 69, pp. 893-898, 2018/01/01/ 2018, doi: https://doi.org/10.1016/j.procir.2017.11.070.
[93] *Tool-life testing with single-point turning tools*, ISO 3685:1993 1993.
[94] *Tool life testing in milling - Part 1: Face milling*, ISO 8688-1:1989, 1989.

[95] *Tool life testing in milling - Part 2: End milling*, ISO 8688-2:1989, 1989.
[96] N. Sharma and K. Gupta, "Influence of coated and uncoated carbide tools on tool wear and surface quality during dry machining of stainless steel 304," *Materials Research Express,* vol. 6, no. 8, p. 086585, 2019.
[97] G. D. Sonawane, R. Bachhav, and A. Kulkarni, "Comparative machinability aspects of austenitic and duplex stainless steels during dry turning," *JOM,* vol. 76, no. 8, pp. 4484-4498, 2024.
[98] Y. Seid Ahmed, J. M. Paiva, D. Covelli, and S. C. Veldhuis, "Investigation of coated cutting tool performance during machining of super duplex stainless steels through 3D wear evaluations," *Coatings,* vol. 7, no. 8, p. 127, 2017.
[99] A. Naskar and A. Chattopadhyay, "Investigation on flank wear mechanism of CVD and PVD hard coatings in high speed dry turning of low and high carbon steel," *Wear,* vol. 396, pp. 98-106, 2018.
[100] K. M. Gupta, K. Ramdev, S. Dharmateja, and S. Sivarajan, "Cutting characteristics of PVD coated cutting tools," *Materials Today: Proceedings,* vol. 5, no. 5, pp. 11260-11267, 2018.
[101] K.-D. Bouzakis, N. Michailidis, G. Skordaris, E. Bouzakis, D. Biermann, and R. M'Saoubi, "Cutting with coated tools: Coating technologies, characterization methods and performance optimization," *CIRP Annals,* vol. 61, no. 2, pp. 703-723, 2012/01/01/ 2012, doi: https://doi.org/10.1016/j.cirp.2012.05.006.
[102] K. D. Bouzakis *et al.*, "The effect of substrate pretreatments and HPPMS-deposited adhesive interlayers' materials on the cutting performance of coated cemented carbide inserts," *CIRP Annals,* vol. 59, no. 1, pp. 73-76, 2010/01/01/ 2010, doi: https://doi.org/10.1016/j.cirp.2010.03.065.
[103] T. Enomoto, T. Sugihara, S. Yukinaga, K. Hirose, and U. Satake, "Highly wear-resistant cutting tools with textured surfaces in steel cutting," *CIRP Annals,* vol. 61, no. 1, pp. 571-574, 2012/01/01/ 2012, doi: https://doi.org/10.1016/j.cirp.2012.03.123.
[104] F. Klocke, T. Schroeder, E. Bouzakis, and A. Klein, "Manipulation of coating and subsurface properties in reconditioning of WC–Co carbide cutting tools," *Surface and Coatings Technology,* vol. 202, no. 4, pp. 1194-1198, 2007/12/15/ 2007, doi: https://doi.org/10.1016/j.surfcoat.2007.06.023.
[105] S. Shoja, O. Bäcke, A. Fazi, S. Norgren, H. O. Andrén, and M. Halvarsson, "Enhanced steel machining performance using texture-controlled CVD alpha-alumina coatings: Fundamental degradation mechanisms," *International Journal of Machine Tools and Manufacture,* vol. 197, p. 104137, 2024/04/01/ 2024, doi: https://doi.org/10.1016/j.ijmachtools.2024.104137.
[106] B. Denkena, A. Lucas, and E. Bassett, "Effects of the cutting edge microgeometry on tool wear and its thermo-mechanical load," *CIRP annals,* vol. 60, no. 1, pp. 73-76, 2011.
[107] K. Zhuang, C. Fu, J. Weng, and C. Hu, "Cutting edge microgeometries in metal cutting: a review," *The International Journal of Advanced Manufacturing Technology,* vol. 116, no. 7, pp. 2045-2092, 2021.
[108] I. Arriola, E. Whitenton, J. Heigel, and P. Arrazola, "Relationship between machinability index and in-process parameters during orthogonal cutting of steels," *CIRP annals,* vol. 60, no. 1, pp. 93-96, 2011.
[109] Y. S. Ahmed, J. M. Paiva, B. Bose, and S. C. Veldhuis, "New observations on built-up edge structures for improving machining performance during the cutting of superduplex stainless steel," *Tribology International,* vol. 137, pp. 212-227, 2019/09/01/ 2019, doi: https://doi.org/10.1016/j.triboint.2019.04.039.
[110] P. Sivaiah and D. Chakradhar, "Performance improvement of cryogenic turning process during machining of 17-4 PH stainless steel using multi objective optimization techniques," *Measurement,* vol. 136, pp. 326-336, 2019/03/01/ 2019, doi: https://doi.org/10.1016/j.measurement.2018.12.094.
[111] M. Abouridouane *et al.*, "Microstructure-based approach to predict the machinability of the ferritic-pearlitic steel C60 by cutting operations," *Procedia CIRP,* vol. 82, pp. 107-112, 2019.
[112] C. Hu, L. Chen, Z. Zhao, A. Gong, and W. Shi, "Effects of Controlled Cooling-Induced Ferrite–Pearlite Microstructure on the Cold Forgeability of XC45 Steel," *Journal of Materials Engineering and Performance,* vol. 27, no. 6, pp. 2772-2781, 2018/06/01 2018, doi: 10.1007/s11665-018-3388-5.
[113] A. Marder and B. Bramfitt, "Effect of continuous cooling on the morphology and kinetics of pearlite," *Metallurgical Transactions A,* vol. 6, no. 11, pp. 2009-2014, 1975.
[114] H. Colpaert, *Metallography of steels: interpretation of structure and the effects of processing*. Asm International, 2018.

[115] M. Field and J. F. Kahles, "Review of surface integrity of machined components," *Annals of the CIRP,* vol. 20, no. 2, pp. 153-163, 1971.
[116] V. P. Astakhov, "Machinability: existing and advanced concepts," *Machinability of advanced materials,* pp. 1-56, 2014.
[117] A. Malakizadi, D. Mallipeddi, S. Dadbakhsh, R. M'Saoubi, and P. Krajnik, "Post-processing of additively manufactured metallic alloys–A review," *International Journal of Machine Tools and Manufacture,* vol. 179, p. 103908, 2022.
[118] Y. Ozcatalbas and F. Ercan, "The effects of heat treatment on the machinability of mild steels," *Journal of Materials Processing Technology,* vol. 136, no. 1, pp. 227-238, 2003/05/10/ 2003, doi: https://doi.org/10.1016/S0924-0136(03)00273-5.
[119] K. Liu, X. P. Li, and S. Y. Liang, "The mechanism of ductile chip formation in cutting of brittle materials," *The International Journal of Advanced Manufacturing Technology,* vol. 33, no. 9, pp. 875-884, 2007/07/01 2007, doi: 10.1007/s00170-006-0531-5.
[120] L. Jiang, Å. Roos, and P. Liu, "The influence of austenite grain size and its distribution on chip deformation and tool life during machining of AISI 304L," *Metallurgical and Materials Transactions A,* vol. 28, no. 11, pp. 2415-2422, 1997/11/01 1997, doi: 10.1007/s11661-997-0198-z.
[121] R. Arif, G. Fromentin, F. Rossi, and B. Marcon, "Investigations on Strain Hardening During Cutting of Heat-Resistant Austenitic Stainless Steel," *Journal of Manufacturing Science and Engineering,* vol. 142, no. 5, 2020, doi: 10.1115/1.4046612.
[122] T. Baker, "Processes, microstructure and properties of vanadium microalloyed steels," *Materials Science and Technology,* vol. 25, no. 9, pp. 1083-1107, 2009.
[123] T. Baker, "Microalloyed steels," *Ironmaking & Steelmaking,* vol. 43, no. 4, pp. 264-307, 2016.
[124] A. DeArdo, M. Hua, K. G. Cho, and C. Garcia, "On strength of microalloyed steels: an interpretive review," *Materials Science and Technology,* vol. 25, no. 9, pp. 1074-1082, 2009.
[125] L. J. Sirtuli, D. Boing, V. Bushlya, and S. Norgren, "Study of initial notch wear during turning of stainless steel with (CVD) Al2O3/Ti (C, N) coated cemented carbide tools," *International Journal of Refractory Metals and Hard Materials,* p. 107116, 2025.
[126] S. Olovsjö, A. Wretland, and G. Sjöberg, "The effect of grain size and hardness of Waspaloy on the wear of cemented carbide tools," *The International Journal of Advanced Manufacturing Technology,* vol. 50, no. 9, pp. 907-915, 2010.
[127] S. Olovsjö, A. Wretland, and G. Sjöberg, "The effect of grain size and hardness of wrought Alloy 718 on the wear of cemented carbide tools," *Wear,* vol. 268, no. 9-10, pp. 1045-1052, 2010.
[128] N. Subhash, T. Jagadeesha, and M. Law, "Investigations on machinability and machining stability of turning super duplex stainless steel," *International Journal of Machining and Machinability of Materials,* vol. 22, no. 5, pp. 386-405, 2020.
[129] T. Gladman, "Precipitation hardening in metals," *Materials science and technology,* vol. 15, no. 1, pp. 30-36, 1999.
[130] N. Kamikawa, Y. Abe, G. Miyamoto, Y. Funakawa, and T. Furuhara, "Tensile behavior of Ti, Mo-added low carbon steels with interphase precipitation," *ISIJ international,* vol. 54, no. 1, pp. 212-221, 2014.
[131] J. Angseryd, E. Olsson, and H.-O. Andrén, "Effect of workpiece sulphur content on the degradation of a PCBN tool material," *International Journal of Refractory Metals and Hard Materials,* vol. 29, no. 6, pp. 674-680, 2011.
[132] N. Ånmark and T. Björk, "Effects of the composition of Ca-rich inclusions on tool wear mechanisms during the hard-turning of steels for transmission components," *Wear,* vol. 368, pp. 173-182, 2016.
[133] P. Fiorini and G. Byrne, "The influence of built-up layer formation on cutting performance of GG25 grey cast iron," *CIRP Annals,* vol. 65, no. 1, pp. 93-96, 2016.
[134] Y. Yamane, H. Usuki, B. Yan, and N. Narutaki, "The formation of a protective oxide layer in machining resulphurized free-cutting steels and cast irons," *Wear,* vol. 139, no. 2, pp. 195-208, 1990.
[135] O. Bletton, R. Duet, and P. Pedarre, "Influence of oxide nature on the machinability of 316L stainless steels," *Wear,* vol. 139, no. 2, pp. 179-193, 1990.
[136] R. Kiessling, "Non-metallic inclusions in steel," *ISI PUBLICATION NO. 115, IRON AND STEEL INSTITUTE, LONDON. 118 P,* 1968.
[137] P. Różański and J. Paduch, "Modification of non-metallic inclusions in steels with enhanced machinability," *Archives of Metallurgy and Materials,* pp. 285-307-285-307, 2003.
[138] M. Merchant and N. Zlatin, "Basic reasons for good machinability of free machining steels," *Trans. ASM,* vol. 41, pp. 647-677, 1949.

[139] H. Yaguchi, "Effect of MnS inclusion size on machinabilty of low-carbon, leaded, resulfurized free-machining steel," *Journal of Applied Metalworking,* vol. 4, no. 3, pp. 214-225, 1986/07/01 1986, doi: 10.1007/BF02833929.
[140] E. Trent, "Cutting steel and iron with cemented carbide tools," *Journal of Iron and Steel Institute,* pp. 1001-1015, 1963.
[141] A. Bjerke *et al.*, "Understanding wear and interaction between CVD α-Al2O3 coated tools, steel, and non-metallic inclusions in machining," *Surface and Coatings Technology,* vol. 450, p. 128997, 2022.
[142] S. Ruppi, B. Ho, and M. Huhtiranta, "Wear characteristics of TiC, Ti (C, N), TiN and Al2O3 coatings in the turning of conventional and Ca-treated steels," *International Journal of Refractory Metals and Hard Materials,* vol. 16, no. 4-6, pp. 353-368, 1998.
[143] T. Baker and C. JA, "Morphology of manganese sulphide in steel," 1972.
[144] H. Liu and W. Chen, "Effect of total oxygen content on the machinability of low carbon resulfurized free cutting steel," *steel research international,* vol. 83, no. 12, pp. 1172-1179, 2012.
[145] R. Kiessling, "Influence of nonmetallic inclusions on the properties of steel," *J METALS,* vol. 21, no. 10, pp. 48-54, 1969.
[146] E. Rollason and J. Williams, "METALLURGICAL AND PRACTICAL MACHINING PARAMETERS AFFECTING BUILT-UP-EDG FORMATION IN METAL CUTTING," *J Inst Met,* vol. 98, pp. 144-153, 1970.
[147] C. H. Leung and L. H. Van Vlack, "Solution and Precipitation Hardening in (Ca, Mn) Sulfides and Selenides," *Metallurgical Transactions A,* vol. 12, no. 6, pp. 987-991, 1981/06/01 1981, doi: 10.1007/BF02643479.
[148] Y. Yang, D. Zhan, G. Qiu, X. Li, Z. Jiang, and H. Zhang, "Inclusion evolution in solid steel during rolling deformation: a review," *Journal of Materials Research and Technology,* vol. 18, pp. 5103-5115, 2022/05/01/ 2022, doi: https://doi.org/10.1016/j.jmrt.2022.05.018.
[149] C.-h. Leung and L. H. Van Vlack, "Solubility limits in binary (Ca, Mn) chalcogenides," *Journal of the American Ceramic Society,* vol. 62, no. 11-12, pp. 613-616, 1979.
[150] A. Slagter, J. A. Setyadji, E. L. Vogt, D. Hernández-Escobar, L. Deillon, and A. Mortensen, "Nanoindentation hardness and modulus of Al2O3–SiO2–CaO and MnO–SiO2–FeO inclusions in iron," *Metallurgical and Materials Transactions A,* vol. 55, no. 5, pp. 1469-1483, 2024.
[151] S. Subramanian, H. Gekonde, X. Zhang, and J. G, "Design of steels for high speed machining," *Ironmaking & steelmaking,* vol. 26, no. 5, pp. 333-338, 1999.
[152] A. Bjerke *et al.*, "Onset of the degradation of CVD α-Al2O3 coating during turning of Ca-treated steels," *Wear,* vol. 477, p. 203785, 2021.
[153] T. Malkiewicz and S. Rudnik, "Deformation of non-metallic inclusions during rolling of steel," *Journal of the Iron and Steel Institute,* vol. 201, no. 1, pp. 33-&, 1963.
[154] S. Rudnik, "Discontinuities in hot-rolled steel caused by non-metallic inclusions," *IRON STEEL INST J,* vol. 204, no. 4, pp. 374-376, 1966.
[155] D. Brooksbank and K. Andrews, "Stress fields around inclusions and their relation to mechanical properties," *Production and Application of Clean Steels, 1972, 186-198,* 1972.
[156] A. Ghosh, *Secondary steelmaking: principles and applications*. CRC Press, 2000.
[157] S. Jacobson and S. Hogmark, "Tribofilms: on the crucial importance of tribologically induced surface modifications," 2010.
[158] K. Adachi and K. Kato, "Formation of smooth wear surfaces on alumina ceramics by embedding and tribo-sintering of fine wear particles," *Wear,* vol. 245, no. 1-2, pp. 84-91, 2000.
[159] A. Blomberg, "Friction and wear of ceramics," Acta Universitatis Upsaliensis, 1993.
[160] O. O. Ajayi and K. C. Ludema, "Mechanism of transfer film formation during repeat pass sliding of ceramic materials," *Wear,* vol. 140, no. 2, pp. 191-206, 1990.
[161] W. D. Callister Jr and D. G. Rethwisch, *Materials science and engineering: an introduction*. John wiley & sons, 2020.
[162] S. Hogmark, S. Jacobson, and E. Coronel, "On adhesion in tribological contacts-causes and consequences," *Tribologia,* vol. 26, no. 1, pp. 3-16, 2007.
[163] E. Coronel, "Solving problems in surface engineering and tribology by means of analytical electron microscopy," Acta Universitatis Upsaliensis, 2005.
[164] N. Matsui and K. Watari, "Wear reduction of carbide tools observed in cutting Ca-added steels for machine structural use," *ISIJ international,* vol. 46, no. 11, pp. 1720-1727, 2006.
[165] T. Matsui *et al.*, "Behavior of MnS on Belag Formation and Observation on Carbide Tool," *Key Engineering Materials,* vol. 656, pp. 500-505, 2015.

[166] J. Yuan, G. S. Fox-Rabinovich, and S. C. Veldhuis, "Control of tribofilm formation in dry machining of hardened AISI D2 steel by tuning the cutting speed," *Wear,* vol. 402, pp. 30-37, 2018.
[167] X. Song, Y. Takahashi, W. He, and T. Ihara, "Study on the protective effect of built-up layer in dry cutting of stainless steel SUS304," *Precision Engineering,* vol. 65, pp. 138-148, 2020.
[168] "What is steel and how is steel made?" The European Steel Association (EUROFER). (accessed 2026).
[169] C. K. Gupta, *Chemical metallurgy: principles and practice*. John Wiley & Sons, 2006.
[170] I. H. Aziz *et al.*, "Recent developments in steelmaking industry and potential alkali activated based steel waste: A comprehensive review," *Materials,* vol. 15, no. 5, p. 1948, 2022.
[171] J. H. Park and Y. B. Kang, "Reoxidation phenomena of liquid steel in secondary refining and continuous casting processes: a review," *steel research international,* vol. 95, no. 11, p. 2300598, 2024.
[172] L. Holappa and O. Wijk, "Inclusion engineering," *Treatise on process metallurgy,* pp. 303-321, 2024.
[173] E. T. Turkdogan, "Ladle deoxidation, desulphurisation and inclusions in steel–Part 1: Fundamentals," *Archiv für das Eisenhüttenwesen,* vol. 54, no. 1, pp. 1-10, 1983.
[174] T. Kizu and T. Urabe, "Hot ductility of sulfur-containing low manganese mild steels at high strain rate," *ISIJ international,* vol. 49, no. 9, pp. 1424-1431, 2009.
[175] M. Morinaga, Y. Murata, R. Hashizume, and Y. Sawaragi, "Remarkable improvement in steam oxidation resistance due to the presence of sulfur in high Cr ferrtic steels," *ISIJ international,* vol. 41, no. 3, pp. 314-316, 2001.
[176] W. E. Bryson, *Heat treatment: master control manual*. Carl Hanser Verlag GmbH Co KG, 2015.
[177] S. Kalpakjian and S. Schmid, *Manufacturing, engineering and technology SI 6th edition-serope kalpakjian and stephen schmid: manufacturing, engineering and technology*. Digital Designs, 2006.
[178] P. J. Greening, "Mechanics of rolling continuously cast stock," Doctor of Philosophy, Department of mechanical and production engineering, The University of Aston in Birmingham, Birmingham, 1987.
[179] L. Zhang and B. G. Thomas, "Inclusions in continuous casting of steel," in *XXIV National Steelmaking Symposium, Morelia, Mich, Mexico*, 2003, vol. 26, p. 28.
[180] B. Thomas, "Continuous casting (metallurgy)," *Yearbook of science and technology,* pp. 1-6, 2004.
[181] M. C. Flemings, "Solidification processing," *Metallurgical transactions,* vol. 5, no. 10, pp. 2121-2134, 1974.
[182] H. GOTO, K.-i. MIYAZAWA, K.-i. YAMAGUCHI, S. OGIBAYASHI, and K. TANAKA, "Effect of cooling rate on oxide precipitation during solidification of low carbon steels," *Tetsu-to-hagané,* vol. 79, no. 9, pp. 1082-1087, 1993.
[183] H. GOTO, K.-i. MIYAZAWA, and H. HONMA, "Effect of the primary oxide on the behavior of the oxide precipitated during solidification of steel," *Tetsu-to-hagané,* vol. 81, no. 7, pp. 715-720, 1995.
[184] J. Campbell, "Melting, remelting, and casting for clean steel," *steel research international,* vol. 88, no. 1, p. 1600093, 2017.
[185] C. Capdevila, F. G. Caballero, C. García-Mateo, and C. G. De Andrés, "The role of inclusions and austenite grain size on intragranular nucleation of ferrite in medium carbon microalloyed steels," *Materials transactions,* vol. 45, no. 8, pp. 2678-2685, 2004.
[186] T. Baker and J. Charles, "Deformation of MnS inclusions in steel," *J. Iron Steel Inst.,* vol. 210, no. 9, pp. 680-690, 1972.
[187] R. Diederichs, R. Bülte, G. Pariser, and W. Bleck, "Modelling of manganese sulphide formation during solidification, Part II: Correlation of solidification and MnS formation," *Steel research international,* vol. 77, no. 4, pp. 256-264, 2006.
[188] Q. Yu, X. Yang, C. Lai, and Z. Tong, "Study on mns inclusion aggregation along continuous casting slab thickness of medium carbon structural steel," *Metals,* vol. 12, no. 1, p. 56, 2021.
[189] R. J. Fruehan, "Ladle metallurgy principles and practices," *(No Title),* 1985.
[190] C. Sims, "Trans. Met. Soc," in *AIME*, 1959, vol. 215, pp. 367-393.
[191] W. FORGENG, "Techniques for the Study of," in *Electric Furnace Steel Conference, Proceedings*, 1961, vol. 18, p. 7.
[192] D. You, S. K. Michelic, P. Presoly, J. Liu, and C. Bernhard, "Modeling Inclusion Formation during Solidification of Steel: A Review," *Metals,* vol. 7, no. 11, p. 460, 2017. [Online]. Available: https://www.mdpi.com/2075-4701/7/11/460.

[193] J. Burja, M. Koležnik, Š. Župerl, and G. Klančnik, "Nitrogen and nitride non-metallic inclusions in steel," *Mater. Tehnol,* vol. 53, no. 6, pp. 919-928, 2019.
[194] C. Lorig and A. Elsea, "Occurrence of intergranular fracture in cast steels," *Transactions,* vol. 55, p. 160, 1947.
[195] F. Pickering, "Formation of Inclusions in Rimming Steels," *Steel Times,* vol. 189, no. 5026, p. 686, 1964.
[196] E. Turkdogan and R. Fruehan, "Fundamentals of iron and steelmaking," *The Making, Shaping and Treating of Steel, Steelmaking and Refining Volume, 11th ed., RJ Fruehan, ed., AISE Steel Foundation, Pittsburgh,* vol. 11, pp. 125-126, 1998.
[197] R. Kiessling, "Non-Metallic Inclusions in Steel. V," *The Institute of Metals, 1989,* p. 194, 1989.
[198] L. Luyckx, J. R. Bell, A. McLean, and M. Korchynsky, "Sulfide shape control in high strength low alloy steels," *Metallurgical Transactions,* vol. 1, no. 12, pp. 3341-3350, 1970.
[199] X. Wang, X. Li, Q. Li, F. Huang, H. Li, and J. Yang, "Control of string shaped non-metallic inclusions of CaO-Al2O3 system in X80 pipeline steel plates," *Acta Metall Sin,* vol. 49, no. 5, pp. 553-561, 2013.
[200] Y. I. Ito, S. Nara, Y. Kato, and M. Suda, "Shape control of alumina inclusions by double calcium addition treatment," *Tetsu-To-Hagane/Journal of the Iron and Steel Institute of Japan,* vol. 93, no. 5, pp. 355-361, 2007.
[201] D. Zhao, H. Li, C. Bao, and J. Yang, "Inclusion evolution during modification of alumina inclusions by calcium in liquid steel and deformation during hot rolling process," *ISIJ International,* vol. 55, no. 10, pp. 2115-2124, 2015.
[202] C. Liu and B. Webler, "Evolution of non-metallic inclusions during heat treatment," *Metallurgical Research & Technology,* vol. 117, no. 4, p. 408, 2020.
[203] Y. Song, H. Zhang, and L. Ren, "A review of research on MnS inclusions in high-quality steel," *Engineering Reports,* vol. 6, no. 5, p. e12892, 2024.
[204] H. Exner, "Qualitative and quantitative surface microscopy," *Physical metallurgy,* pp. 943-1032, 1996.
[205] G. Vander Voort and A. Roosz, "Measurement of the interlamellar spacing of pearlite," *Metallography,* vol. 17, no. 1, pp. 1-17, 1984.
[206] E. Zinngrebe, P. Šedá, C. Van Hoek, and B. Van Arendonk, "Analysis and significance of non-metallic inclusions in non grain-oriented electrical steel," *ISIJ international,* vol. 53, no. 11, pp. 1913-1922, 2013.
[207] A. Okayama and T. Nishi, "Effect of Observed Number of Inclusions on the Diameter Distribution at Two-Dimensional Inspection," *ISIJ international,* vol. 51, no. 12, pp. 2064-2068, 2011.
[208] P. Woodard, S. Chandrasekar, and H. Yang, "Analysis of temperature and microstructure in the quenching of steel cylinders," *Metallurgical and materials transactions B,* vol. 30, no. 4, pp. 815-822, 1999.
[209] G. Wang and Y. Li, "Effects of alloying elements and temperature on thermal conductivity of ferrite," *Journal of Applied Physics,* vol. 126, no. 12, 2019.
[210] D. R. Lide, *CRC handbook of chemistry and physics: a ready-reference book of chemical and physical data*. CRC press, 1995.
[211] K. Holmberg and A. Matthews, *Coatings tribology: properties, mechanisms, techniques and applications in surface engineering*. Elsevier, 2009.